Bioinspired interface management in composites: Exploring peptide-polymer conjugates as precision compatibilizers

Dissertation

zur Erlangung des akademischen Grades
doctor rerum naturalium

(Dr. rer. nat.)

im Fach Chemie

eingereicht an der

Mathematisch-Naturwissenschaftlichen Fakultät
der Humboldt-Universität zu Berlin

von

M.Sc. Valeria Samsoninkova

Präsidentin der Humboldt-Universität zu Berlin
Prof. Dr.-Ing. Dr. Sabine Kunst

Dekan der Mathematisch-Naturwissenschaftlichen Fakultät
Prof. Dr. Elmar Kulke

Gutachter: 1. Prof. Dr. Hans G. Börner
2. Prof. Dr. Erhard Kemnitz
3. Prof. Dr. Helmut Cölfen

Tag der mündlichen Prüfung: 10.07.2019

Content

Abstract

Nature provides fascinating examples of composite materials with exceptional mechanical properties such as bone or nacre. Intensive research of last years explored the structure–function relationships in those hierarchically structured materials. Bioinspired materials represent a new class of materials build according to architecture principles found in natural materials. Recently the internal material interfaces in biomaterials have come into focus of studies and the control of interface properties seems to be one of the key factors towards outstanding mechanical properties. Nature uses proteins as connecting molecules – compatibilizers between an inorganic component and organic matrix. These natural compatibilizers are able to recognize inorganic surfaces and mediate the internal material interface. This thesis aims to evaluate the applicability of principles of interface management derived from nature to synthetic system.

The current concept is based on the sequence specific recognition of the inorganic surface by peptides. Peptide sequences can be biocombinatorially selected from a phage display library, allowing to identify sequences able to recognize specific inorganic surfaces. Peptide-polyethylene oxide (PEO) conjugates, consisting of a previously identified specifically binding peptide sequence and polymer-block, are incorporated in the polymer composite material, composed of MgF_2 nanoparticles particles and PEO. Peptide-polymer conjugates can be considered as the simplified version of natural compatibilizers.

Incorporation of the conjugates into the composite leads to simultaneous improvement of mutually exclusive properties such as stiffness and toughness. Improved stiffness expresses in 2-3 times higher elastic modulus values. Structural studies involving electron microscopy and spectroscopic techniques revealed suppression of particle aggregation and corresponding structural size effect responsible for improvement in the mechanical performance. Elastic modulus is sensitive to aggregate's size changes and their distribution especially in the nanometer range.

Concept of bioinspired compatibilizer was expanded to the implementation of different peptide sequences out of set of peptides identified as selective binders to the surface. Evaluation of secondary interactions, including solubility and self-aggregation tendency, revealed that the smaller the affinity for peptide-peptide interaction, the higher the availability of peptide sequences for an inorganic surface. Sequences with low solubility due to aggregation are less efficient in surface recognition. Peptide-polymer conjugates containing well soluble peptides allowed to achieve better stabilization and further improvement of mechanical properties. Employing advanced NMR techniques, binding motif was identified in the most efficient peptide sequence, revealing role of particular amino acids in the interaction and recognition of inorganic surface.

This bioinspired concept of interface modification via peptide-polymer conjugates represents a versatile tool for new material development.

Zusammenfassung

Die Natur bietet faszinierende Beispiele von Materialien mit besonderen mechanischen Eigenschaften wie Knochen oder Perlmutt. Durch intensive Forschung in den letzten Jahren konnten die Zusammenhänge zwischen der Struktur und Funktion in diesen hierarchisch strukturierten Materialien identifiziert werden. Bioinspirierte Materialien stellen eine neue Gruppe der Materialien dar, die nach den Architekturprinzipien der Biomaterialien aufgebaut sind. Vor kurzem sind die Grenzflächen der Biomaterialien in den Fokus der Forschung gerückt, da sie eine der entscheidenden Faktoren hinsichtlich der hervorragenden mechanischen Eigenschaften zu sein scheinen. Die Natur benutzt Proteine als natürliche Kompatibilisatoren – Moleküle, die anorganische Komponenten mit der organischen Matrix verbinden. Diese natürlichen Kompatibilisatoren können die anorganische Oberfläche erkennen und damit die Grenzfläche stabilizieren. Diese Arbeit beschäftigt sich mit der Aufgabe, die Anwendbarkeit des Konzeptes der Kompatibilisatoren aus den Biomaterialien auf synthetische Systeme zu prüfen.

Das Konzept der Arbeit basiert auf der Erkenntnis, dass Peptide anorganische Oberflächen erkennen können. Die Peptidsequenzen können biokombinatorisch aus Phagen-Display-Bibliotheken identifiziert werden. Diese Methode erlaubt Sequenzen zu finden, die bestimmte anorganische Oberflächen erkennen können. Peptid-Polyethylenoxid (PEO) Konjugate, die bioinspirierten Kompatibilisatoren, die davor identifizierte spezifische adhärierende Peptidsequenz und einen Polymerblock enthalten, sind in das Material eingeblendet, welches aus MgF_2 Nanopartikeln und PEO besteht. Peptid-Polymer Konjugate können als eine vereinfachte Version der Grenzflächenproteinen betrachtet werden,

Das Einblenden der Konjugate in die Komposite führt zur gleichzeitigen Verbesserung von Steifigkeit und Zähigkeit. Die verbesserte Steifigkeit, erreicht durch die Zugabe von dem Konjugat, äußert sich in einem zwei- bis dreifach höherem elastischen Modul. Die Analyse der Materialstruktur mit den mikroskopischen und spektroskopischen Methoden zeigt die Unterdrückung der Aggregation und den entsprechenden Größeneffekt, der für die Verbesserung der mechanischen Eigenschaften verantwortlich ist. Der elastische Modul ist sensitiv gegenüber den Größen der Aggregate speziell im Nanometerbereich.

Das Konzept der bioinspirierten Kompatibilisatoren wurde um das Implementieren von anderen Peptidsequenzen erweitert, die aus dem Set von spezifisch bindenden Sequenzen stammen. Die Evaluierung der sekundären Wechselwirkungen wie Löslichkeit und Selbst-Aggregation hat gezeigt, dass je kleiner die Affinität zur Peptid-Peptid Wechselwirkung, desto höher ist die Verfügbarkeit der Sequenz für die anorganische Oberfläche. Die Peptidsequenzen mit der geringeren Löslichkeit aufgrund der Aggregation sind weniger effizient in der Erkennung der Oberfläche. Peptid-Polymer-Konjugate, die gut lösliche Peptidsequenzen enthalten, erlauben bessere Stabilisierung der Nanopartikel und sind damit effizienter in der Verbesserung der mechanischen Eigenschaften. Durch die Anwendung von NMR war es möglich, ein Bindungsmotiv aus der effektivsten Peptidsequenz

zu identifizieren und die Rolle der einzelnen Aminosäuren in der Interaktion des Peptids mit der anorganischen Oberfläche zu zeigen.

Diese Arbeit zeigt, dass das Konzept der Biomaterialien von den Biomolekülen an der Grenzfläche übertragbar auf die synthetischen Systeme ist. Das Konzept von der bioinspirierten Grenzflächenmodifizierung mit Peptid-Polymer Konjugaten ist ein versatiles Tool für die Entwicklung neuer Materialien.

1. Motivation and goals

Nature provides fascinating examples of composite materials such as bone, nacre, silk and others.[1, 2] These materials show exceptional properties and are perfectly adapted to their purpose and environment.[3] Intensive research throughout the last decades revealed the structure–function relationships in those hierarchically structured materials.[4, 5] Mechanistic insights have been provided elucidating the origins of superior mechanical performance.[2, 4] These efforts allowed to deduce the structural principles of biomaterials and transfer these principles to address challenges of engineering materials.[6-8] This field has been evolving very fast, creating a new scientific direction of bioinspired materials, promising to open completely new dimensions for material science.[1, 9]

This work is dedicated to the exploration and transfer of one recently discovered structural principle of biomaterials – biomolecules at interface - to synthetic hybrid composites. The control of interfaces seems to be one of the key factors toward remarkable mechanical properties.[10] In established design strategies of synthetic composites, the effect of interface modulation on mechanical properties have been frequently underestimated as attention was often set on constituents and hierarchical superstructures. Biomaterials tailor the internal material interfaces frequently through protein-based interface active molecules such as proteins or proteoglycans, making out of brittle constituents stiff and tough materials.[11] For instance, the high fracture toughness of abalone shells arises from its interface design, where proteins build a "glue"- like phase between aragonite platelets. This organic layer is made responsible for energy dissipation, realizing impact resistance and fracture toughness.[11] Nature uses also very specific proteins for these purposes, they are able to recognize the inorganic phase of material and specifically binds to it, ensuring very efficient mediation of the interface.[12]

In contrast to biomaterials, the improvement of both stiffness and toughness remains frequently problematic or not feasible in synthetic composites.[13] Hence, bioinspired concepts are mandatory to exploit material-specific interactions for the realization of material-specific compatibilizers. These might offer opportunities to more precisely modulate mechanical properties in synthetic composite materials and ultimately improve contradictory properties such as toughness and stiffness.

Considering functions of interfacial proteins found in biomaterials, rationalized and simplified versions of protein-based interfacial stabilizers –peptide-polymer conjugates- can be explored. The combination of synthetic polymers and monodisperse biosegments, e.g., peptides,[14] nucleotides[15] or saccharides,[16] proves the enormous potential to control binding or adsorption properties, making these bioconjugates a valuable toolbox for material and biomedical applications.[17, 18] For instance, peptides can be identified by phage display to show material-specific adsorption onto inorganic or soft-matter surfaces.[19] Such sequences were utilized to mediate the growth of inorganic nanoparticles or to functionalize surfaces.[20-23] Moreover, derived peptide-block-poly(ethylene glycol) (peptide-PEG) conjugates can effectively stabilize sols in solution, providing ease of redispersibility of

inorganic nanoparticles.[24] Specific compatibilizers might be envisioned to stabilize inorganic–polymer composites as the peptide segment could be tailored for sequence-specific adsorption to the inorganic constituents and the polymer block could contribute to effective blending into a surrounding polymer matrix.

The concept of bioinspired compatibilizers (**Fig. 1**) will be evaluated in the present thesis on a model system. This system contains nanometer-sized MgF_2 particles and poly (ethylene oxide) matrix. The biologically inspired peptide-PEG compatibilizer combines a peptide segment for sequence-specific adsorption onto MgF_2 nanoparticle surfaces and a PEG block to improve blending into the PEO matrix, allowing precise interface design. The inorganic constituents proved to have interesting properties such as high hardness, bactericidal activity, and low refractive index, which might be of interest for potential applications.[25, 26] PEO matrix material is known to have reduced interactions with peptides or proteins as PEO coatings show anti-fouling character. Thus, it can be expected that the peptide–MgF_2 interactions might not be dramatically perturbed by nonspecific peptide–matrix interactions. The utilized peptide-PEG compatibilizer was based on a recently described stabilizer for MgF_2 sol nanoparticles. The peptide sequence Thr-Gln-Tyr-Tyr-Ala-Tyr- Ser-Thr-Thr-Gln-Lys-Ser (TQYYAYSTTQKS) had been identified previously by phage-display biopanning as sequence that specifically binds onto MgF_2 and later modified to conjugate Ac-GTQYYAYSTTQKS-PEG.[24]

- The applicability of the biomaterials structural principle of “glue-like” interface biomolecules to synthetic system
- The effect of bioinspired compatibilizer on the mechanical properties of hybrid composites
- Structure of new composites and its connection to the mechanical performance
- The applicability the different peptide sequences as compatibilizer, differences in their behavior and efficiency; parameters impacting their performance
- Interaction of peptides with the inorganic surface and types of forces driving them; role of residues in these interactions

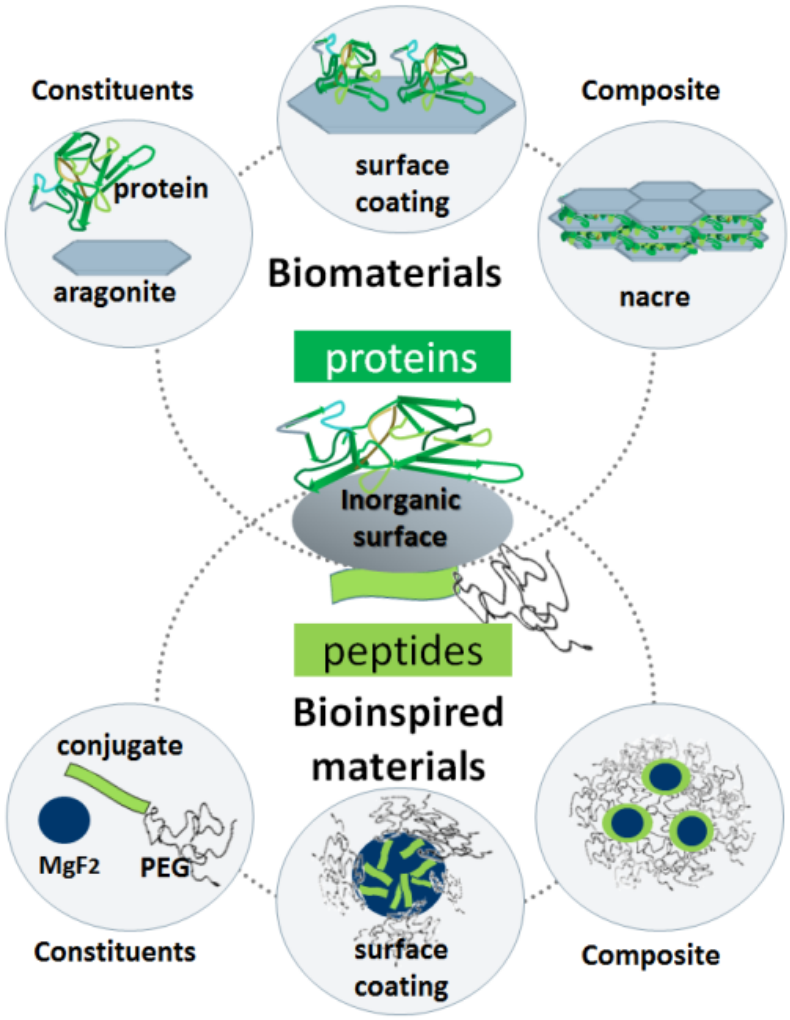

Fig. 1. Illustration of bioinspired concept of tailor-made compatibilizers for hybrid material: inspired by biomaterials such as nacre, where aragonite constituents are “glued” together by a protein layer that is specifically tailored to bind to the surface of inorganic building blocks and generates a distinct interface (top). From this concept a peptide–polymer conjugate could be abstracted as a simplified synthetic analog (bottom). The bioconjugate requires a peptide segment that enables specific binding to an inorganic constituent such as MgF_2 and a polymer block that effectively blends into the surrounding polymer matrix.[27]

2. Theoretical background

This chapter is dedicated to the presentation of theoretical background underlying this research. First section will cover the relevance and necessity of biomaterials investigation as well as development of bioinspired materials. The focus will go to the role of interfaces in the biomaterials and bioinspired materials and modification of interfaces through compatibilizers. Interface modification in biomaterials and compatibilizers in nature will be covered first and then analyzed in comparison to the conventional compatibilizers used in the industry for commercial applications. This research study focuses on the peptide-nanoparticle interactions and application of peptides as compatibilizer, therefore the second section will be dedicated to the peptides and their known applications in material science. The attention will be primarily drawn to the adhesion of peptides to the inorganic surfaces and modification of their properties, as it is the most crucial step in compatibilization and interface modulation.

2.1. Role of interface in conventional and natural composites

2.1.1. Interfaces of biomaterials and natural compatibilizers

Nature vital evolution originates very specific mechanisms to build biomaterials with exceptional mechanical properties.[1, 28] All these materials such as bone or nacre are usually contain hard and soft phases arranged in the hierarchical architectures from nano to macroscale.[2] These sophisticated hierarchical arrangements allow achieving “property amplification”: making from brittle minerals and proteins remarkable mechanical performance of the final material. To name one well studied example of such “amplification”: mollusk shells are mostly made of minerals (around 95%) and contain only a small portion of organic phase (around 5%),[29] but nacre has high stiffness (70-80 GPa), high tensile strength (70-100 MPa) and high fracture toughness (4-10 MPa/$m^{1/2}$).[30, 31] At the same time, fracture toughness of mineral phase in nacre – aragonite is around 0.25 MPa MPa/$m^{1/2}$, which means that toughness of final material is up to 40 times higher as of its main component.[2]

Hierarchical structure implies that constituents of different size have to be joined to make a material. Nature creates the interfaces of different types that govern, to a large extent, all properties of the hierarchically structured biomaterials and the control of interface properties seems to be one of the key factors toward remarkable mechanical properties. Due to this, recently the internal material interfaces in biomaterials have come into the focus.[32][33] Biomaterials tailor the internal material interfaces frequently through protein-based molecules forming a “glue” at the interface (**Fig. 2**)**,** which enables stress mediation.[10]

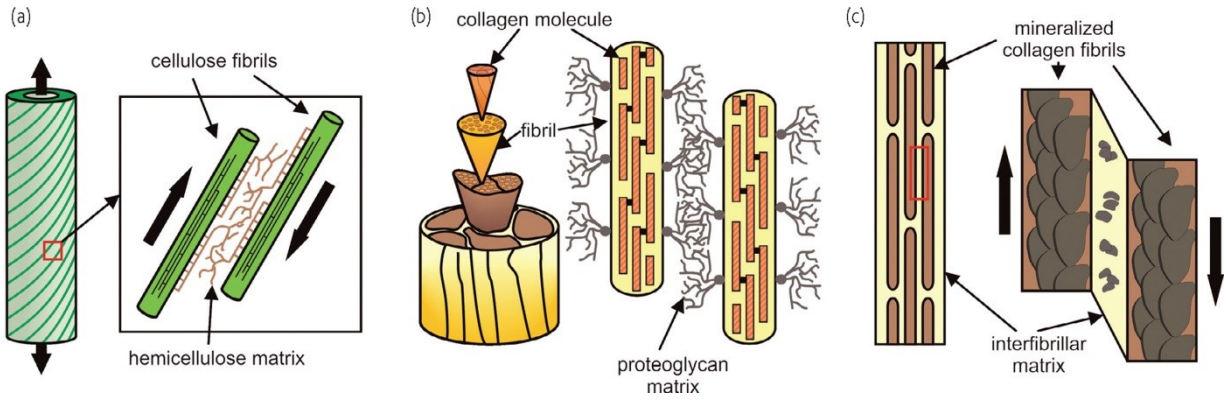

Fig. 2. ”Glue” like phase at the Interfaces between (a) cellulose fibrils in the wood cell wall (b) collagen fibrils in the tendon and (c) mineralized collagen fibrils in bone. Figure is adapted from reference [32].

There are many fascinating examples of biomaterials, where proteins at the interfaces play a crucial role in the mechanical performance. The incorporation of soft interface, consisting of chitin and collagen like proteins, significantly improves the fracture resistance of brittle silica in the skeleton of deep sea sponges.[34] Soft interfaces can also provide deformability in materials such as wood cell wall and tendon. Sliding of cellulose fibrils against each other in wood is possible thanks to the hemicellulose matrix, where cellulose fibers are incorporated in (**Fig. 2a**).[35] Proteoglycan matrix containing collagen fibrils in tendon ensures plastic flow (**Fig. 2b)**.[36] In bone, the interfibrillar layer, consisting of negatively charged polyelectrolytes between mineralized collagen fibrils, is correlated with the plastic flow in the matrix (**Fig. 2c)** [37].

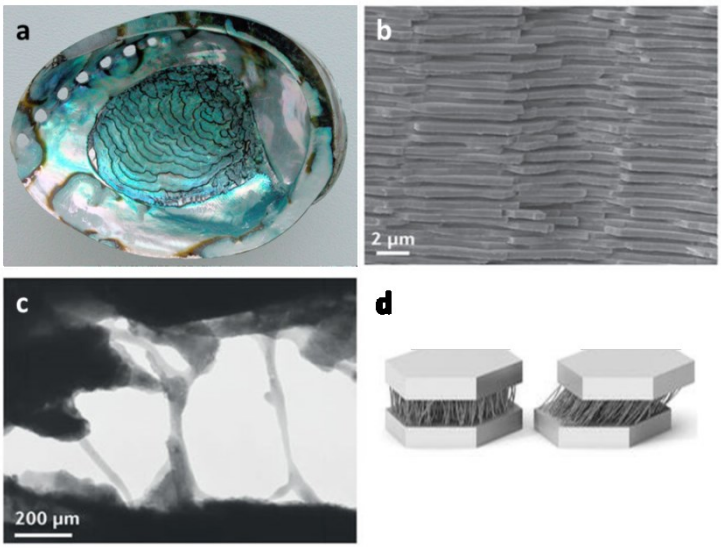

Fig. 3. Illustration for the interface management strategies on the example of nacre. a Picture of nacre. Outer shell of nacre consists of aragonite platelets glued together by a number of proteins arranged is a brick-and-mortar structure (b). c. Various proteins (c) are involved in gluing the aragonite platelets together. Proteins allow sliding platlets one on another, contributing significantly to remarkable toughness. Picture was adapted from references [2, 33].

Exceptional properties of nacre are also due to its special structural complexity. Nacre consists of 95 vol.% of layered aragonite ($CaCO_3$) platelets (~200–900 nm thick with a diameter of 5–8 μm), bonded by a thin (~10–50 nm) layer of organic material (**Fig. 3 a,b,c**).[2] The exceptional toughness of nacre is ensured through several toughening mechanisms, the most powerful mechanism among them is sliding of aragonite tablets against one another, which generates relatively large deformations accompanied by energy dissipation (**Fig. 3 d**).[31, 38] Sliding and pullout of the tablets are mediated by the thin (10-50 nm) interfaces between the tablets, which are rich in organic phase, consisting of β-chitin fibrils, sandwiched between two proteinnacrous layers.[39] The protein layers are bonded to the tablets, forming a continuous connection.[39, 40] About 40 protein sequences have been identified from the organic layer in nacre up to now.[41] Two of the most well studied proteins, which are commonly brought in relation to mechanical response, are chitin and Lustrin A, the later of which could add to toughening through unfolding.[11, 42] Interestingly, Lustrin A can specifically interact with aragonite due to Ca-binding domains providing a tailor made interface between the mineral and the protein phases.[43] In addition, another protein was extracted, named Pif 97. This protein with its chitin- and aragonite binding sites may function as a link between aragonite and chitin.[12] Presence of mineral-binding domains in Lustrin A and Pif again emphasizes the fact that nature uses abilities of proteins for recognition of surfaces to realize higher functions, such as connecting inorganic blocks and creating special interfaces.

2.1.2. Interfaces and compatibilizers in conventional polymeric composites

This section is dedicated to the conventional approaches for compatibilizers, which are well established in the industry. A composite material by definition is a material made of two or more constituents with significantly different physical or chemical properties that, when combined, produce a material with characteristics different from the individual components. Polymers used as matrix to produce composites are often blended with different fillers- to enhance mechanical performance. Inorganic fillers can be of various types and shapes, they can be particles, fibers, flakes etc.[44, 45] The common problem in the composites is that components are very different in their nature and are therefore not compatible. Various types of compatibilizers are used to enhance compatibility of different components and realize homogeneous distribution of the filler and bonding to the matrix. Only the particulate filled composites and their compatibilizer will be considered, as studied system in this work is based on particles.

Homogeneous distribution of the filler is assumed in most of the cases, which, however, rarely occurs and special particle structures develop in the composites. Two types of interactions must be considered in particulate filled composites: particle-particle and matrix-filler interactions. Particle-particle interactions induce aggregation, while matrix-filler

interaction leads to the interphase with special structure and properties different from both components. Aggregation increases with decreasing size of the filler, as far as strength of adhesion between the particles is determined by the size and surface energy. The easiest way for modification of interfacial interactions is the surface treatment of fillers. With a few exceptions, the surfaces of most particulate fillers are less than optimum for interaction with polymers. Therefore, surface modifiers are used to improve the interaction. The wide range of compatibilizers (surface modifiers) are offered and used commercially, ranging from the inexpensive fatty acids, to silanes, titanates and zirconates.[44, 45]

There are two main types of surface treatments of fillers: those that involve covalent chemical bonding and those that do not. The reasons for using them are different. Chemical bonding treatments are designed to improve the adhesion between filler and polymer, promoting better mechanical properties. Non-bonding treatments in contrast are designed very often to improve fillers ease of handling and dispersion. One of the most typical examples of this type are long chain fatty acids. They can be adsorbed on the filler surface, changing its character so that it is more compatible with hydrophobic polymers and easier to disperse. Coupling agents, representing another group of surface treatment, have two reactive chemical groups, one to bond to the filler and one to the polymer. The most common example is the organosilanes that are applied to the surface of inorganic fillers in order to improve their adhesion to polymers.[46]

The oldest and most commonly used modification of fillers is the coverage of the surface with a small molecular weight organic compound.[47] Saturated fatty acids (very often stearic acid) are typical examples of non-coulpling agents. The principle of the treatment is the preferential adsorption of the polar group of the surfactant onto the surface of the filler. Fatty acids are very well applicable for basic filler, where acid groups can give strong interaction. This treatment is easy applicable, inexpensive and can lead to easier processing. However, one of crucial questions of non-reactive treatment is the amount of agent to use, which is critical for the efficiency of the treatment. It could be dependent on the type of interaction, size of treating molecule, alignment on the surface. The insufficient amount does not bring desired effect, while excesses lead to the deterioration of the mechanical properties.[48] As a result of the treatment, the surface free energy of the filler decreases drastically.[49] Such changes consequently lead to a decrease of both types of interactions: particle-particle and particle-matrix. Reduction of particle-particle interactions leads to the decrease in aggregation and improved dispersion. In parallel to some useful effects, coatings with saturated fatty acids normally interact weakly and the tails of acids are normally too short to entangle with the polymer matrix. This results in filler debonding at relatively low stresses, expressed very often in a lowering of elastic modulus and strength, but leading to improved elongation at break and toughness. [50] Toughness improvement is caused by a plastic deformation of the matrix, which is the main energy adsorbing process in impact. [51]

Silanes represent a big class of compounds widely used as coupling agents with general formula.

$$(R)_{4-n} – Si – X_n$$

The X is a group chosen to react with surface hydroxyls of the filler, usually halogen or alkoxyl. Organo-silanes rely on reaction with surface hydroxyl, due to the fact that most of them are effective only for fillers with surface hydroxyls such as silica, silicates, oxides and hydroxides. Apart from this, silanes can react with themselves in the presence of moisture. Silane coupling agents are much more widely used in particulate filled composites than the non-coupling ones. This is because of their ability to improve filler polymer adhesionand filler dispersion. Silane coupling agents produce around the filler a layer, which consist of physisorbed and chemisorbed molecules, building an interphase of a graded structure, where exact properties of this phase control the reinforcement.[52] The nature of this interphase will depend on the silanes, coating condition, nature of the filler, the matrix and compounding condition.[53] Silanes are applicable for all organic resins, but the degree of improvement varies with the nature of the resin.[54] Application of silanes mostly leads to improved strength, although deformability and impact characteristics decrease. [55]

As an alternative to silanes, other coupling agents were introduced, especially for the cases, where silanes are not applicable e.g carbon black. Examples of these alternative coupling agents are organo-titanates or organo-zirconates. Organo-titanates are derivatives of ortho-titanic acid $Ti(OH)_4$ and therefore the organo-titanes are similar to silanes. They are designed to have a group that readily hydrolyse to titanium hydroxyl groups, which can condense with surface hydroxyls. The main use of organo-titanates appears to be in giving dispersion of particles.[56] It is claimed that the major part of their effectiveness is due to chemical removal of the surface water layer on the particles, which significantly improves dispersion.[44]

Block-copolymers have also found their application as coupling agents.[57] They can be used for the cases where the commonly used coupling agents can't effectively improve the compatibility and interfacial adhesion, as in the cases, where polymers have no functional groups present for such coupling agents to react with. The good compatibility between the matrix polymer and the block copolymer coupling agent is desirable for the improvement in the interfacial adhesion.[58] They proved to contribute to the efficient dispersion of particles, better interfacial adhesion and improvement of mechanical properties. [59, 60]

One-more quite commonly used strategy, especially in the field of nanocomposites, is grafting method, when polymer attached to the nanoparticles ensures their distribution in the polymer matrix. There are mainly two methods to create grafted nanoparticles: "grafting to" and "grafting from". In a grafting-to method, a preformed and functionalized polymer is attached to the surface. Although the grafting-to method has the advantage of a simple and modular approach, there are drawbacks. Steric repulsion between already attached and diffusing to the surface polymer chains limits the available graft density. In the grafting-from method, the surface is functionalized with an initiator or chain transfer agent and the polymer if grown from the surface. Controlled radical polymerization offer an attractive method for the functionalization of the interface between the nanoparticles and polymer matrix, allowing the control over multiple molecular variables including chain composition,

molecular weight, architecture as well as end- and side-group functionality. [61, 62] Polymer brushes attached to the nanoparticles may also undergo variations such as bimodal brushes consisting of homopolymer with two different distinct polymer lengths or brushes composed of block copolymers.[63]

Surface treatment is obviously the most convenient route to modify interactions and composite properties. Conventional compatibilizers relay solely on the interaction of surface groups of a filler with the compatibilizer, allowing to use the same compatibilizers for different fillers. This represents a simplified concept in comparison to the natural compatibilizers where special proteins are able to recognize the surface of the mineral components. The approaches used by nature and current compatibilizers relay on a very different principles. Ability of peptides to recognize the surfaces and specifically adhere to it makes peptide-polymer conjugates studied in this project to the tailor-made compatibilizers. They are selected and optimized for the specific inorganic surfaces. Therefore peptide-based conjugates should be considered as more advanced compatibilizers in comparison to conventional ones.

A very important point is also effect of this compatibilizers on the final composite properties. A strong thin interphase results in brittle materials, while a soft interphase leads to lower modulus and higher impact resistance.[64] Generally conventional compatibilizers improve toughness but tend to lower modulus, which means that improvement of one property (toughness) goes on the cost of other property (elastic modulus) and there is a need to compromise. This phenomenon does not occur in the natural composites, which again emphasizes the differences between conventional and compatibilizers from the nature.

2.1.3. Bio-based and bioinspired compatibilizers for composites

In the two previous subchapters it was discussed that nature uses proteins for the interface stabilization. Afterwards the conventional compatibilizers were considered, where completely different types of compounds are employed as compatibilizers. This subchapter will be dedicated to the latest scientific publications where researchers tried to utilize the more advanced compatibilizers derived from biosources. This class of compounds could be considered as an intermediate stage between conventional and compatibilizers of biomaterials. Compounds will fall into the category of bio-based in case if they are derived from renewable sources such as soy, lignin etc. In contrast, bioinspired compatibilizers can be considered as such, if they utilize principles of architecture from biomaterials, which can be also realized on the basis of synthetic components.

In the last years, many efforts have been made for the development of bio-based composites allowing full degradation in the soil. Alongside utilization of bio-based filler and application of biocompatible and degradable polymers, there were attempts to find a way to compatibilize the interface between two components by means of bio-based or bioinspired compatibilizers.

The following substances of different nature were proposed for use as coupling agent or comaptibilizers. Asolectin from soybeans (mixture of natural polyunsaturated phospholipids) was applied to cellulose-based composites to compatibilize hydrophilic filler and hydrophobic polymer matrix and allowed improvement of elastic modulus. [65] Oxidized wax was used as a compatibilizer for nano silica clay and low density polyethylene composites and lead to improved elastic modulus values and decreased tensile strength.[66] Lignin, containing both polar hydroxyl groups and non-polar hydrocarbon and benzene rings, was applied to compatibilze coconut fiber-polypropylene composites leading to improved flexural strength and decreased tensile properties.[67]

Amino acids and proteins also have found their application in this research area. Conventional compatibilizers were modified with the amino acids, attempting to make them biocompatible. Lysin-based diisocyanate acted as compatibilizer for bamboo fibers for two different polymer matrixes leading to slight simultaneous improvements of elastic modulus, tensile strength and toughness.[68] Study of mussel adhesives inspired researchers to use dopamine (3,4-dihydroxy-L-phenylalanine) as a compatibilizer for hemp poly- L-(lactic-acid) (PLLA) composite. This allowed slight improvements to elastic modulus, strength and toughness.[69] Clay was modified with dopamine and incorporated into polypropelene (PP) leading to enhanced UV resistance and mechanical performance.[70] Soy proteins performed the role of compatibilizer for PP composites reinforced with lignocellulose allowing an improvement to elastic modulus only.[71]

Above described approaches for interface modification obviously have some similarities with the strategy applied within this study as they also utilize proteins, separate amino acids or complex mixtures of biopolymers. The most significant difference in comparison to the peptide-polymer conjugates is that selected compatibilizers are mostly non-specific for the given filler surface in comparison to our proposed concept. The interaction of bespoke compatibilizer seems to be based on the presence of certain functional groups suitable to the interaction with the filler making them more comparable with silans.

2.1.4. Stiffness and toughness in biomaterials and conventional composites

As described in the previous chapter, interface management in conventional composites realized through compatibilazers allows to improve toughness but not necessarily stiffness. This represents often an undesired effect. New concept of bioinspired compatibilization may help to address this issue. Therefore this section will provide an overview about the relation between stiffness and toughness in conventional composites and biomaterials.

Unfortunately, although these properties may seem to many to be similar, changes in material structure often affect the stiffness and toughness in very different ways. Microstructures which restrict plasticity (or more generally inelasticity) will display high

strength properties, but this again can lead to lower toughness by minimizing the local relief of high stresses. Indeed, although there are exceptions, toughness is usually inversely proportional to strength, such that the design of strong and tough materials is inevitably a compromise. [72]

Since structural materials are often used in applications where catastrophic fracture is not an option, such as critical medical implants, nuclear containment vessels, aircraft jet engines, gas pipelines, it can be argued that the property of toughness is far more important than strength.[13] There is a demand for materials with optimal combination of strength and toughness.

Whereas engineers and material scientist are looking for strategies to find an optimum between these properties, there are biomaterials known, where nature has already provided a way for the optimization of mutually exclusive properties. Nature can create composite structures that are hierarchically organized at the nano, micro and meso levels to achieve orders of magnitude increases in strength and toughness compared to their constituent phases.[28] (**Fig. 4)** From a fracture-mechanics perspective, it is clear that most of these biological materials derive their fracture resistance through the presence of a series of extrinsic toughening mechanisms acting at various length-scales. [1, 2] Again considering example of nacre, aragonite platelets provide strength, while inter-lamellar shear in the proteinos layers provide sufficient inelastic deformation to permit redistribution of stress and ensuring toughness. The prominent multi-scale toughening mechanism in nacre occurs via viscoplatic energy dissipation within biopolymer layers, where the tables are able to slip over one another. Suggested concepts include an organic layer acting as a glue involving breaking of sacrificial bonds in the biopolymer at the molecular level, [11] the breaking of aragonite minerals bridges that are located between the mineral layers [73] and the surface roughness of platelets by itself hindering inelastic shearing.[74] Recently natural principles of design were utilized for the development of complex lamellar composites consisting of ceramic lamellae and separated by lubricating polymeric layers leading to composites with high stiffness and toughness.[3] This provides a good example that following natural principles of design may offer a way out of stiffness and toughness dilemma.

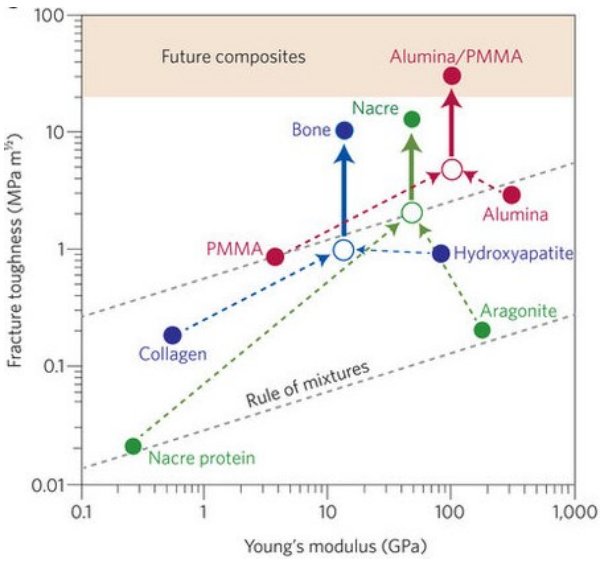

Fig. 4. Ashby plot for selected natural materials like nacre and bone and synthetic material (alumina/PMMA) designed by mimicking the architecture of nacre. Plot represents mechanical properties of the constituents and compares it with the properties of final materials emphasizing the role of architecture of these materials. Dashed lines represent properties of materials as they would be homogeneous mixtures of the constituents. Graph was adapted from reference [2].

2.2. Peptides for material science applications

The previous chapters were dedicated to various options of interface compatibilization employing different classes of compounds for this purpose. Irrespective of the type of compatibilizer, they have to bind efficiently enough to the surface to fulfill its function. This chapter is dedicated solely to the peptides and their interaction with inorganic surfaces with the special focus on the material science applications. The binding of conventional compatibilizers relay on the presence of interaction groups, while sophisticated proteins in natural materials are able to recognize the surface. Peptides are also able to recognize different surfaces and various aspects of recognition phenomenon will be discussed in this chapter. This phenomenon is of high relevance as the concept of bioinspired compatibilization relay on the ability of peptides to recognize certain inorganic surfaces. The aim is to show the versatile abilities of peptides and corresponding application and state of the knowledge about this phenomenon. At first, overview will be given about the inorganic surfaces and binding peptides and developed biotechnological methods for peptide identification. Ability of peptide to recognize inorganic surfaces and to bind to it created a branch in nanotechnology called “bioinspired nanotechnology”, which uses this unique ability very successfully for bioinspired synthesis of nanoobjects. At last, focus will be shifted to the nature of this recognition and interaction with the surface.

2.2.1. Peptides as specific binders to inorganic surfaces

In the previous chapters it was discussed that nature uses proteins frequently in biomaterials for interface management. Nature has developed certain proteins to specifically fulfill their functions. In order to do so proteins are able to recognize certain inorganic surface and adhere to it. Proteins and peptides are closely associated with biomaterials in nature contributing significantly to material properties through involvement of proteins in sophisticated architectures. They also evolved to play a key role in the nucleation, growth and organization of nanostructured biocomposite material.[75] It is realized via specific, non-covalent interactions with the aqueous material interface. Over the course of the years, researches have tried to make use of their natural abilities of proteins and peptides in recognition of surface. One obvious way was identification of material binding peptides from many known examples of inorganic binding proteins found in nature. Some of such examples were repeating peptides from sillaffin proteins for silica formation[75, 76] and peptides mimicking protein from magnetotactic bacteria in controlling morphology and size of magnetite nanoparticles.[77] An alternative to using biologically derived peptides is the use of combinatorial peptide libraries for material specific peptide selection.[78] Combinatorial based peptide libraries are constructed from display peptides on bacteriophages or cell surfaces. They are constructed to select sequences for a specific target from a larger population of peptides.[79] Phage display technology is based on the construction of a polypeptide library fused to a bacteriophage coat protein. Filamentous bacteriophages consist of a genome of circular single-stranded DNA (ssDNA) and a flexible rod-shaped cylinder, which is composed of five coat proteins. All the coat proteins can be used for display. Random peptide libraries are the most common type of phage display libraries and they code up to 10^9 peptide sequences. The phage selection procedure, also referred as biopanning, is based on affinity selection, which is a characteristic aspect of the phage display technology that selects for ligands against any target. A selection cycle basically contains four stages: (i) incubation of target molecules with a phage display library, (ii) washing off unbound phage, (iii) elution of the bound phage, and (iv) amplification of the eluted phage (**Fig. 5**). Three to four rounds of selections are generally carried out in a biopanning experiment. Phage eluted in the final step can be used to infect a suitable bacterial host, from which the phagemids can be collected and the relevant DNA sequence excised and sequenced to identify the relevant, interacting peptides.[80]

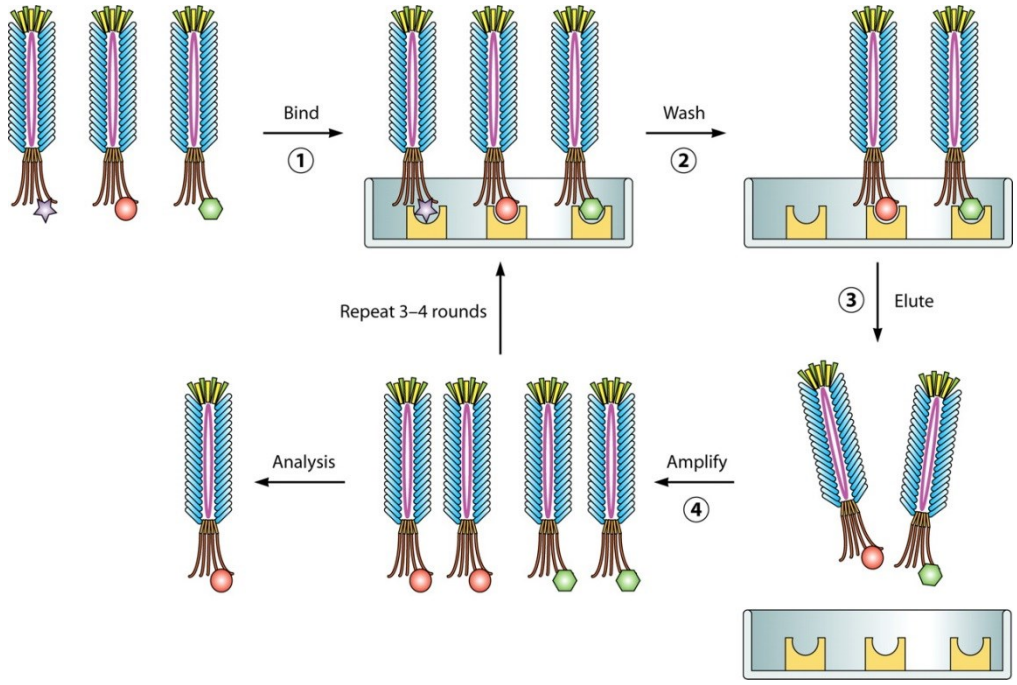

Fig. 5. Schematic representation of selection of peptides for the specific targets through phage display libraries. 1. Target surface is incubated with the phage library 2. Washing away of unbound phages 3. Elution of bound phage 4. Amplification of eluted phages. As a final step, DNA is extracted from selected phage and send for sequencing to obtain a peptide sequence. Figure was adapted from reference [80].

From large peptide libraries, first peptides were identified that were able to recognize gold surface.[81] This field grew rapidly and material binding peptides were identified for a big range of surfaces. Specifically binding peptides were identified first for metals Ti [82] , Ag[83]. Afterwards, the circle was expanded to oxides SiO_2 [84], ZnO [85] and Cu_2O [86]. Later, more complex structures were targeted such as zeolites, [87] indium nitride semiconductor surface[88], hydroxyapatite [89] and carbon structures such as nanotubes [90], a graphene [91]. Further studies found peptide binding not only to inorganic surfaces but also to organic substrates like polystyrene [89], cellulose [92] and others [19].

2.2.2. Peptides for synthesis and stabilization of nanoparticles

Identification of peptide sequences binding to a certain target is only the first step, but a very important one, on the way to the utilization of this peptide (protein) property to applications. This chapter will present examples of peptides adsorption on the different surfaces and application resulting from this ability of peptides. First, this phenomenon was explored and tested on single amino acids. [93] The effect of single amino acids was explored on the behavior of nanoparticles and it was possible to achieve stabilization and guided

assembly of nanoparticles [94] and nanorods of Au.[95] Then, not only single amino acids but peptides were employed for prevention of aggregation.[96, 97] (**Fig. 6)** Protecting clusters as a coating consisting of peptides were realized around Au nanoparticles.[98][99] Additionally, self-assembly of peptides became a common tool to assemble nanoparticles.[100] The response of peptides to changes in pH lead to different state of aggregation of Ag nanoparticles [101] and gave the opportunity to obtain differently shaped structures. [102][103][104] Additionally, self-assembled peptides systems were used as a templates to obtain different nanoparticles structures with enhanced properties, as for example Pd-networks for catalytic applications.[105] Helical nanoparticle structures, obtained on the basis of peptide helical structures, showed tunable plasmonic circular dichroism properties (**Fig. 7).** [106, 107] Uniform interparticle spacing was achieved through a unique design of peptide-structures.[108] Introduction of polymer and its conjugation with the peptide brings additional functionality to the final system. Conjugated peptides systems in the form of peptide-polymer conjugates were explored and utilized for different material science applications too such as functionalization of Gd_2O_3 nanoparticles, crystallization modifiers, stabilizer of nanoparticles[14][109][110][24]

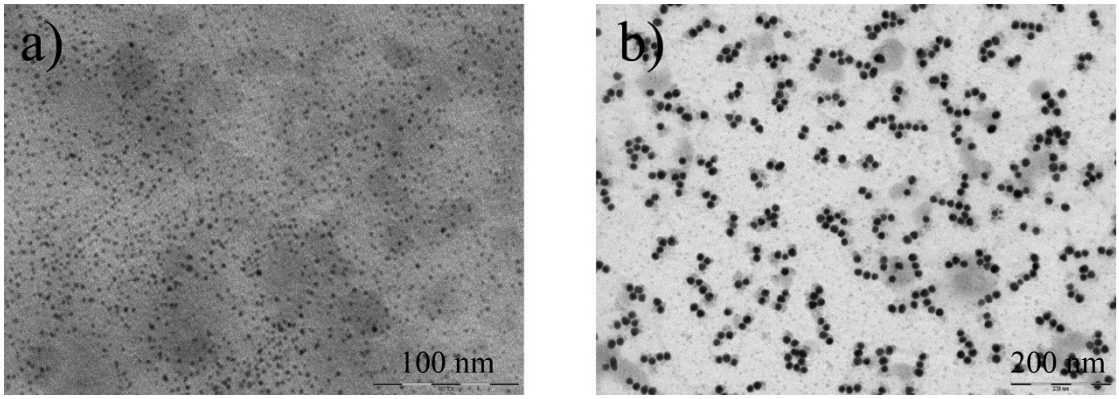

Fig. 6. TEM images of gold nanoparticles stabilized by peptide (GCGGCGGKGGCGGCG). (a) 2.5 nm Au nanoparticles (b) 15 nm Au nanoparticle. Particles of different sizes can be stabilized by peptides via their adhesion on the surface. As a result of that, aggregation of nanoparticles can be prevented. Picture was adapted from reference. [97]

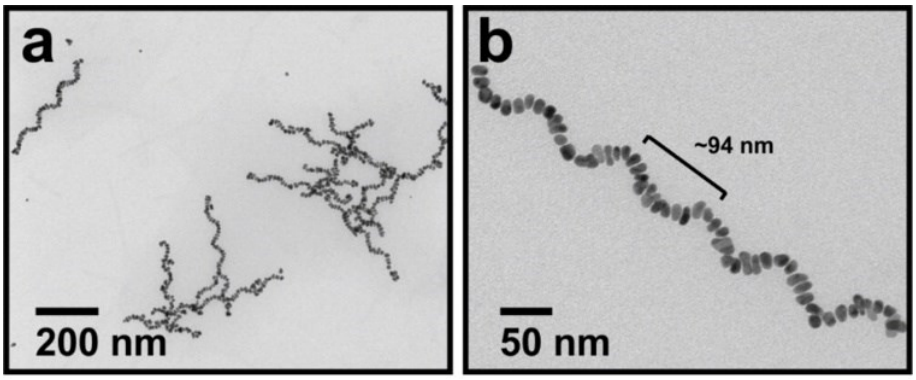

Fig. 7. TEM pictures of gold nanoparticles-assemblies formed by peptides. Tailored peptide-based conjugates can direct the assembly of nanoparticles. Gold-binding peptide conjugate molecules, R-PEPAu (R = organic tail; PEPAu = AYSSGAPPMPPF bind to gold nanoparticle surfaces during particle synthesis directing particle assembly. (a, b) TEM images of single-helical gold nanoparticle superstructures after 15 h of reaction and (c) negative-stained TEM image after 30 min of reaction with measured pitch of the helix. Figure was adapted from reference [107]

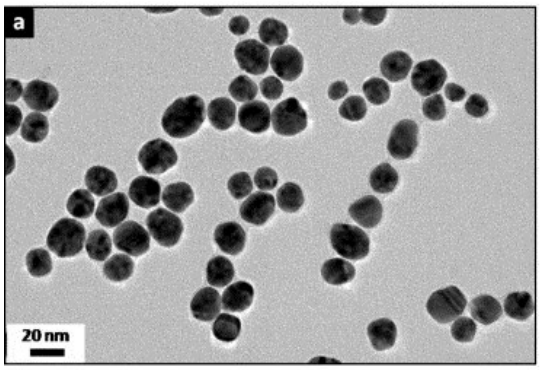

Fig. 8. TEM picture of gold nanoparticles. Monodisperse spherical gold nanoparticles were formed after 3 days incubation at room temperature with 0.5 mM $HAuCl_4$ with the dodecapeptide TGTSVLIATPYV. Picture was adapted from reference [111].

One of areas, which should be mentioned, where peptide sequences found its application, is peptide-guided synthesis of nanomaterials, allowing control of sizes and shapes. Shape and size-tunable synthesis was realized for Au nanostructures with peptides[112] (**Fig. 8**), where the physicochemical properties were tuned using different peptide sequences. [113] Then it was extended to other inorganic particles such as Ag [114, 115], Pd [116] One-dimensional Pt nanostructures with controllable morphologies were obtained with short peptides,[117] including ultra small Pt crystals.[21, 118] Directed nanocrystal assembly was realized also for semiconductors.[119] Nanocrystals of metal oxides such as TiO_2 were obtained following the same methodology.[120] Some other fascinating abilities of peptides were explored such as differentiation between crystallographic surface orientation of the same material.[121] Many of the above described examples of synthesis of nanoparticles were driven by catalytic applications and later studies showed that peptides can even control activity of nanoparticles in catalytic reactions. [122]

2.2.3. Peptide-nanoparticle interactions

The ability of proteins and peptides to recognize surfaces was utilized in many applications, but there is little knowledge available about the relationship between a primary peptide sequence and their ability to bind and functionalize at the nanostructured interfaces. Some aspects of this topic are covered within this thesis on the example of one sequence. In this chapter the current knowledge available to this topic is presented to give an overview about different aspects of this complex topic.

The structure of biomolecules at the interfaces and understanding the nature of interaction still remains challenging, although some significant steps were made towards the understanding this type of interactions.[123] This knowledge would allow more rational design of biomolecules allowing more control over production, functionalization and modification of nanomaterials.[124] This lack of understanding is becoming very distinct by comparing the qualities and structures of laboratory grown inorganic materials with equivalent biomaterials produced in nature. Marine organisms are able to synthesize and to control the mineralization of highly oriented calcium carbonate crystal with defined geometries, while laboratory grown nanoparticles exhibit random geometries and orientations and do not have the same physical properties. The complexity of the interface develops from having peptides and biomolecules with various conformations, structures, chemistries, polarities, chiralities, electrostatic charges and binding affinities. It combines with diverse nanocrystal surfaces, which have different facets, oxidation states, surface charges, crystallographic orientation and defects.[125] Each of these properties has been shown to effect binding.[126] Multistep adsorption was proposed with formation of multilayers, in which the prevailing interactions (electrostatic, hydrophobic, hydrogen bonding) and their relative contribution to binding event are governed by the identity of peptide itself, substrate surface functionality, peptide bulk concentration and pH of solution.[84]

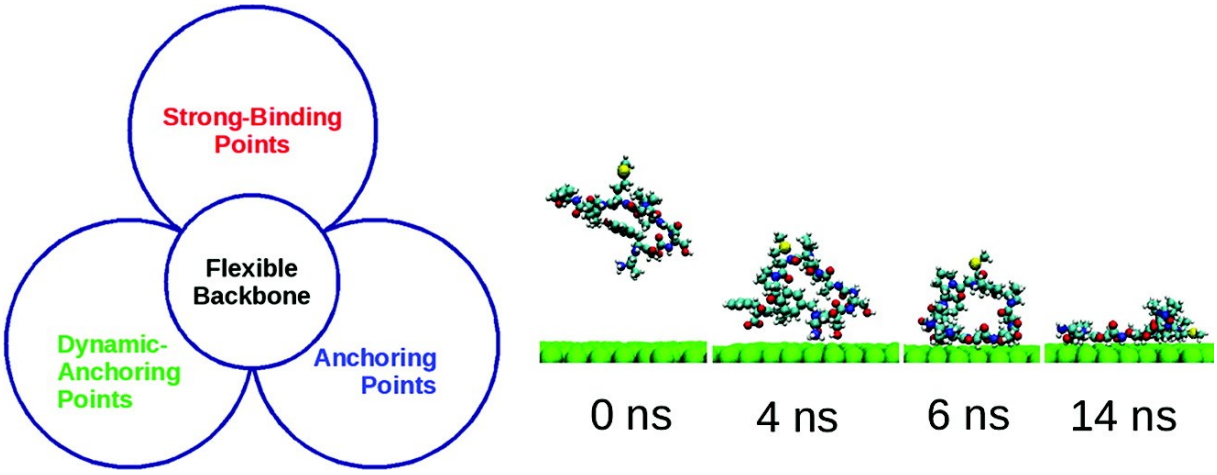

Fig. 9. Molecular dynamics study of the binding process of peptide AYSSGAPPMPPF onto gold surfaces. The binding process can be separated into the following steps: diffusion, anchoring, crawling and binding. Figure is adapted from reference[127].

Computer simulations provided a significant contribution for the understanding of the interactions at the interfaces. A multistep mechanism was proposed for the binding process, where certain amino acid residues seem to play a specific role in either ensuring anchoring or binding or providing flexibility to the backbone (**Fig. 9).** [127] It was attempted to differentiate between binding peptides considering enthalpic and entropic factors as a main driving forces.[128] The role of sequence and conformation, interpeptide forces and the role of water were also addressed in simulations,[129, 130] followed by the contribution of different forces for adsorption of different peptides.[131]

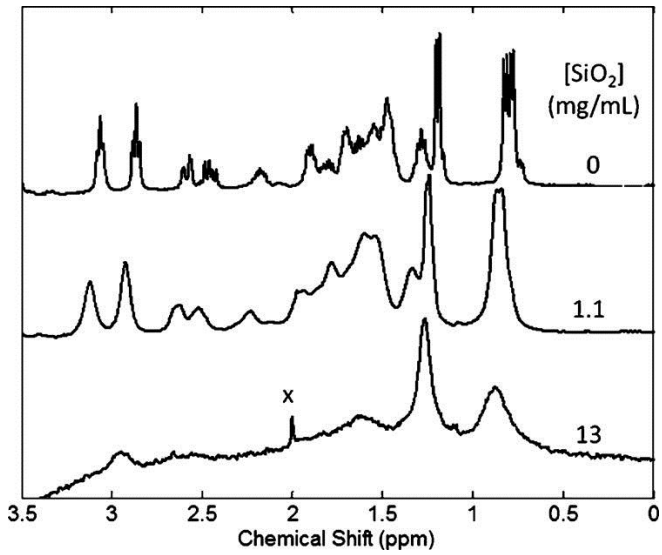

Fig. 10. The effect of 14 nm silica nanoparticles on the proton NMR spectrum of the peptide RKLPDA. In the absence of nanoparticles, sharp lines are observed for the peptide. The lines slightly broaden and shift as the nanoparticle concentration is increased to 1 mg/mL and are greatly broadened at higher (13 mg/mL) nanoparticle concentrations. The line broadening is a consequence of the change in proton chemical shift for the peptide upon binding to the nanoparticle. The figure was adapted from the reference [132]

Circular Dichroism (CD) and Infrared (IR)-spectroscopies can mainly deliver proof of interaction and allow following the changes in the secondary structures of peptides upon a binding event. Monitoring of Amide I and Amide A bands in IR spectra, studied using examples of peptides bound to differently sized nanoparticles of Au, lead to the observation that both bands shift upon binding and curvature of differently sized nanoparticles impact peptide conformation.[133] Curvature depended β-sheet structure was also confirmed for amyloid derived peptides on the Au nanoparticles.[134] Changes of conformation upon binding were also characterized for graphene substrate from α-helix in the powder form to a complex reticular structure.[135] Changes in the structure of peptides upon binding were also proven by CD on several examples. [136-138]

Nuclear magnetic resonance spectroscopy (NMR-spectroscopy) can provide more insight in the structure at the interface and the role of single amino acids in the interaction. Recent studies with high resolution solution NMR showed that solution NMR can be used for structure determination at the interface for short peptides bound to different types of nanoparticles. First, NMR experiments with SiO_2, TiO_2 particles showed changes in the spectra of peptides in the presence of nanoparticles. Lines are broaden and shift in the presence of smaller amount of nanoparticles, which is a typical behavior for peptides in the fast exchange regime. Broader lines are observed for peptides with significantly higher amount of nanoparticles, because the peptide is fully bound and slowly tumbling in the solution (**Fig. 10).** More detailed insight with saturation transfer difference (STD) technique revealed that interactions with NP surface occur predominantly as a consequence of side chain interactions with the surface.[132] Some NMR studies employing standard 2D techniques were realized for Zn and ZnO binding peptides. Histidine (His) with its imidazole ring and glutamic acid with carboxyl O were involved in the interaction with Zn shown on the example of one peptide.[139] A set of ZnO binding peptides identified through phage display were analyzed. The authors concluded that the charge state of peptides play a major role for ionic interactions, although polar interactions of nonionic amino acid residues play an important role in the binding driven in this case by His and Serine.[85]

3. Results and discussion

3.1. Peptide-PEG conjugates as compatibilizers for composites

3.1.1. Composite development

The concept of bioinspired compatibilizers was tested in the present study on a model system, consisting of nanometer-sized MgF_2 particles, poly(ethylene oxide) matrix and compatibilizer. The biologically inspired peptide-PEG compatibilizer combined a peptide segment for sequence-specific adsorption onto MgF_2 nanoparticle surface and a PEG block to improve blending into the PEO matrix.

Magnesium fluoride proved to have interesting properties, which make this material suitable for various applications. It has a very low water solubility 0.16 g L^{-1} and it is non-toxic [140]. Low water solubility provides a long term stability under expose to water, which ensures very slow and continuous release of magnesium and fluorine ions. Both ions are known for their biological activity. These two properties make magnesium fluoride useful for potential applications in the biomedical area. [141, 142] Magnesium fluoride has also a very low refractive index n=1.38 and shows high transparency within a broad spectral window that it is often used in antireflective coatings [26]. These set of properties of this material makes it a good candidate for various applications. Due to that it was selected for the model system. This work is dedicated to the test of the concept and the inorganic components were selected in a way that composites for various applications can be created on its basis.

Magnesium fluoride used for preparation of the composites was obtained in a form of nanoparticles present in an optically clear sol form. Nanoparticles were obtained through sol-gel synthesis route developed in the group of Prof. Kemnitz at the Humboldt University [25]. More detailed information is provided in the experimental part of the thesis. Synthesis of nanoparticles in performed in methanol and in this medium sol remains stable. Addition of water causes irreversible gelation and formation of xerogel. The obtained nanoparticles evidence pores and high specific surface area of 390 m^2g^{-1}. [24] Magnesium fluoride crystallizes in the rutile structure and is in the dimensions of 5 nm. [25]

Polyethylene oxide with M = 900 000 g/mol was selected as a matrix component. PEO matrix material is known to have reduced interactions with peptides or proteins as PEO coatings show anti-fouling character. Thus, it can be expected that the peptide–MgF_2 interactions might not be dramatically perturbed by nonspecific peptide–matrix interactions. Due to these reason, PEO was a good candidate as a matrix polymer especially as this work aims mainly for the prove of the concept of bioinspired compatibilization, and it was important to ensure that polymer matrix will not disturb peptide – nanoparticle interactions.

The bioinspired compatibilizer consists out of peptide segment (13 amino acids residues in length) and PEG-block with the molecular weight of Mn = 3200 g/mol. The

utilized peptide-PEG compatibilizer was based on a recently described stabilizer for MgF_2 sol nanoparticles. The peptide sequence Thr-Gln-Tyr-Tyr-Ala-Tyr-Ser-Thr-Thr-Gln-Lys-Ser (TQYYAYSTTQKS) had been identified previously by phage-display biopanning as sequence that specifically binds onto MgF_2. This sequences was modified to conjugate Ac-GTQYYAYSTTQKS-PEG, which contains in the beginning Gly(G) as a spacer.[24] This sequence will be abbreviated as **pep-I-PEG**. Conjugates were obtained through solid-phase peptide synthesis method described more in detail in the experimental part of the thesis. Short PEG block makes the conjugates well water soluble. Also PEG block of conjugate would allow better blending into the PEO matrix.

The preparation procedure of the composites consisted of two steps: solution casting and hot pressing (**Fig. 11**)**.** An appropriate amount of the peptide-polymer conjugate was dissolved in methanol, after which a corresponding amount of MgF_2 sol was added. The mixture was stirred for a minimum of 4 hours to allow the conjugate to adhere to the inorganic surface. A 5 wt% aqueous solution of PEO (900 kg mol^{-1}) was added. The mixed solution was cast into a small bowl and the material was dried under an extraction hood for 12 hours. The material that was obtained after the solution casting step was not suitable for the mechanical testing experiments, which require even and homogeneously thick composites. A hot pressing procedure was applied to eliminate unevenness in thickness of composites. Hot pressing of the composite materials was performed on the SPECAC machines from Specac Limited (Orington, UK) at a constant temperature of 70°C. The composites are cooled down in the special cooling device with circulating water. The average thickness of the composite ranges from 80-120 µm. More detailed description of preparation procedure is provided in the experimental section of the thesis.

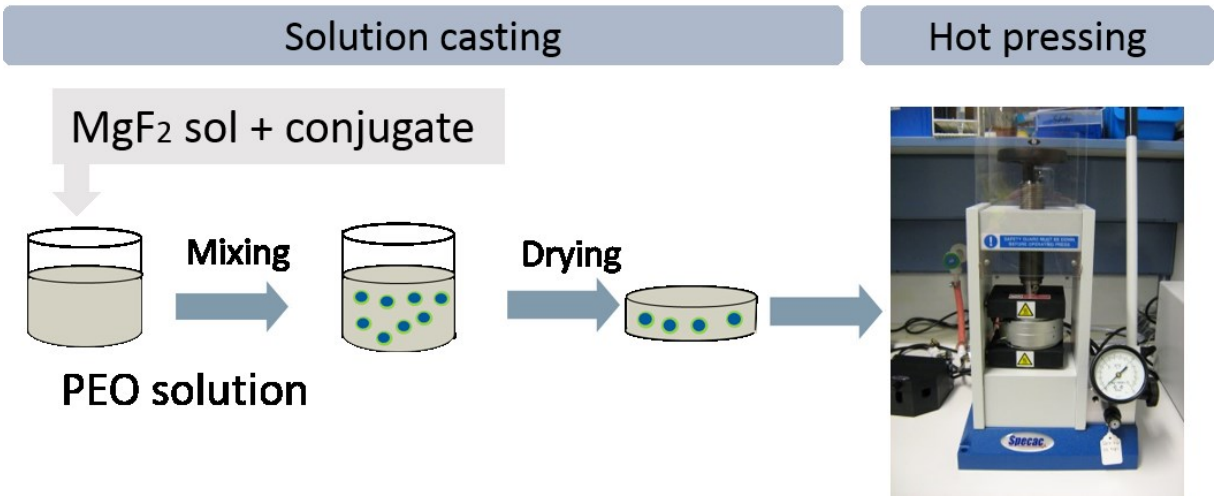

Fig. 11. Preparation procedure for all composites showing solution casting procedure and hot pressing step.

To evaluate a mechanical performance, tensile testing experiments were performed for all composites described in the thesis. Samples in a typical bone form were punched out of pressed composites. Normally 4 bone shaped samples can be made out of one composite. Experiments were performed on the two tensile testing machines: small devices for precise

measurements of small forces and at standard Zwick machine. For the tensile testing experiment, a sample is fixed in the holder of the machine. The sample will be pulled apart with the constant speed, while the needed force and the displacement will be measured. Based on these two experiment parameters, elastic modulus, yield strength and toughness are calculated. More details about mechanical tested are provided in the experimental section of the thesis.

3.1.2. Mechanical properties of composites

3.1.2.1. Impact of MgF_2 nanoparticles on the properties of composites

Tensile testing experiments were performed to assess the influence of nm sized MgF_2 particles on the composite performance; elastic modulus and yield strength were calculated as the main parameters to evaluate the impact of the filler.

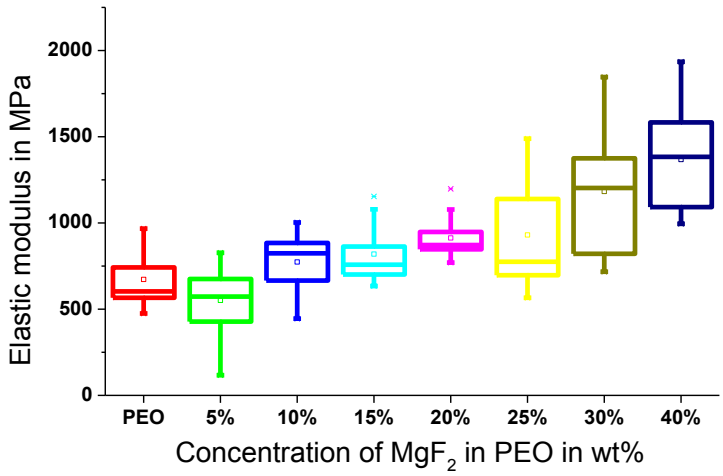

Fig. 12. Elastic modulus of PEO composites with increasing MgF_2 filler content (5-40wt%). Elastic modulus increases with each step of increase of filler concentration.

As **Fig. 12** shows, stepwise addition of the inorganic filler leads to the slow increase of elastic modulus. The change in elastic modulus for the filler content ranging 5-20wt% was 200-300 MPa. Further increase of inorganic filler content causes significant distortion of the polymer matrix evident in a very broad distribution of elastic modulus values. 30-40wt% of filler nearly doubles the values of elastic modulus reaching 1500 MPa compared to neat PEO. Experiments clearly show that the MgF_2 particles can be blended into PEO matrix up to 40 wt%, which is a high filling content. Preparation of the composites with the higher filler content was not possible.

The values of elastic modulus obtained for PEO that are around 600 MPa are in a good agreement with the previously published literature: for PEO with the molecular weight of 1000 000 g/mol elastic modulus of 720 MPa was reported. [143]

On the one hand, the introduction of the filler in the matrix leads to higher stiffness expressed in higher elastic modulus values, but on the other hand experiments clearly indicate that filler makes composites very brittle. The composites became more and more brittle with increased filling content; highly filled composites can be easily broken.

It is well known that particles introduced into the polymer matrix tend to aggregate, especially if it is a nanofiller. The same phenomenon of increasing aggregation was shown for unstabilized composites. This fact would explain big inhomogeneity of elastic modulus values for highly filled composites, where bigger aggregates create significant weak points in the material.

3.1.2.2. Impact of conjugate on the mechanical performance

The optimal concentration of the conjugate will be found in an empirical way on the example of different MgF_2 concentrations: 10wt%, 15wt%, 30wt%. Under the optimal concentration we understand the concentration of conjugate with the best mechanical properties. All experiments were performed with the conjugate **pep-I-PEG**. Changes of elastic modulus will be monitored to discover the optimal concentration of the conjugate for the system. 0.5 mol%, 1mol%, 3 mol%, 5 mol%, 8 mol% conjugate concentrations, calculated in reference to the filler concentration, were selected as a starting set of concentration for test. More increments were introduced on the later stages of experiments in case much smaller amount of conjugates was needed. **Fig. 13 a,c,e** shows, for all filling contents elastic modulus increased with the **pep-I-PEG** addition. Elastic modulus doubles for lower filler content: from 800 MPa for unstabilized composites to 1500-1600 MPa for stabilized ones. For 30wt% filled composites, elastic modulus increases by 1/3: from 1200 MPa to 1600 MPa. In all cases it follows the same trend: the values of elastic modulus increases with the step by step increase of conjugate concentration, reaching its maximum at a certain point and then dropping down to the level of not stabilized composites. It should be noted that the conjugate concentration with maximal values are different depending on the filler content. 3 mol% conjugate concentration appears as the optimal one for 10 and 15 wt% filler content and 0.5 mol% for 30wt% filler content. Higher conjugate concentration is not beneficial for the improvement of elastic modulus values for all filler contents. The difference between different maximum points for different filler content can be potentially explained as a competition between two processes: aggregation of particles and adhesion of conjugates on the surface of nanoparticles. With the increasing MgF_2 content the tendency to the aggregation increases as far as interparticle distances decreases and this process may be faster than the adhesion process. After many particles had formed bigger aggregates, smaller surfaces were offered for conjugate adhesion. This would lead to a smaller amount

of conjugates needed to cover this surface. This idea can be also supported by the fact that the values of elastic modulus for higher filled composites (30wt%) are very similar to the composites with lower filler content (10-15wt%)and are in the range of 1500 MPa.

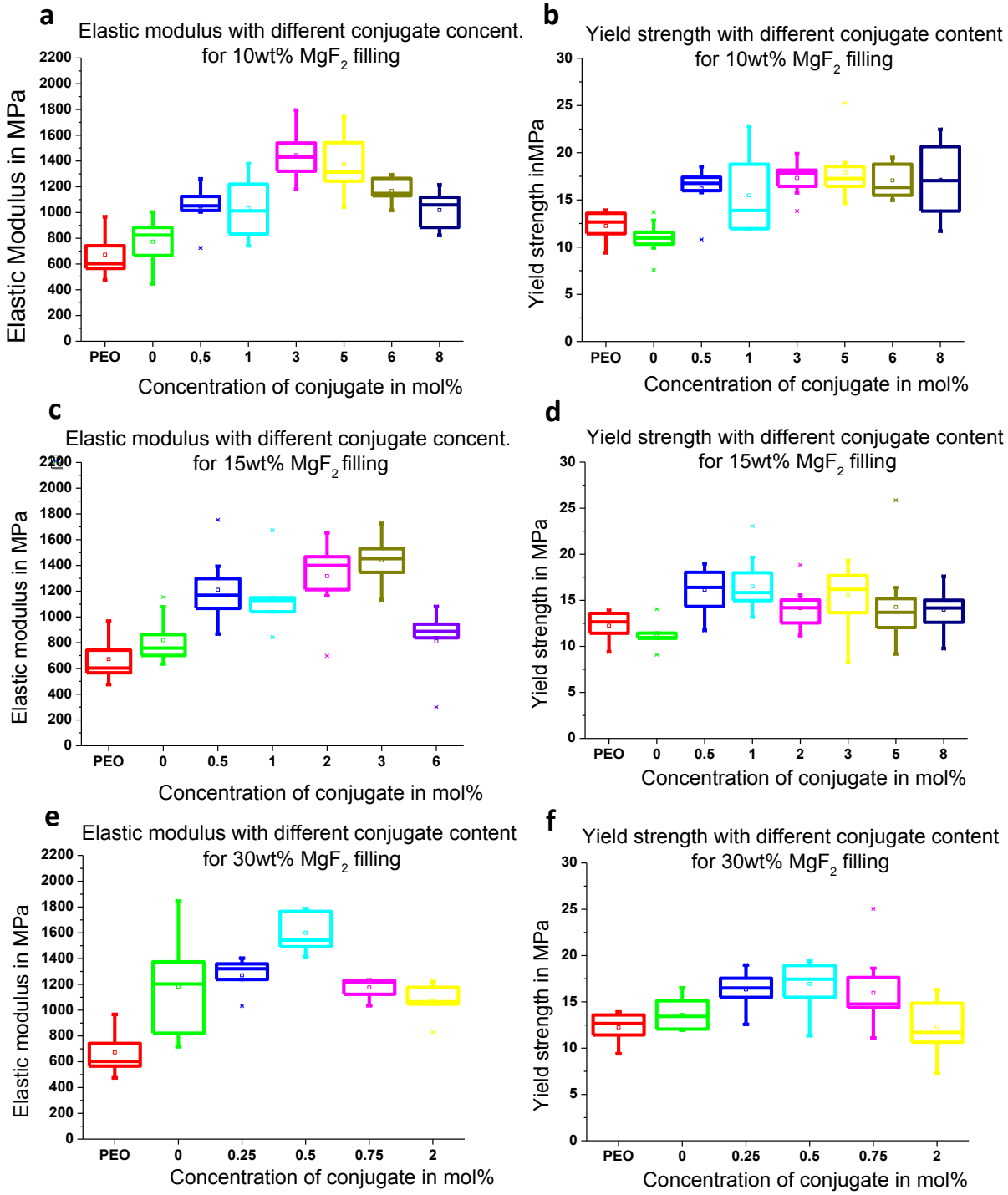

Fig. 13. Elastic modulus and yield strength of composites containing 10wt% (a, b), 15wt% (c,d) and 30wt% (e,f) MgF_2 filler content with various conjugate concentrations (0.5;1,2;3;6;8 mol%). Both properties improve for all filler concentrations and show dependency from conjugate concentration.

The presence of the maximum values can be explained by the effect of surface saturation. After the surface of the particles is covered with the conjugates, they are

expected to be protected by PEO. The next conjugates can not adhere and will stay in the matrix, which has a negative effect of the mechanical performance.

Following the trend of elastic modulus, yield strength values increase with addition of the conjugate for all fillings contents of MgF_2: for 10wt% from 11 MPa to 17 MPa (**Fig. 13 b)**, for 15wt% from 11 MPa to 16 MPa (**Fig. 13d)** , for 30wt% from 12 MPa to 15 MPa (**Fig. 13f)**, meaning that the addition of the conjugate leads to the strengthening of the composites. Opposite to the elastic modulus trend, stepwise increase of the conjugate concentration does not lead to the increase in the yield strength values, the values stay on the same level for 10wt% filler, while slightly decreasing for 15wt% and 30wt%.

The values for yield strength show the efficiency of binding between the filler and the matrix.[144] Considering this fact, the increase of yield strength with conjugate addition indicates that the inorganic component is becoming more efficiently connected to the matrix. Yield strength parameter then could be considered as an indicator for the strength of peptide-nanoparticle interaction. The fact that the yield strength does not depend on the conjugate concentration could be expected because different conjugate concentration does not change the strength of conjugate – particle interaction and the binding of matrix with the filler and its efficiency. Slight decrease of yield strength values indicate that the higher the inorganic content, the more difficult is to provide sufficient binding.

From these experiments optimal concentration of conjugates for further experiments was found and 15wt% filler content will be used for next tests.

Elastic modulus

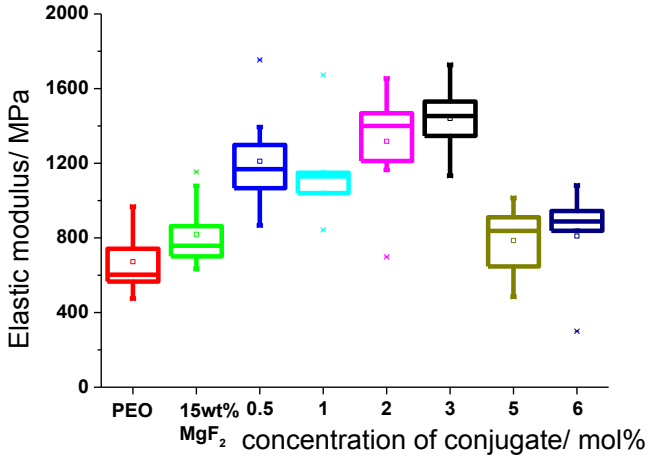

Fig. 14. Elastic modulus for 15wt% MgF_2 filled composites with 0.5;1;2;3;5;6 mol% conjugate addition. Elastic modulus improves with rising conjugate concentration, while excessive concentration (6-8 mol%) does not provide positive effect.

Initial mechanical properties were evaluated on a set of samples, containing PEO, 15 wt% MgF_2 and a range of compatibilizers **pep-I-PEG** from 0.5 to 6 mol%. **Fig. 14** shows the elastic modulus of the composite materials depending on compatibilizer concentration. A remarkable increase of the elastic modulus from 720 MPa for a non-stabilized composite, to

1450 MPa was evident by using 3 mol% of the compatibilizers. Below 3 mol% conjugate insufficient stabilization takes place and upon addition of more than 3 mol% the elastic modulus decreases. Considering that the addition of the 15 *wt.*% of MgF_2 to the PEO matrix only results in a small elastic modulus change from ~600 MPa (pure PEO) to ~720 MPa, the effect of the peptide-PEG compatibilizer is significant. That the changes of elastic modulus are statistically significantly different was proven via t-test with different variances performed in Excel. This test delivers p-values, it should be below 0.05 if the considered values are significantly different. According to the result of this test, changes of elastic modulus of composites containing 0.5; 1; 2;3 mol% conjugate in comparison to the composites without conjugate are significantly different with p-values 0.004; 0.006; 0.0005; $2.1*10^{-6}$ correspondingly.

Tensile toughness

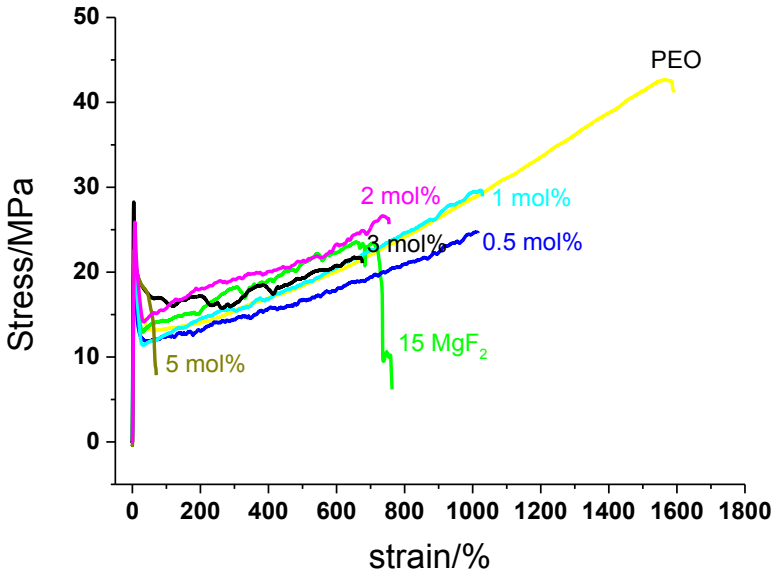

Fig. 15. Representative stress-strain curves for 15wt% MgF_2 filled composites with 0.5; 1;2;3;5; mol% conjugate addition and pure PEO as a reference. Graph indicates increase in tensile toughness for certain conjugate concentration (0.5 and 1 mol%) in comparison to unstabilized composites. Tensile toughness is calculated as integral area under the stress-strain curve.

Table 1. Values for elongation at break and tensile toughness for differently stabilized 15wt% MgF_2 filled composites.

Conjugate concentration in mol% [a]	Elongation at break in %	Tensile toughness in MJ/m^3 [b]
0	730±200	150±60
0.5	900±180	165±40
1	930±160	190±45
2	790±200	160±70
3	690±230	150±50
5	70±40	12±7

a. mol% is calculated in relation to n(MgF_2) b. Tensile toughness is calculated as an area under the stress-strain curve obtained in tensile testing experiments

Besides the positive effect on the elastic modulus of the composites, addition of specific compatibilizers results in a desired increase in tensile toughness**. Fig. 15** and **Table 1** show the stress-strain curves of composites with different compatibilizer concentrations and indicates a maximum increase of the tensile toughness from 150 MJ/m^3 (non-stabilized) to 190 MJ/m^3 in the presence of 1 mol% compatibilizer. The composites evidence higher toughness mainly due to higher elongation at break values. Elongation at break could be improved from 700% strain without compatibilizer to 1000% strain if 0.5-1 mol% is used. The high tensile toughness was evident for composites with 0.5-1 mol% of compatibilizer and with higher amounts of conjugate the toughness decreases to values comparable to those found for unfilled composites. Addition of 5 mol% of conjugate makes the material extremely brittle. The possible reasons and explanations for these observations will be discussed in detail in further chapters.

The simultaneous increase of elastic modulus and tensile toughness in synthetic composites is highly desirable but typically not easily achievable with established compatibilizers. The addition of conjugate leads to the simultaneous improvement of these contradicting properties, emphasizing the effectiveness of the used concept.

3.1.2.3. Comparison of stabilized and non-stabilized composites

Addition of the conjugate pep-I-PEG to the system leads to changes of various properties such as elastic modulus and tensile toughness, where elastic modulus almost tripled. This outperforms the improvement of elastic modulus, which could be achieved with the addition of double amount of inorganic filler. The elastic modulus with 15wt% filling with 3 mol% of conjugate is higher than with 40wt% filler without compatibilization as shown in the (**Fig. 16**).

On one hand addition of the filler brings increasing of elastic modulus and strength of the composites but on the other hand it reduces the ductility of material and makes it finally more brittle. Considering the same example of 40wt% filled composites, stabilized

composites possess not only higher elastic modulus values but show much higher toughness in the same time (**Fig. 16, table**). This comparison emphasizes the advantages of peptide-polymer conjugates application in composites allowing the simultaneous improvement of stiffness and toughness.

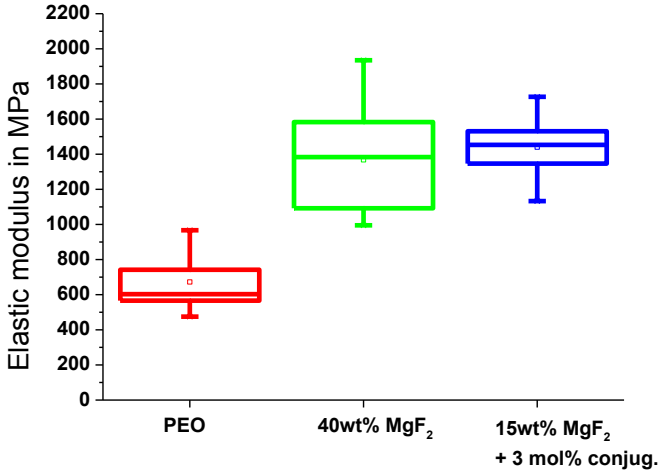

Composite	Toughness in MJ/m^3
40 wt% MgF_2	0.54
15 wt% MgF_2 + 3 mol% con	150

Fig. 16. Comparison of elastic modulus and toughness of stabilized 15wt% MgF_2/3mol% with non-stabilized composites 40wt% MgF_2: graph indicates comparable values of elastic modulus for 40wt% filled non-stabilized composites and 15wt% stabilized composites.

3.1.2.4. Impact of peptide and PEG in conjugate on composite properties

To prove that the improvement of the properties is only possible with specifically binding peptide sequences, two reference experiments were performed. In one experiment the original sequence will be changed and in another one the peptide-PEG conjugate will be replaced by just PEG 3000. Elastic modulus will be monitored as parameter indicating the efficiency of alternative compatibilizers.

In the first experiment, compatibilizer, containing scrambled sequence, was investigated. In the scrambled sequence, peptide segment is composed of the same amino acids residues but in different order. The scrambled compatibilizer **pep-I-PEG*** was not capable to stabilize MgF_2 filler particles and the control composite exhibited an elastic modulus compared to non-compatibilized composites (**Fig. 17**). Removing of conjugate from

the system and leaving just PEG also does not improve mechanical performance (**Fig.17**)**.** This highlights the importance of the presence of the compatibilizer at the inorganic surfaces and makes it likely that the improved elastic modulus is originating from effects involving the interfaces.

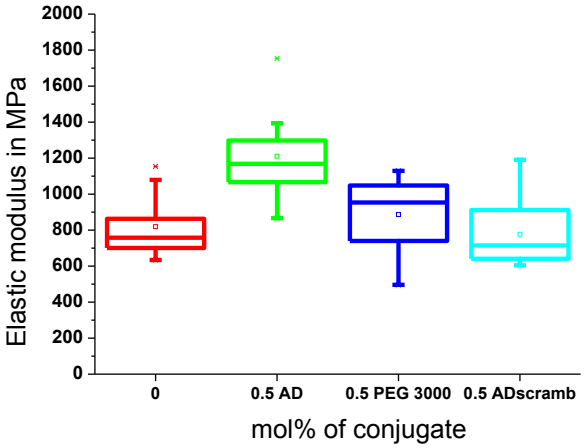

Fig. 17. Elastic modulus of 15wt% MgF_2 filled composites containing 0.5 mol% of original, modified (scrambled) peptide sequence and PEG 3000 instead of peptide. Reference experiments indicating the unique ability of peptide–PEG conjugate act a compatibilizer: changing the peptide sequence keeping the amino acids the same (scrambled sequence) does not allow to improve elastic modulus, PEG 3000 used as a compatibilizer lead to slight increase of elastic modulus. 15 wt% MgF_2 filled composites used as a reference and pep-PEG and PEG were used in 0.5 mol% concentration.

3.1.2.5. Impact of conjugate on the polymer matrix in composites

It became clear from the previous experiments that incorporation of particles alone into the polymer matrix of PEO increases elastic modulus and strength but reduces dramatically toughness. The incorporation of particles together with conjugates allows improving elastic modulus, where experimental data shows that only a certain amount of conjugate is beneficial and excessive amount has a negative effect. To address this issue, the impact on the polymer matrix of the pure conjugate was studied. Tensile testing experiments were performed on the composites, containing no inorganic part but different amounts of conjugate. The amount of used conjugate was identical with the amount used for 15wt% filled composites. These experiment shows that conjugate by itself present in unbound form in the matrix significantly changes the properties of the matrix, where the influence of the conjugate is becoming more pronounced with the increasing concentration (**Fig.18**). Elastic modulus and yield strength of PEO matrix is increasing with the conjugate addition, while toughness is decreasing, which is also expressed in lower elongation at break values. This data together suggests that conjugate act a reinforcing agent. The reinforcement

would be only possible if the filler is introduced into PEO matrix, which has a much higher elastic modulus as matrix itself. It suggest that with higher conjugate concentration one does not deal with peptide-polymer conjugates by itself but with some other conjugate-based structures, as by introduction of conjugate into the polymer matrix softening would be expected. Interestingly to note that 0.5-1 mol% conjugate addition does not significantly impact the polymer matrix, causing just minor changes. Severe changes start from 3 mol% making the material very brittle. This data allows to address the issue of overstabilization and indicates that in case of higher concentration of conjugate (above 3 mol%) in filled composites most probably excess of conjugate is present in the polymer matrix, making the material brittle.

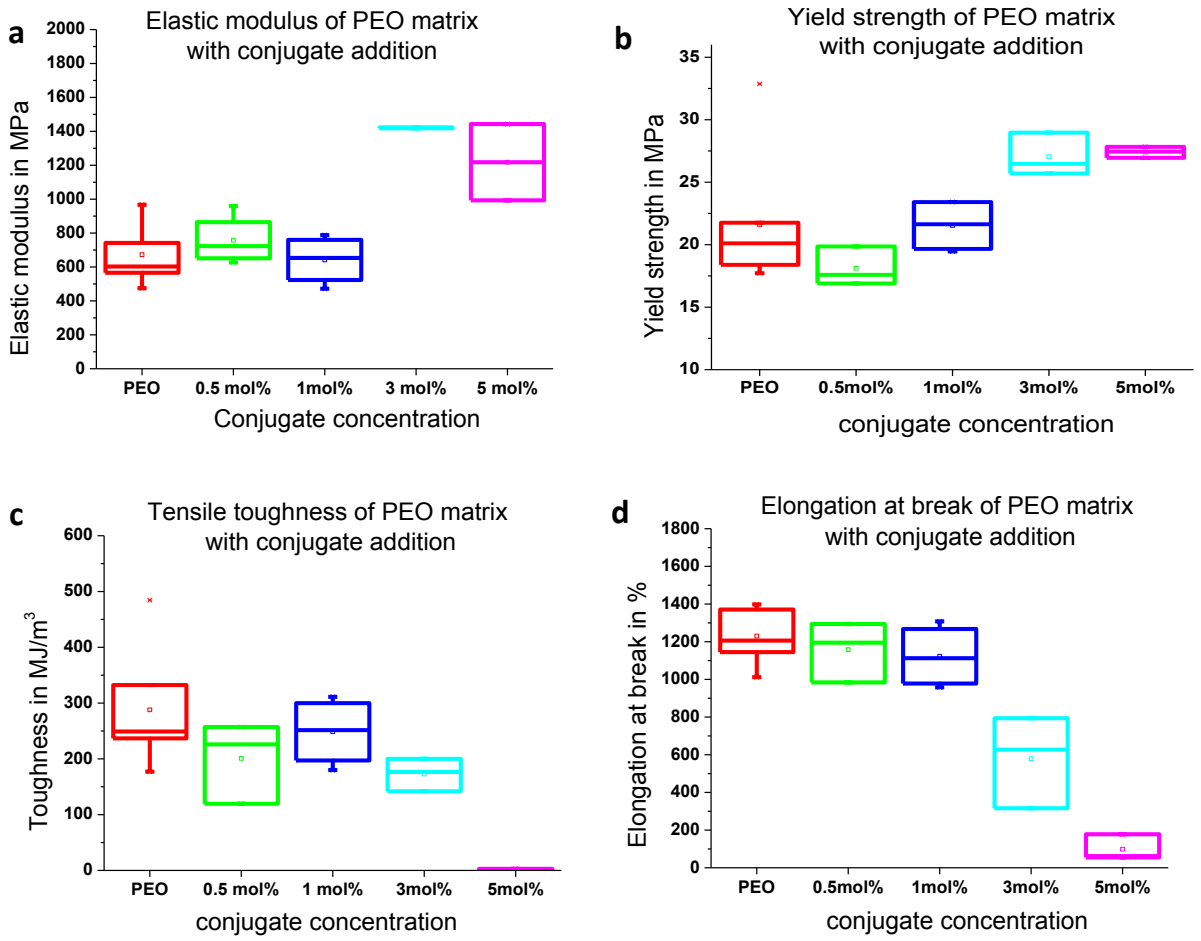

Fig. 18. Changes in the mechanical properties of PEO matrix with the addition of various amounts of pure conjugate, evidencing increase in elastic modulus (a) and yield strength (b) with rising conjugate amount and decrease in tensile toughness (c) with corresponding lower elongation at break values (d).

3.1.3. Internal structure of composites

3.1.3.1 Non-stabilized composites

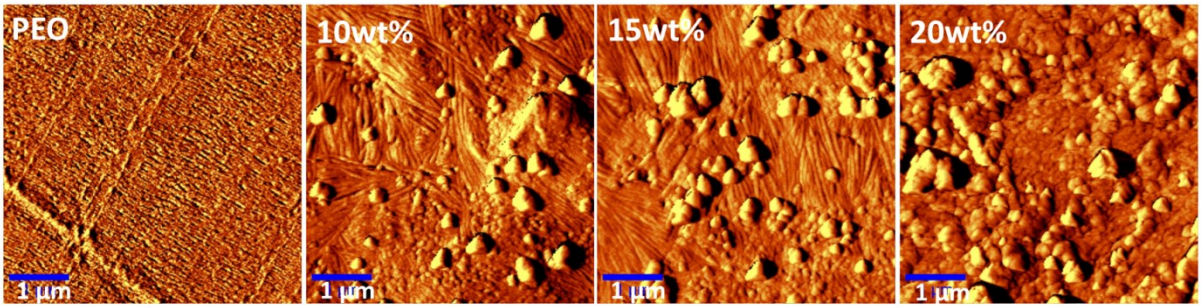

Fig. 19. AFM micrographs (phase micrograph) of composites filled with different amounts of MgF_2 NP (0wt%; 10wt%; 15wt%;20%) showing progression of aggregation of particles with increasing filler content.

Composites with different amount of filler were studied with AFM in order to follow the impact of filler on the polymer matrix (**Fig. 19**). PEO was considered as a reference sample and AFM is able to show lamella structure of PEO. AFM reveals formation of aggregates, which are increasing in size with increasing filler content. The visible aggregates on the micrographs are in submicrometer range and consist of small particles. The higher is the filler content, the more particles build aggregates and consequently are less evenly distributed. These observations are expected as it is a well-known fact that reinforcing of composites with the filler lead to its aggregation, which is especially pronounced for nanofiller.

3.1.3.2. Stabilized composites

High resolution scanning electron microscopy (HR-SEM) study

Samples with 15 wt% MgF_2 filling and different **pep-I-PEG** content (1 mol%, 3 mol% and 6 mol%) were investigated in HR-SEM in back-scattered electron (BSE) mode to evaluate size and distribution of the particles in the composites depending on conjugate concentration. Backscattered electrons were detected in order to distinguish the particles from the matrix. In comparison to the secondary electrons, backscattered electrons are sensitive to the elemental composition. MgF_2 particles will appear as the bright spots in comparison to the matrix. Electron microscopy pictures were done on a Jeol LEO 1550 with acceleration voltage 9 kEV, which was found as the optimal accelerating voltage for these samples. Lower voltage levels did not eject enough backscattered electrons to generate sufficient contrast. As a drawback of the quite high voltage level, samples can be quickly

damaged during measurement leading to visible cracks in micrographs. The samples were sputtered with Pt/Pd before measurement.

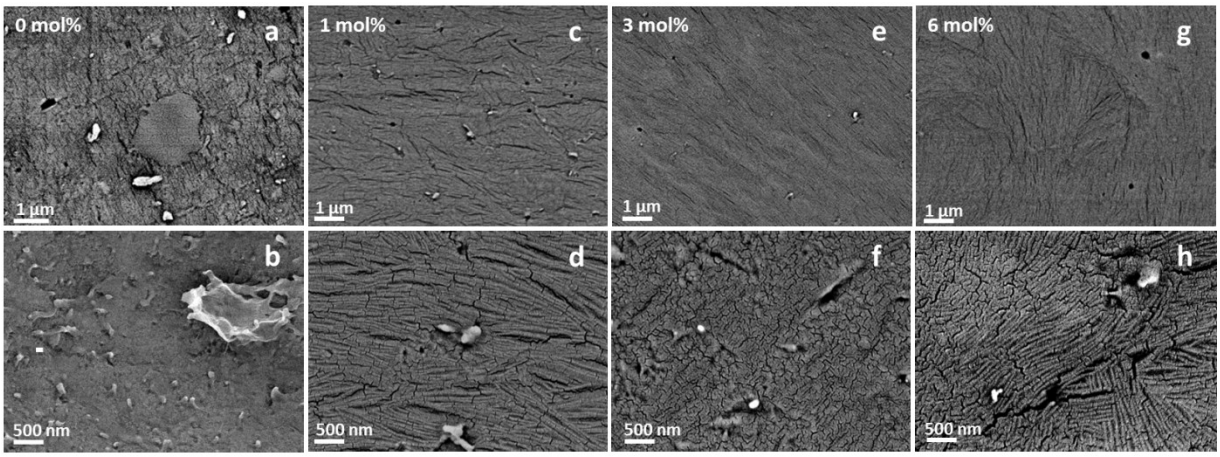

Fig. 20. SEM micrographs obtained in BSE mode of the 15 wt% filled composites with a,b - 0 mol%, c,d – 1 mol%, e,f – 3 mol%, g,h – 6 mol% conjugate indicating suppression of particle aggregation with stepwise increase of conjugate concentration. Electron microscopy pictures were measured on the Jeol LEO 1550 with acceleration voltage 9 keV.

SEM micrographs reveal the transition in the filler sizes depending on the conjugate concentration as represented in the **Fig.20**. MgF_2 particles added to the matrix from the sol with the particle size of 5 nm aggregate severally and cause formation of aggregates in the µm range visible on SEM micrographs (**Fig.20 a,b**). This process is naturally occurring and based on the tendency of very small particles with high surface area and high energy to reduce it by aggregation. Each portion of conjugate added to the system reduces the size of formed aggregates and µm aggregates disappear moving to submicron and nm particles (aggregates)(**Fig.20 c-f**). Particles in the highly stabilized composites can be only found with higher magnification (**Fig.20 g,h**). This study clearly evidences the size transition but it does not provide quantitative information about the sizes of filler in the composites with different conjugate concentration. To eliminate this gap particle-size distribution diagrams were generated based on the scanning electron microscopy study. To obtain particle-size distribution diagrams, the size of randomly selected particles was measured in all samples, keeping the number of measures particles the same per sample. The statistics is built on the basis of 200 randomly selected particles. The size of the particles was measured with Image J program. The procedure of size calculation is described in the experimental section.

Particle-size distribution diagrams (**Fig. 21, Fig.22**) povide more detailed information about the average sizes of particles in composites with different conjugate concentration. It should be noted that this procedure does not consider the particles below 10 - 20 nm due to limits in resolution of the measurement method. Composites without addition of conjugate have a combination of aggregates in various sizes ranging from µm aggregates to nm particles with domination of submicron aggregates of 100-300 nm in sizes. Firstly, addition of 0.5 mol% conjugate prevents only the formation of larger aggregates (larger than 3 µm) keeping nm and submicron aggregates unchanged. Further addition of conjugate leads to

narrower particle-size distribution and in the case of 3 mol% all measured particles are smaller than 1 µm. In case of 6 mol%, larger aggregates disappear and around 80% of the particles are below 100 nm. These observations evidences that addition of conjugate in the systems lead to better stabilization of nanoparticles and a step by step decrease in aggregate sizes in a particular range accessible by this technology. One should note that conjugates cannot stabilize the particles to the full extent and keep them the same as in the sole.

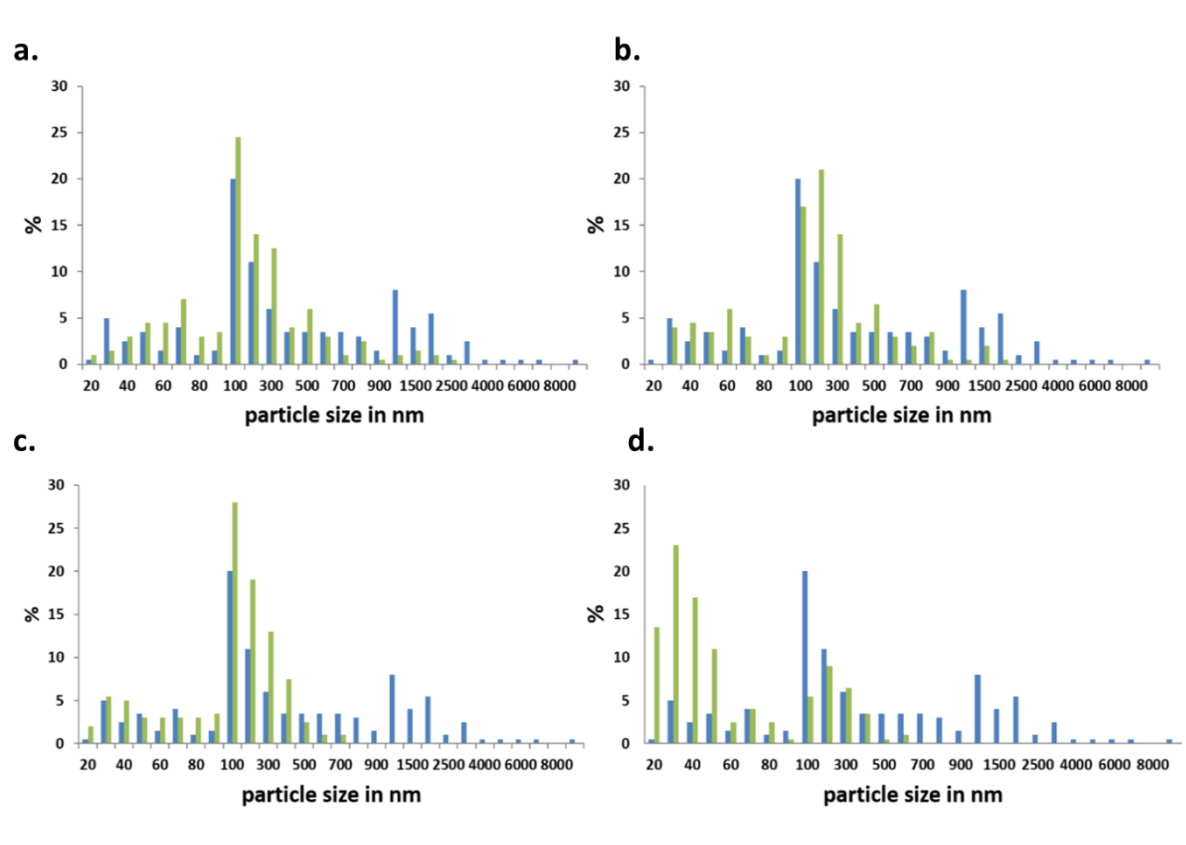

Fig. 21. Particle-size distribution histograms for 15wt% filled composites with different conjugate amount presented in green: 0.5 mol% (a); 1 mol (b); 3mol% (c) ;6 mol% (d). Particle size-distribution for composites without conjugate is taken as reference on all graphs and presented in blue. Diagrams are based on the results of SEM (BSE) study and consider 200 randomly selected particles.

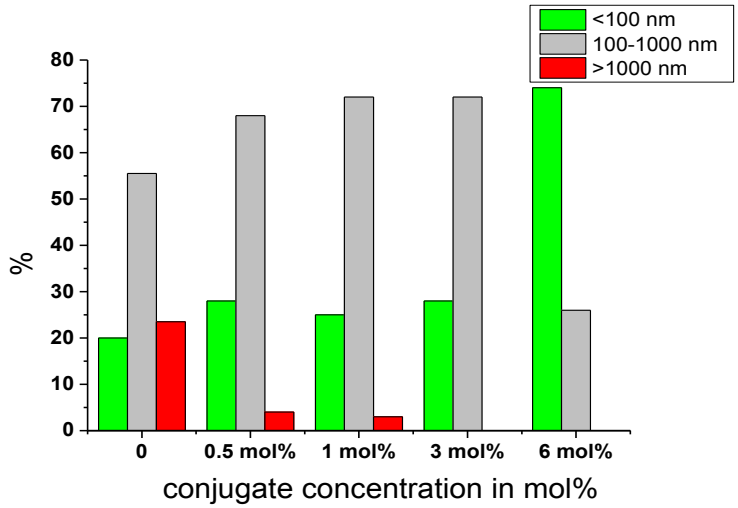

Fig. 22. Particle-size distribution for 15wt MgF_2 filled composites, showing the estimation of distribution between different size of aggregates (≤100 nm, 100-1000 nm, ≥1000 nm) depending on conjugate concentration.

Transmission electron microscopy (TEM) study

TEM was also employed to follow the changes of particle/agglomerate sizes in the different composites. In comparison to the SEM study, TEM micrographs can provide a valuable insight in the form of aggregation and organization of on the nanoscale and allow closer look at the particles below 50 nm. Micrographs are taken in the bright field mode (BF) meaning that heavier elements will appear dark, so MgF_2 particles will look like dark spots. The measurements were taken from the liquid samples. Small amounts of solution prepared for casting were taken for TEM measurements and then further diluted. A couple of drops were placed on the copper grid and dried.

TEM micrographs were taken for 15wt% filled composites with 1,3,6 mol% conjugate (**Fig. 23**). The samples without conjugate evidence severe aggregation, particles assembled randomly together, forming aggregates of 3-4 µm. TEM study confirm results of SEM measurements, evidencing the same dimensions of aggregates. Already addition of 1 mol% conjugate causes significant changes in the aggregation process. Large aggregates above 1 micron are becoming less densely packed. Apart that, the portion of large aggregates is decreasing that most of observed aggregates in TEM are in the range of 200-600 nm. These observations aligning again very well with results obtained out of SEM measurements. Further addition of conjugate – 3 mol% - strengthens this phenomenon, causing aggregates to become even smaller. Aggregates above 1 micron are not visible at the TEM micrographs any more, what again correlates with SEM results. The structure of formed aggregates is more distinct and constituents are becoming clear. The formed aggregates are built from spherical particles around 10 nm in diameter, which are dense packed in higher ordered

structures of ca 100 nm in size. The continuous transition in sizes is observed with the step by step addition of the conjugate: starting from large aggregates to subsequently smaller aggregates and particles. The TEM study suggests the suppression of aggregation of the inorganic MgF_2 particles and indicates more effective dispersion of the particles with increasing amounts of compatibilizers.

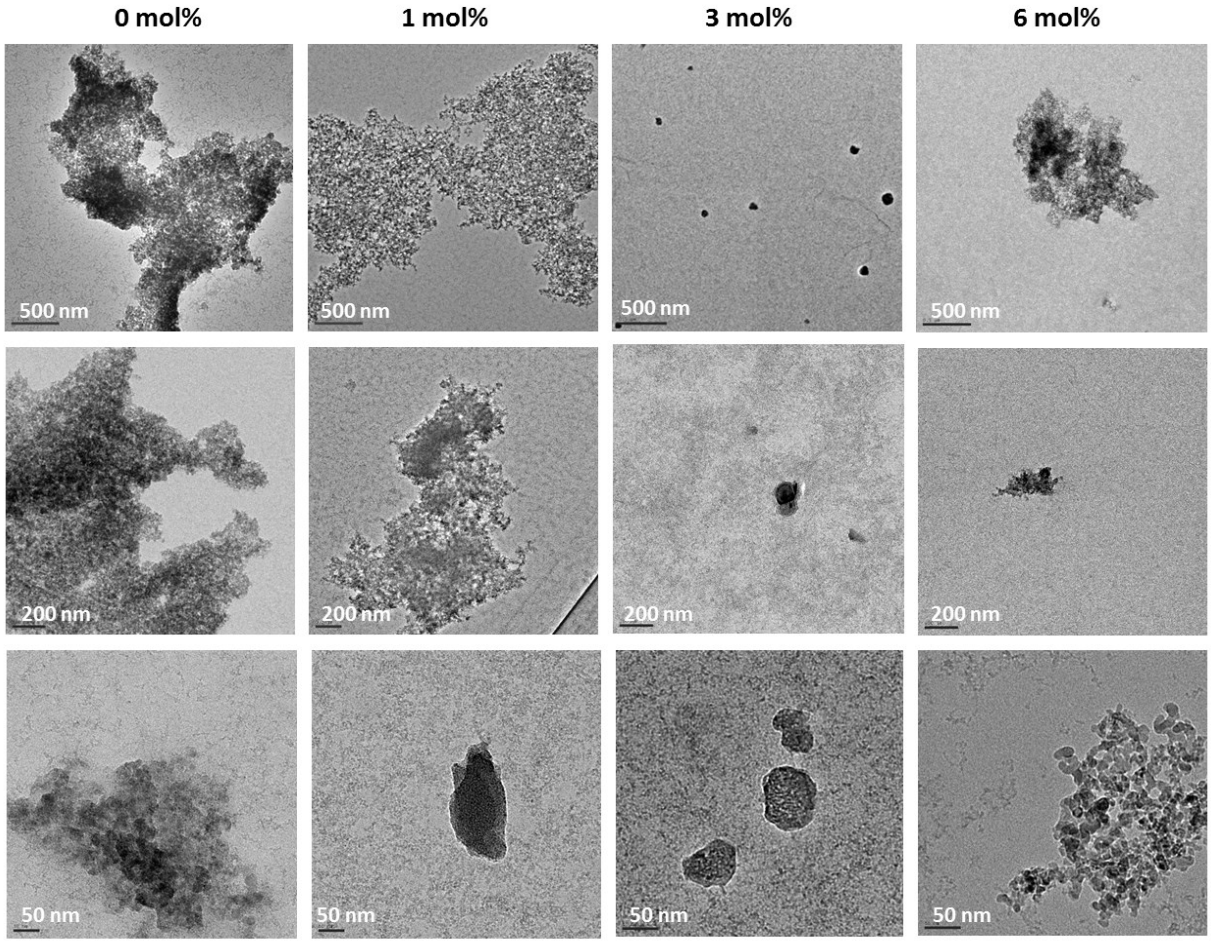

Fig. 23. Representative TEM micrographs measured on 15wt% MgF_2 filled composites with 0;1;3;6 mol% conjugate indicating step by step suppression of aggregation with stepwise addition of conjugate visible from changes of aggregate morphology and form.

It should be noted that suppression of aggregation takes place on the different length scales. Most obviously the aggregation is suppressed on the micrometer length scale. With rising conjugate concentration, the micrometer large aggregates start to disappear. This observation perfectly correlates with the SEM study and obtained particle-size distribution diagrams. The aggregation on the submicron and nanoscale is not significantly influenced by the conjugate, the aggregates just slightly decrease in size. The changes are visible not only in the sizes of particles but also in the form. Aggregates take different shapes depending on the conjugate content. Again this effect is more pronounced on the micrometer length scale. For unstabilized composites large amounts of particles are bulked together. The more conjugate is present in the system the more defined is the shape of the particles and the

grainier they are. The bulked aggregates start to become more distinct with a defined structure, where the smaller particles held together can be clearly distinguished from each other. This effect is especially well observed on the example 1 mol% and 3 mol% stabilized composites.

.At the same time, micrographs evidence that conjugates are not able to suppress aggregation completely and keep all the particles as provided initially in the sol. Besides changes in aggregation, TEM reveals that the smaller particles tend to be aggregated in networks (**Fig. 24 left**) and present in all composites, irrespective of conjugate concentration. The nanoparticles are connected with each other and form a network structures. Interestingly, particles below 5 nm were found in the SAXS study, performed by Britta Seidt at the Max-Planck Institute of Colloids and Interfaces, and particles in the same sizes are visible on the TEM micrographs. (**Fig. 24, right**)[25, 27, 145]

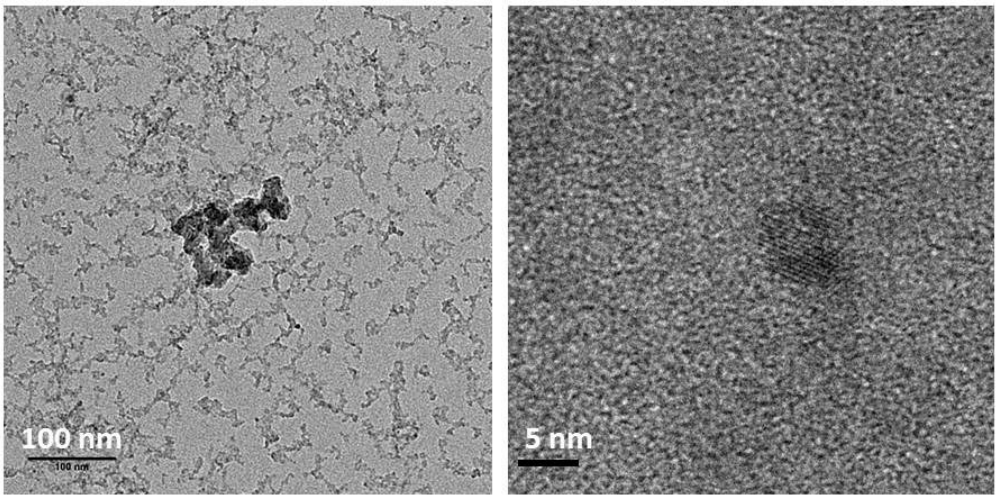

Fig. 24. TEM micrographs of MgF_2 particles single and in a form of a network. 100 nm big aggregate is surrounded by a network formed from small particles (left) and separate MgF_2 particles in higher magnification with the size of ~5 nm (right). TEM micrographs are measured on 15wt% filled composites with 0.5 mol% conjugate (left) and with 3 mol% conjugate (right).

The fact that the aggregation cannot be completely suppressed by the conjugate can be potentially explained by the speed on the interaction processes. The aggregation may be faster than the adhesion of peptide to the particles and would logically result in aggregation taking place first followed by the adhesion of conjugate to larger particles, which are formed in aggregation process.

Adhesion of conjugate to the surface of particles would lead to the formation of so called core-shell structures where a shell will be formed from a conjugate layer. Visualization of such morphologies in TEM appeared to be challenging mainly due to the organic nature of the layer and possibly its thickness. Nethertheless, all TEM micrographs show that the types of formed morphologies are entirely different as without the addition of conjugate. It indicates that conjugates adhere to the surfaces of the particles. This adhesion process also

cause several different morphologies to arise, most of them on the submicrometer to nanometer range.

One of the most common morphologies present in all stabilized composites, and not found in composites without conjugate, are aggregates with a granular structure (**Fig. 25).** They consist of smaller particles (around 10 nm) which are randomly arranged. Small constituents of the aggregates can be well distinguished from each other. This kind of morphologies could possibly be formed by the particles which are partly coated with conjugates, realizing the intermediate stage of aggregation.

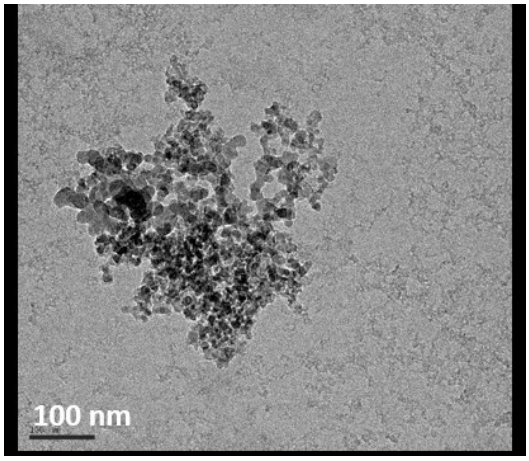

Fig. 25. TEM micrograph of aggregate with a granular structure formed from MgF_2 particles found in 15wt% filled stabilized composites.

To conclude, electron microscopy study of the composites shows that conjugates suppress aggregation in the composites preventing formation of bigger micrometer aggregates. This effect is more pronounced with increasing concentration of conjugate. The suppression leads to more efficient distribution of the particles in the composites.

3.1.3.3. Aggregation of conjugate in composites

Mechanical experiments suggest the presence of rigid structures in the polymer matrix with the addition of conjugate (**pep-I-PEG**). In parallel TEM study of 15wt% filled composites with various conjugate concentration reveals rod-like structures in the composites, where the number of rods is dramatically increasing with the rising conjugate concentration (**Fig. 26**). Rod-like structures apparently tend to stick to each other and form bigger aggregated structures.

To estimate the size of aggregates, 80 aggregates were selected per sample and analyzed with Image J following the procedure described in experimental section. (see Fig.52) This estimation is semi-quantitative as TEM sample preparation and drying can cause

additional aggregation. Despite the limitations of the applied procedure, the estimation of sizes of rod-based aggregates depending on the conjugate concentration still provides meaningful results (**Fig. 27**). With each step of concentration increase, structures formed of rods become larger. The aggregates are below 1µm in the range of 0.5-1 mol% conjugate content. But after this concentration level, aggregates start to be larger than 1µm.

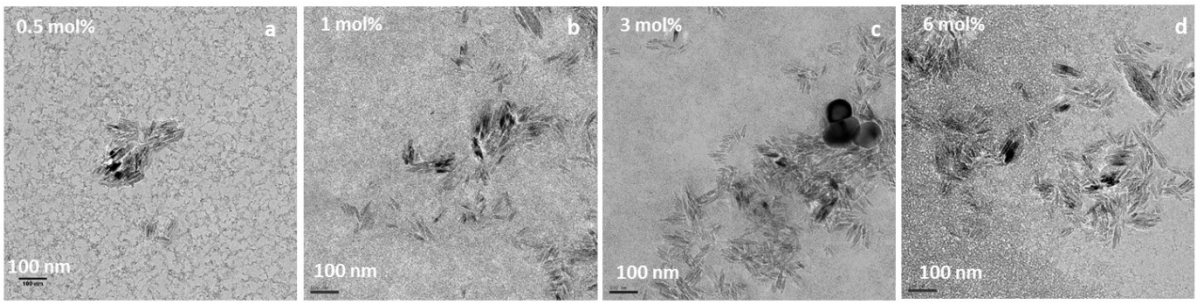

Fig. 26. Representative TEM micrographs of rod like structures formed as a result of self-assembly of conjugates using the example of 15wt% MgF_2 composites with 0,5;1;3;6 mol% conjugates (a-d) Rods are assembling in aggregates, which increase in size with raising concentration.

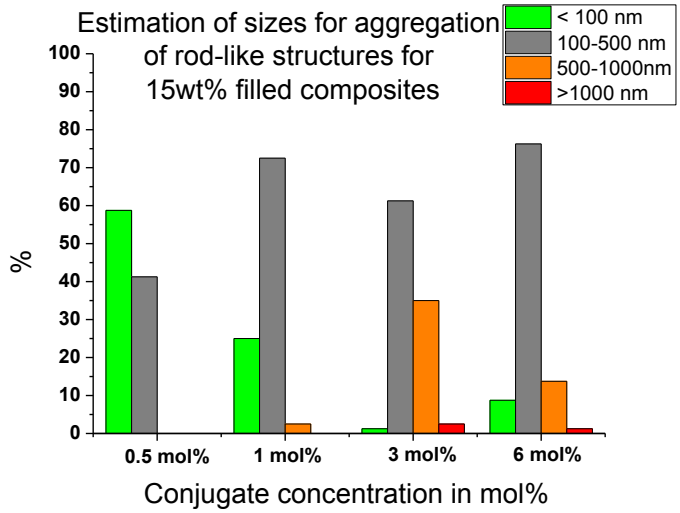

Fig. 27. Size-distribution diagram of aggregate formed from rod-like structures for of 15wt% filled composites. The estimation of sizes is based on TEM micrographs and 80 randomly selected aggregates.

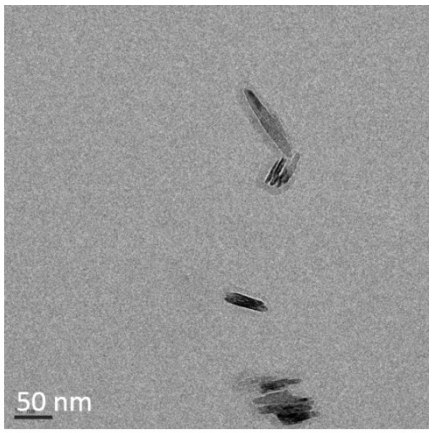

Fig. 28. Representative TEM micrographs of rod like structures measured on the sample containing only conjugate in methanol solution in 3 mol% equivalent.

To clarify the connection between the rod-like structures and conjugate, methanolic solution of conjugate was analyzed alone without blending into polymer matrix and absence of other constituents. Careful TEM investigation of the samples containing only conjugates visualized the formation of anisometric, rod-like objects with 50-80 nm in length and ~10 nm in width (**Fig.28).** The objects appear to be related to self-assembled β-sheet fibrils that have been obtained by peptide-guided organization of peptide-PEG conjugates as described recently. [146]

Conjugate with the increase in concentration has a higher probability of interaction with themselves then with the inorganic surface. If this process is favored conjugates are not available to fulfill their function in the composites. One should note that the size of rods remains and does not depend on the conjugate concentration, the number of rods is increasing with rise in concentration leading to larger aggregates. Considering the estimation of aggregates sizes and the competition between these two processes, one can conclude that starting from 3 mol% on one hand the aggregation of inorganic particles suppressed, but on other hand the aggregation of supramolecular structures formed from conjugates start to become pronounced and weakens the materials.

Analysis of IR spectra obtained from composites with different conjugate concentration shows vibrational Amide I band at 1628 and 1690 cm^{-1}, which are characteristic for extended cross-β-sheet structures (**Fig. 29**).[147] The FT-IR spectra of composite materials with varying amounts of **pep-I-PEG** compatibilizer provides evidence that the typical β-sheet bands become more pronounced with increasing amounts of the conjugate. This observation suggests that conjugates in the material depending on the concentration can undergo the self-assembly process and supports the observation done in TEM study.

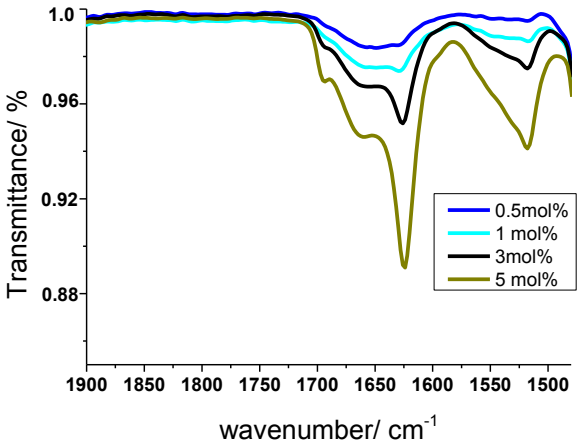

Fig. 29. FT-IR ATR spectra of the composites giving Amide I & II vibrational bands and indicate the formation of β-sheet secondary structures.

3.1.4. Crystallization behavior of composites

In the previous chapters the mechanical properties of composites were discussed, which are the macroscopic property. To the biggest extend the properties of materials and the corresponding values of the measured properties such as elastic modulus and strength are predefined through the properties of the matrix, as it represents the biggest part of the composite in terms of volume and weight content, although the properties of the matrix can be significantly altered by the modifications as filler introduction. Structural studies performed on composites mainly with electron microscopy methods (SEM and TEM) provides a good insight into the aggregation processes in the composites, which can explain the changes of mechanical properties upon modifications. Scanning electron microscopy methods is also a very good tool to follow the changes of morphology of composites, which reflects changes in the crystallization process but does not provide details of the crystal structure. The organization of crystalline and amorphous parts in the semicrystalline PEO is a very important aspect of structural organization and significantly predefines the mechanical performance. Therefore analysis of crystal organization in the composites is essential and will be covered in this chapter.

All studies and results mentioned in this chapter were performed in collaboration with Britta Seidt from Max-Planck Institute of Colloids and Interfaces. All X-Ray based measurements were realized in the Max-Planck Institute. Further analysis of data and its correlation with other measurements were realized in cooperative work.

3.1.4.1. Crystallinity of non-stabilized composites

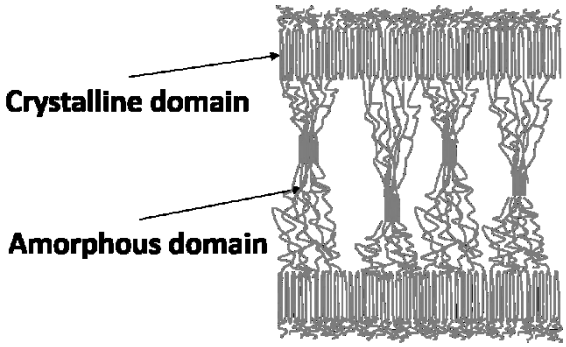

MgF_2 amount in wt%	Crystallinity in %
0 (pure PEO)	65.6
15	63.3

Fig. 30. Schematic representation of crystalline and amorphous domains present in PEO. Table shows crystallinity values for PEO and 15 wt% of MgF_2 filled composites calculated from XRD measurements. For ease of understanding and visualization, empty space is left between amorphous domains.

Crystallinity is specified as a percentage of the volume of the material that is crystalline. By the calculating the crystallinity, relation of crystalline to the amorphous part is defined.

As the first step, crystallinity of polymer and non-stabilized composites is evaluated based on the XRD measurements in order to monitor impact of filler on the crystallization processes. The crystallinity values of pure PEO and 15wt% MgF_2 filled composites are presented in the **Fig. 30.** Pure PEO (M_n = 900 000 g/mol) has crystallinity of 65.6%. This value is in alignment with the published values, where for PEO with different molecular weight the crystallinity in the range of 60-75% was reported.[148, 149] PEO with the molecular weight of 1000 000 g/mol had 60% crystallinity.[150]

Upon introduction of the filler into the system, as expected, crystallinity changes from 65.6% to 63.3%. Lower crystallinity values could be explained by modified (hindered) crystallization processes that crystallites can not be formed in the same way as in the pure PEO. In the preparation step of pressing, the dry composites is melted again and then cooled down, the polymer chains in the composite have a slightly lower possibility to build a crystalline phase in comparison to pure PEO. This can be influenced the presence of aggregates, which hinders the formation of crystalline domains. Very similar behavior in crystallinity changes was reported for PEO composites filled with hydroxyapatite nanoneedls.[151] Increasing the amount of nanofiller in PEO matrix leads to the retardation of PEO crystallization and the amount of amorphous phase increases. [152]

3.1.4.2. Crystallinity of stabilized composites

As it was shown in the previous subchapter, with the introduction of an inorganic filler into the system crystallinity decreases and now the introduction of conjugate (**pep-I-PEG**) is evaluated on the example of 15wt% MgF_2 composites. Crystallinity values of stabilized composites are presented in the **Table 2.** Crystallinity changes upon conjugate addition and it varies depending on the conjugate concentration. The crystallinity grows from 63% for not stabilized 15wt% MgF_2 filled composites to 73% for 3 mol% conjugate addition and then drops down by the concentration beyond 3mol% to 61%. Crystallinity of the composites changes by 10% with conjugate addition and, interestingly, it reduces for composites with substantial amount of conjugate (8 mol%) and becomes even smaller than for unstabilized composites. These changes would indicate that conjugate in the concentrations between 1-3 mol% contributed to the formation of more crystalline domains in the PEO, while excessive amounts of conjugate have opposite effect.

Table 2. Changes of crystallinity in 15wt% MgF_2 filled composites containing different amount of conjugate.

Conjugate content in mol% [a]	Crystallinity in % [b]
0	63
0.25	67
0.50	67
0.75	66
1.00	68
3.00	73
5.00	66
8.00	61

a. mol% is calculated in relation to n(MgF_2) b. The degree of crystallinity was calculated based on X-Ray diffraction data by comparing the area under the crystalline peaks to the total scattered intensity

It is important to note that the changes in crystallinity exactly follows the trend of changes in elastic modulus values. This fact allows us to correlate both these properties of the system. It is expected as far stiffer composites show normally higher crystallinity.

All previous studies on the structure of the composites showed addition of conjugate suppresses aggregation producing smaller aggregates. Analysis of crystallinity changes supports the changes on the elastic modulus, as far as changes of crystallinity following exactly the trend of elastic modulus. Based on this fact, one can assume that aggregation suppression impacts the crystallization processes of composites. This impact can be explained by the fact that smaller particles present in the composites will represent smaller defects for crystallization processes and crystallite formation is less hindered. This would lead to more formed crystalline domains and corresponding higher crystallinity. There are

also reported results in the literature, where increased crystallinity is attributed to better distribution and smaller size of the filler, often achieved with coupling agents [153-155].

3.1.4.3. SEM study of crystallization in composites

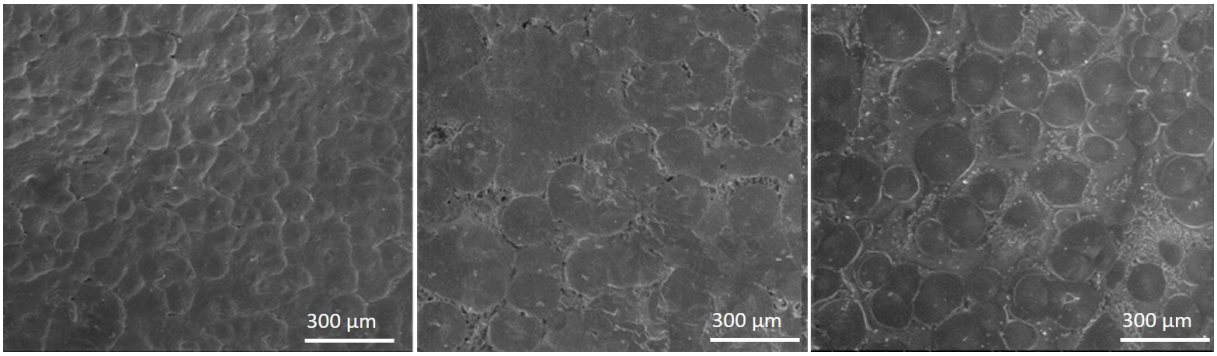

Fig. 31. SEM micrographs of changes in spherulite morphologies formed by crystallization of PEO in different composites: PEO pure (left), 15wt% MgF_2 filled (middle) and 15wt% MgF_2 filled with 1 mol% conjugate (right).

Tracking of the crystallinity changes shows that filler and conjugate introduction into the PEO influences the crystallization process.

Unstrained semicrystalline polymers usually crystallize in a spherulitic manner. Spherulits represent point-nucleated semicrystalline entities, which grow in a spherically symmetrical form until their boundaries impinge. The spherulites are composed of radiating lamellar crystals in which the molecular axis is perpendicular to the growth direction. The lamellas are folded-chain crystals.[156] **Fig. 31 left** represents PEO spherulites formed after drying in the hood before hot pressing step.

The influence of filler and conjugate on the crystallization process of PEO matrix was followed also by SEM, where the changes of morphology were analyzed for different composites in comparison with pure PEO (Fig. **31**). In order to do so, composites were investigated after the drying step in solution casting and before the hot pressing step. PEO as a semicrystalline polymer typically crystallize in spherulite morphologies. On many SEM micrographs MgF_2 particles are found in the middle of the spherulites, is suggests that MgF_2 particles act as additional crystallization sites by the crystallization of the PEO. Addition of inorganic filler obviously has an impact on the crystallization of PEO. The structure of spherulites became less pronounced and some spherulites merged together to form larger ones (**Fig. 31 middle)**. Addition of conjugate again alters the spherulite morphology leading to smaller spherulites that are better separated from each other (**Fig. 31 right)**. All the changes could be explained by aggregation issues. Aggregated particles represent significant distortion for the crystallization of PEO in nicely formed spherulites, which could explain loss of morphology perfection and merging of spherulites. Suppression of aggregation would represent smaller distortion for the spherulites growth, this would restore the morphology of spherulites. Other published studies of crystallization of PEO in the presence of inorganic filler support our observations and showed that filler destroys the perfection of formed

morphologies and suppresses spherulites growth.[157, 158] Introduction of nanofiller enhances this process even more, increasing the number of nucleation sites and smaller spherulite size, which is confirmed in the other publications. [159, 160]

3.1.4.4. Crystallite size of composites

Table 3. Changes of crystallize sizes of PEO depending on the filler amount and conjugate content. 15wt% MgF_2 filled composites are considered with 0-6 mol% of conjugate.

Conjugate content in mol% [a]	Crystallite size in nm [b]
PEO	52.3±1.3
0(15wt% MgF_2)	46.9±1.2
0.5	46.8±1.8
1	45.7±1.3
2	47.6±1.9
3	47.3±0.2
6	45.4±1.1

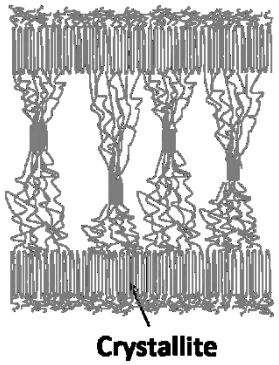

a. mol% is calculated in relation to n(MgF_2) b. Crystallite size was calculated based on (120) PEO reflexes from WAXS study

Introduction of the inorganic phase and conjugate impacts crystallization processes of the composites as it was shown on the example of crystallinity changes and formation of spherulites. But previous measurements do not reveal what exactly is happening with the crystallites in the PEO matrix and how is it connected with the aggregation phenomenon described previously. To get insight into this aspect of crystallization processes, changes in the crystallite sizes of PEO were followed employing WAXS (Wide Angle X-Ray Scattering). The experiments were performed in cooperation with the Department of Biomaterials at the Max-Planck Institute of Colloids and Interfaces by Britta Seidt. Details of the experiment and analysis procedure as well as obtained values are presented in the Dissertation of Britta Seidt. [145] The changes of PEO matrix were monitored during the experiment and, based on the (120) reflex of PEO, crystallite size of PEO matrix in different composites were calculated (**Table 3)**. The calculation of sizes includes oriented and nonoriented crystallites. The size of PEO crystallite in unfilled matrix is 52.3 nm. For PEO with different molecular weight and different state (pallet, melt, powder) the crystallites sizes were reported in the range 35-55 nm. [161] Addition of filler to the matrix reduces the crystallite site to 46.9 nm. At the same time addition of conjugate again allows a significant increase in the size of crystallites: from 46.9 to 47.6 nm. Remarkable is also decrease of crystallite size for 6 mol% stabilized composites, which is smaller (45.4 nm) then unstabilized (46.9 nm) composites. The changes of crystallize sizes can be again referred to size effect. Larger aggregates hinder the growth of crystallites, leading to a decrease in crystallize sizes of unstabilized

composites. Smaller aggregates represent less distortion for growth of crystallites, which lead to a bit larger crystallites after addition of conjugate. Observed changes are consistent with the published literature. [151]

3.1.4.5. Changes of crystallites sizes during tensile testing

Table 4. Crystallite sizes of PEO in nm at 0 and 8% of strain measured for PEO and 15wt% filled stabilized and unstabilized composites.

Strain in %	PEO	0mol%	0.5 mol% [a]	1 mol%	2 mol%	3 mol%	6 mol%
0	52	46	46	45	47	47	45
8	41	26	27	29	33	34	29

a. mol% is calculated in relation to n(MgF_2). Crystallite size calculated based on (120) PEO reflexes from WAXS study taking into account oriented and non-oriented crystallites

After evaluation of overall crystallite sizes, the change of crystallite sizes were studied at the different stages of deformation. This was realized in in-situ tensile testing experiments combined with WAXS were performed on the samples with different composition. These experiments were performed by Britta Seidt (Max-Planck Institute of Colloids and Interfaces), where analysis of the data was also done. Further analysis of the data and establishing the connection with other experiments was realized in a collaborative work. Experiments were done in a specially developed set-up, where X-Ray signal could be measured at the different steps of tensile testing experiment. One of the limitations of the set-up was that composites could be not stretched until the breaking point due to limitation of moving distance in tensile stage. This allowed to analyze only the first part of the stress-strain curve and corresponding properties. In the **Table 4 and 5** the changes of crystallite size are represented after 8% of strain for various composites. Overall the crystallite sizes decrease with increasing strain, although the decrease in crystallite sizes is dependent on the composition. Decrease in crystallize size for pure PEO matrix is much slower in comparison to filled composites: for PEO crystallize sizes decreases from 52 to 41 while in the same time for 15wt% filled composites the changes go from 46 to 26 nm. Addition of conjugate also shows influences on the crystallite size change, making the decrease slower: the 3 mol% conjugate addition reduces crystallites from 47 to 34 nm, while without conjugate it goes from 46 to 26 nm. All described changes suggest that addition of filler and conjugate impacts the deformation mechanisms in composites and it expresses in sizes of crystallites. Also different changes introduced by filler and conjugate separately can be monitored and more precisely expressed by calculation the percentage of change in size in relation to original size for different composites, which is represented in the **Table 5**. Changes in sizes expressed in % from original size immediately indicates that addition of the

filler to the system doubles the speeds of crystallize change: 43.9% for filled composites and 21.4% fore pure PEO matrix. Further introduction of the conjugate slows down the speed from 43.9 to 26.6% for 3 mol% stabilized composites. Graphical representation of the speed of change for crystallize size (**Fig. 32**) clearly indicates that inorganic filler significantly increases the rate of reduction in sizes, while each step of conjugate addition slows the rate of crystallite size reduction. This process takes place up to 3 mol% and then again the rate increases and decreasing in sizes in speeded up in comparison to 3 mol%.

Table 5. Changes of crystallite sizes of PEO and 15wt% MgF_2 filled composites by 8% strain expressed in % of original size.

Strain in %	**PEO**	**0mol%**	**0.5 mol%** [a]	**1 mol%**	**2 mol%**	**3 mol%**	**6 mol%**
0-8%	21.4	43.9	42.3	36.3	30.4	26.6	34.3

a. mol% is calculated in relation to n(MgF_2).

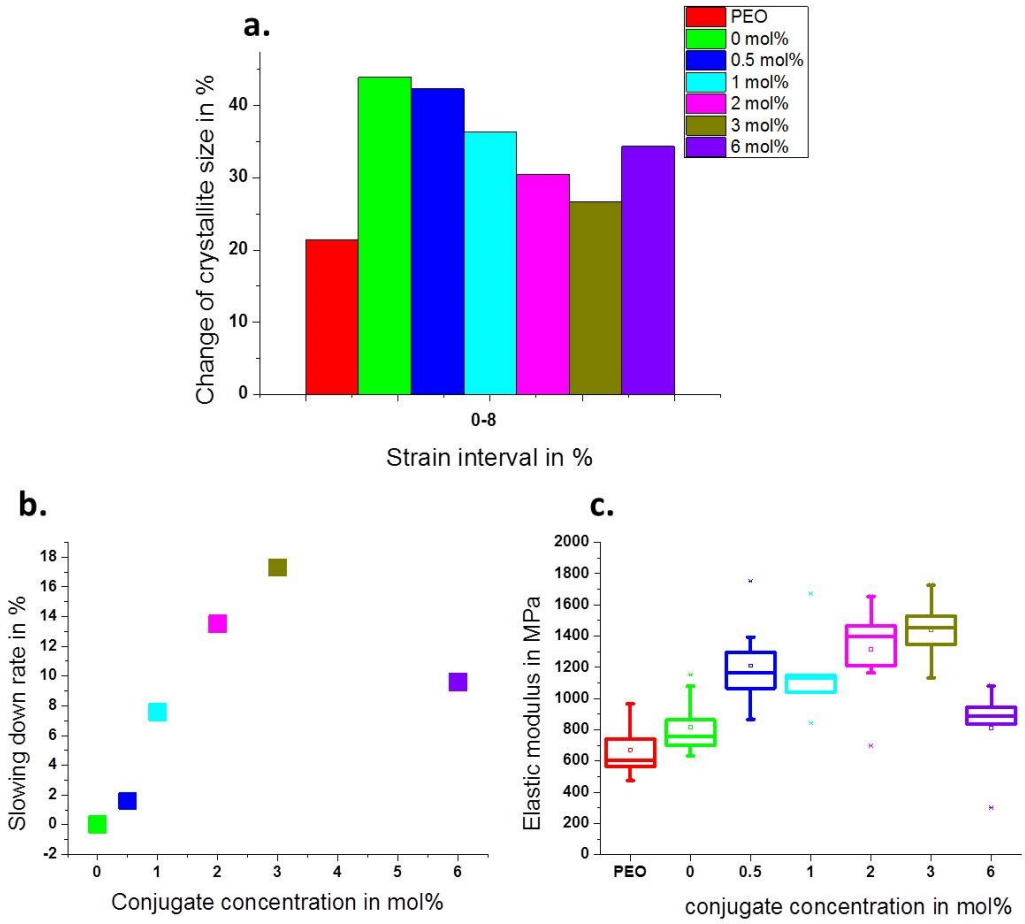

Fig. 32. Graphic representation of dependencies between changes of crystallite sizes and elastic modulus measured on 15wt% composites. (a) speed of crystallite size change in % in composites depending on conjugate content; (b) graphical representation of slowing down rate of crystallite size change depending on the conjugate concentration (b) and corresponding changes of elastic modulus (c).

Fig. 32 represents the impact of conjugate on the system, it takes into account the changes in rate expressed in % depending on the conjugate amount, where the changes for unstabilized composites considered as a value for comparison. Interestingly the represented changes exactly correlates with the changes of elastic modulus. Knowing that the changes of elastic modulus are originating from aggregation suppression therefore the crystallize size changes can be explained by that too. Bigger aggregates seem to speed up the damage of crystallites representing bigger distortion points, while decreasing aggregate sizes with addition of conjugates seem to slow down damage of crystallites.

Due to need to complicated set-up and limited availability of synchrotron sources, the number of performed in situ tensile testing and WAXS studies are very limited. The existing studies concentrated mainly on the study of commonly used polymers and relatively new field of nanocomposites has not come into focus yet. To our knowledge, there are no publications avaliable, where nanocomposites, containing compatibilizers, were studied with this combination of methods, and hence very few information available in this field.

3.1.4.6. Deformation mechanism at early stages

The deformation mechanisms of semicrystalline polymers have been studied for a long time. For most widely used polymer - polyethylene (PE) the following steps in the mechanism were proposed: mechanism starts from moving of lamellas apart with strain accommodated mostly by amorphous phase, then chains get extended and slip initiated in the crystalline lamella, where blocks are pulled out of lamella. [162] Later studies involving more advanced combination of methods (in-situ Raman and WAXS) confirmed that at the early stages of stretching, it is just chains of the amorphous interlamellar layers which undergo deformation. It involves disentanglement, extension and alignment of tie molecules between two adjacent crystalline lamellae. In the plastic domain, the crystalline chains begin to orient towards the tensile axis. Beyond the yield point, amorphous phase cannot accommodate any more the deformation and this is crystals which are affected in turn. Blocks of crystals in equatorial position, attached by tie molecules in extension, are break up into smaller folded chains blocks.[163] Based on this consideration the simplified mechanism is proposed for the composites with conjugate with schematic representation in the (**Fig. 32**) reflecting mainly the impact of conjugate onto the system. There could be two approaches to consider the system - one would consider polymer matrix and particles together with conjugate as inclusion. Results of in-situ-WAXS and tensile testing suggest that the particles and particularly conjugate acts as a stabilizer of the amorphous phase in comparison to the net polymer. [145] The second way of consideration focuses mainly on the role of conjugate on the system and filled polymer without conjugate is considered as a reference for comparison, which represented in the **Fig.33**. Introduction of the filler to the polymer brings aggregates into the system, which most probably are located in the amorphous phase. As discussed previously, bigger aggregates would represent distortion points for the amorphous part of the polymer and restricting their movement. This finally

will lead to stress transfer to the crystalline regions and crystalline lamellas will undergo deformation, which expresses in the decrease of crystallite sizes. Decrease of crystallite sizes may be realized through pulling of more blocks from lamella. Smaller aggregates as of result of aggregation suppression would represent smaller defects and less blocks are pulled out of crystallites, which is again visible in increase of crystallite sizes in comparison to unstabilized composites. So each step of conjugate addition lead to the fact that less and less blocks are pulled out. The conclusion would be that conjugate addition and size effect lead to the retardation of damage of crystalline domains, which expresses in the slowed down decrease crystallite sizes.

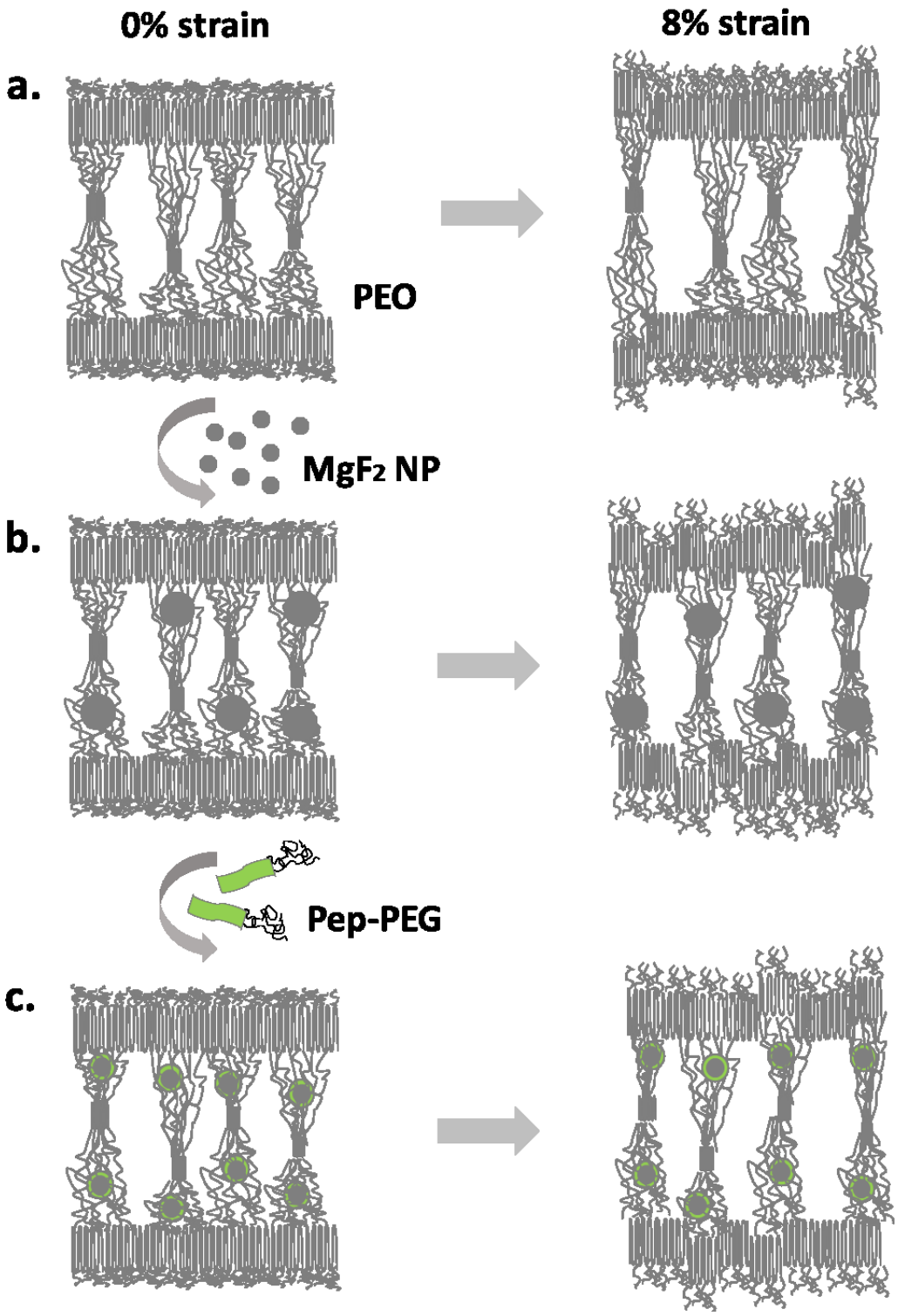

Fig. 33. Schematic representation of deformation mechanisms of PEO (a) and 15wt% MgF_2 filled stabilized and unstabilized composites showing impact of filler and conjugate on it: filler alone present in the polymer leads to faster deformation of crystalline domains in comparison to neat polymer (b), while filler in combination with the conjugate slower down the process in comparison to sample without conjugate(c). Empty space between amorphous domains is left for clarity purposes.

3.1.5. Summary

3.1.5.1. Stiffness and toughness of composites

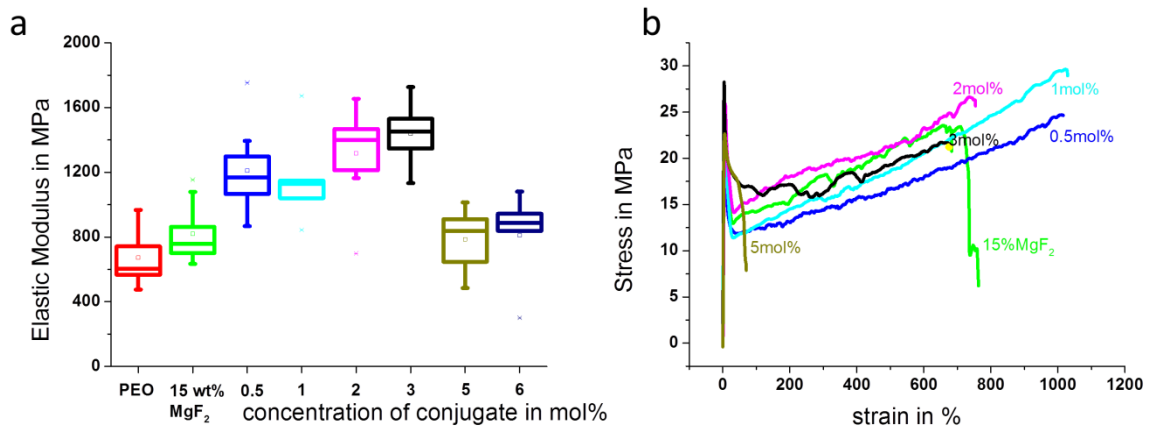

Fig. 34. Analysis of MgF_2/peptide-PEG/PEO composites with 15 wt% MgF_2 filler and different compatibilizer concentrations. a) elastic moduli and b) stress–strain curves showing the tensile toughness (integral area below the curves) and elongation at break.

The simultaneous increase of elastic modulus and tensile toughness in synthetic composites is highly desirable but typically not easily achievable with established compatibilizers. The difficulty arises from the fact that elastic modulus and toughness are mutually exclusive properties. Here, we have shown that the application of peptide-polymer conjugates (**pep-I-PEG**) as compatibilizer improves these properties at the same time i.e. higher elastic modulus and higher tensile toughness (**Fig. 34**).

3.1.5.2. Size effect and its impact on the mechanical properties of composites

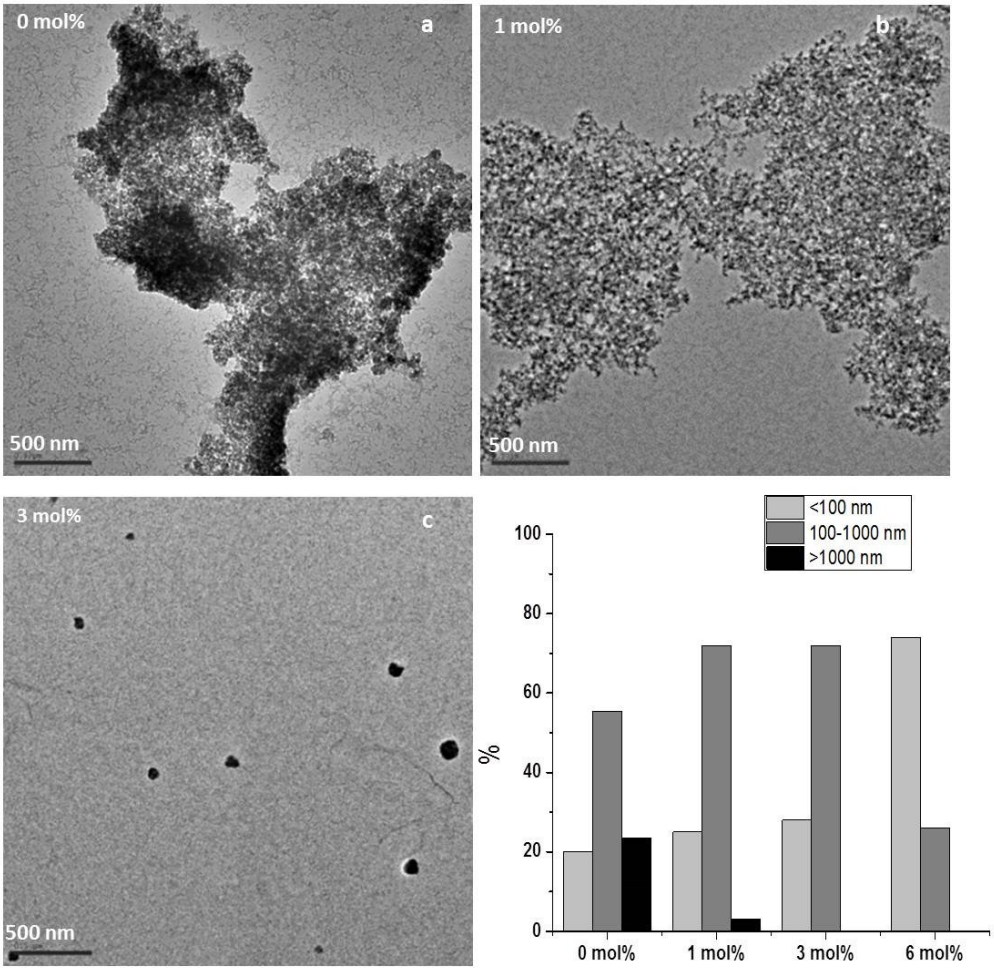

Fig. 35. Representative TEM micrographs from microscopy analysis of MgF_2 particle dispersion in 15 wt% filled composites depending on the compatibilizer concentrations (a) 0 mol%, b) 1 mol%, and c) 3 mol%) and d) particle-size distribution histogram based on image analysis of SEM-BSE micrographs.

Electron microscopy studies (SEM and TEM) performed on the composites proved that aggregation of particles is suppressed by the addition of the conjugate (**pep-I-PEG)** (**Fig. 35**). Both microscopy methods show analogous changes in the composite structures. For instance, TEM micrographs show that the aggregation of the inorganic MgF_2 particles was suppressed. In another words, by increasing the amount of the compatibilizer, the particles are being more efficiently dispersed. A quantitative analysis of the particle-size distribution was obtained from SEM in back-scattered electron mode. The particle-size histogram provides evidence that stepwise increase of conjugate concentration leads to a reduction in the average aggregate sizes. This transition in size of aggregates/particles will be called size effect.

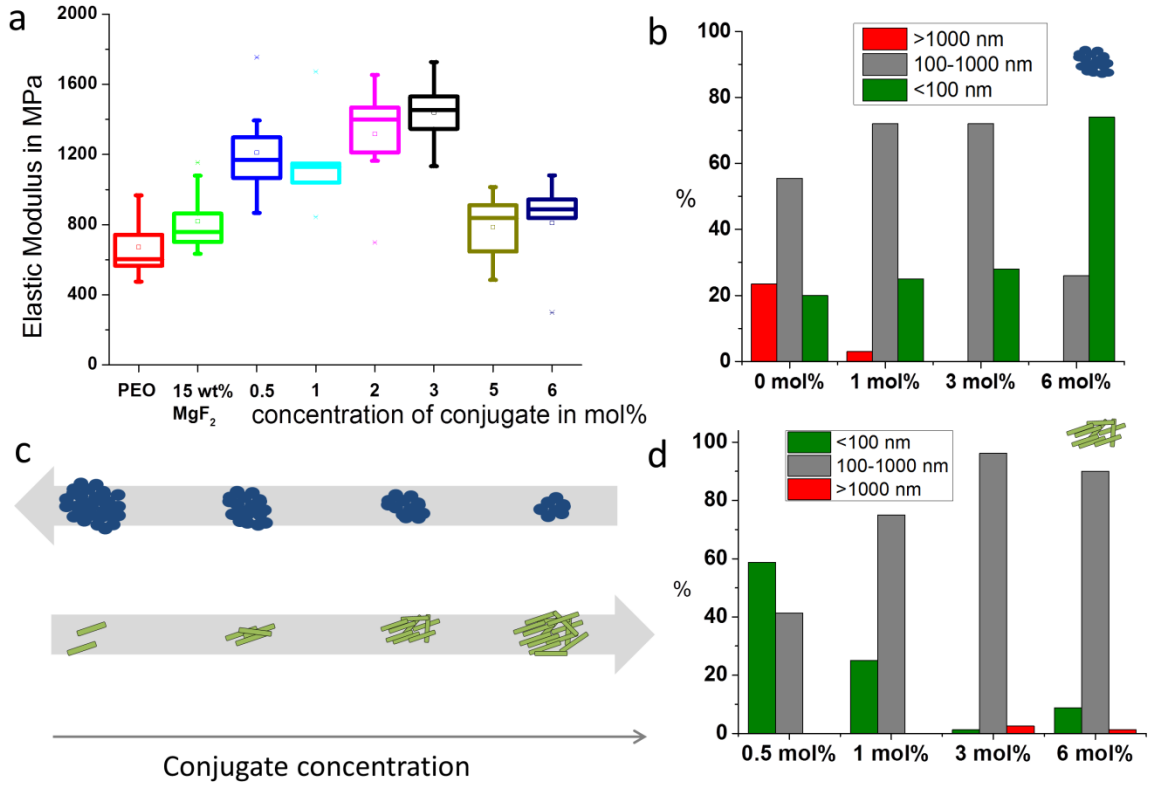

Fig. 36. Graphical representation of connection between changes of elastic modulus in 15wt% MgF_2 filled composites and aggregation. a. Elastic modulus of composites with various conjugate concentration, aggregate-size distribution diagrams for particles (b) and rod like structures (d) depending on conjugate concentration c. schematic representation of aggregation behavior for particles and rod-like structures. Conjugate suppresses aggregation of particles leading to elastic modulus increase, while aggregation in conjugates due to peptide-peptide interaction lowers the elastic modulus.

The obvious transition in average sizes of particle aggregates from dominantly large sizes of >1000 µm to the smaller particles of <100 nm called as size effect can be correlated with the changes in the elastic modulus of the composites. While the aggregates size is decreasing, elastic modulus is increasing (**Fig. 36 a,b,c)**. A reduction of aggregation lead to smaller aggregates and better dispersion of particles, which represents smaller distortions of the polymer matrix. In parallel to aggregation suppression, TEM studies evidence aggregation phenomenon expressed in the formation of rod-like structures. Formation of these structures is probably caused by the conjugate itself. The inverse effect was found in terms of sizes of aggregates in comparison to particles sizes. Estimation of aggregates sizes formed from rod-like structures clearly evidences that aggregates increase in size with the increasing conjugate concentration, overcoming the micrometer boarder for 6 mol% conjugate concentration **(Fig.36 d)**.

The presence of maxima for the elastic modulus for 3 mol% and abrupt decrease for 6 mol% conjugate could be potentially explained through aggregation processes of particles and peptide-polymer conjugates themselves. With increasing conjugate concentration aggregation size of aggregated particles decreases, while aggregate size made of rods increases (**Fig. 36 c**). Decrease in size of aggregates from particles allows improving elastic modulus, but probably at the certain point aggregates made from rods reach the initial size of particle aggregates and let elastic modulus values decrease again. One should also note that size effect is obviously one of the effects leading to the changes of elastic modulus. Improvement in the distribution of the particles coexisting with the size effect could be an even more significant factor, contributing to the changes in the elastic modulus, but the quantification of this parameter for the system is challenging.

Published studies, addressing the question of size effect on the elastic modulus, show that elastic modulus is insensitive to the changes of the particles sizes as far filler element varies in micron range.[144, 164] [165] The situation changes when, instead of micrometer sized particles, nanoparticles are used. Elastic modulus becomes sensitive to it and increases with decreasing size of particles. [166] [167] Literature study also suggests that generally interfacial adhesion, which would change in the composites by mean of conjugate, does not affect the changes of elastic modulus by itself, which was shown previously by variation of different coupling agents in the particulate composites.[168] This can be explained by the simple fact that elastic modulus is measured at relatively low deformation, where no significant phase separation takes place.

Incorporating particles into the system restricts mobility of polymer matrix and introduces a mechanical restrain. The restriction of polymer diffusion is based on the interaction of polymers with the introduced particles. The degree of the restriction will depend on the property of the filler and the matrix. The interaction of polymer with the particles creates an addition phase in the material- called interphase. The effect of interfacial phase makes its contribution to the enchantment of composite modulus, where for particulate filled composites with the size of the filler above 1 μm, this contribution can be considered as negligible. This assumption based on the relation between the interface size to the total volume. The size of formed interface is around 1 nm, which does not considerably contribute to the properties compared to the total volume. Switching from the microcomposites to nanocomsposites introduces changes in the accepted models and the contribution of interface between the polymer and particles can no longer be neglected. Introduced nanoparticles will offer much higher surface areas for the interaction with the polymers compared to micron particles. Even considering the interface in the same size range, the relation between the total volume of interface to the total volume will f composite change dramatically. Also the interface thickness may be comparable to the particle size, which significantly affect elastic properties.[169] Some studies tried to incorporate the role of interface into predictive models for elastic modulus and to correlate it with experimental results. [170] These studies based on particle-interface-matrix unit, found that the smaller the size of hard particles, the better the mechanical enhancement.[171] Additionally, studies, aiming to evaluate effect of particle size combined

with modification of interface by grafting, confirmed improvement of modulus values thank to nanofiller and the better distribution.[172]

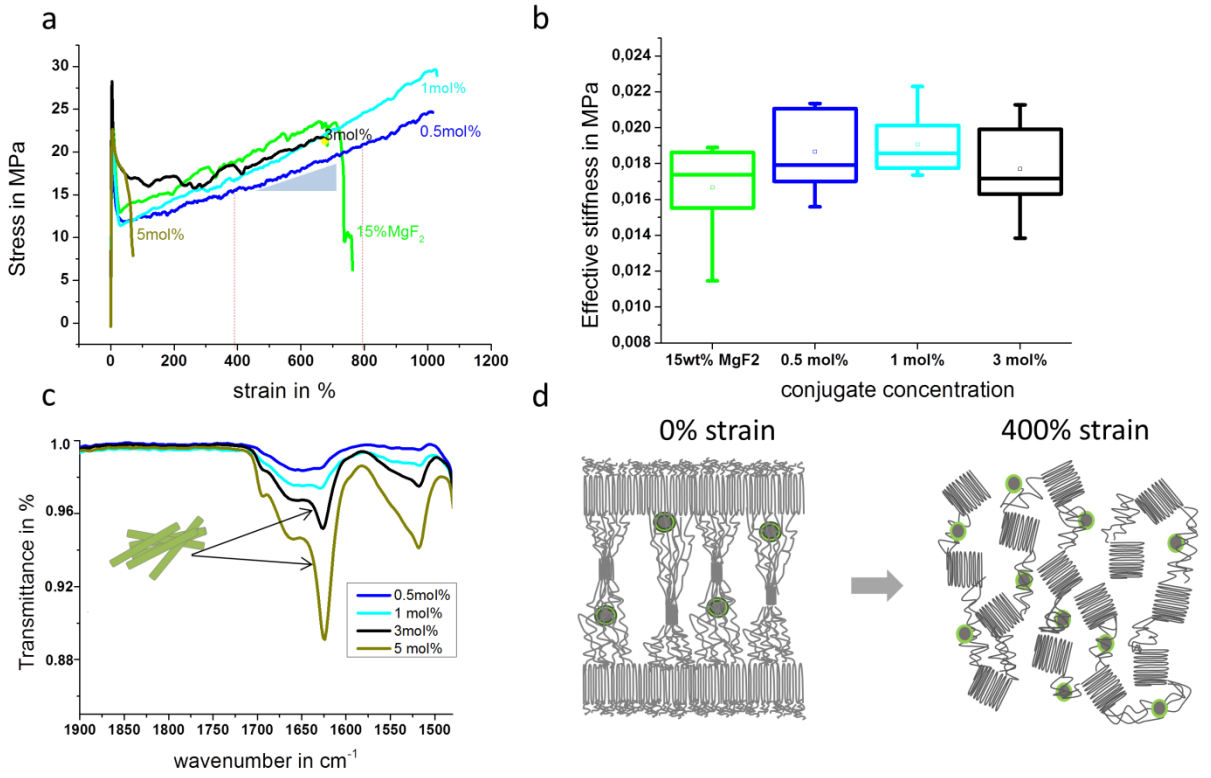

Fig. 37. Graphical representation of size effect impact on the toughness change. a. stress–strain curves showing the tensile toughness (integral area below the curves) and elongation at break with the area between 400-800% for the effective stiffness calculation – slope of the curve for 15wt% filled composites b. Values for the effective stiffness calculated for composites depending on the conjugate concentration c. IR spectra of composites indicating formation of β-sheet-like structures d. Schematic representation of the possible deformation of crystalline phase by 400% strain and reinforcement of amorphous phase by the particles.

The reasons for the toughness changes found in the composites and underlying mechanisms are not straightforward and remain unrevealed due to limitations of accessible methods. But based on the obtained results some hypothesis is provided, which can be a potential explanation for toughness changes.

The potential explanation for observed changes of toughness could be size effect – suppression of aggregation and changes in the aggregate sizes with increased conjugate concentration. Careful comparison of the stress-strain curves obtained on 15wt% MgF_2 filled composites in dependence of the conjugate concentration points to one important aspect: composites with improved toughness show no difference in elongation at break values but have different slopes in the stress-strain curves. Higher slope of the curve leading to an increase the area under the stress-strain curve leads automatically to higher tensile toughness values (**Fig. 37 a**). The slope on the defined region is called effective stiffness and these values calculated for different composites are presented in the **Fig. 37 b.** 400-800% strain region was selected in a way that all composites can be included into consideration.

Analysis of the slopes clearly indicates that composites with 0.5-1 mol% conjugate have more steep slopes and higher values of toughness correspondingly. The necessity to apply a higher force for the deformation, which finds its expression in the effective stiffness, could also be potentially explained again by the presence of the reinforcement of the amorphous phase by smaller particles. How the particles and changes of their sizes can impact the elastic modulus was discussed in the previous chapters. In the early stages of deformation, where deformation of reinforced amorphous phase took place, it expressed in the increase of elastic modulus values. Further deformation would impact the crystalline regions of the polymer matrix requiring the higher forces and leading to the yield strength peaks. A subsequent cold drawing region would deform the crystalline and amorphous parts. The presence of the particles and their sizes could again have an impact on the non-crystalline domains in cold drawing regio leading again to the sort of reinforcement that leads to the increase of toughness (**Fig. 37 d**). This hypothesis could be a potential explanation for the changes of toughness and the fact that both properties changes simultaneously.

Following this hypothesis toughness and elastic modulus should increase with the rising conjugate concentration, as it decreases size of particle aggregates. But experimental values show that elastic modulus and toughness decrease after a certain conjugate concentration. The explanation for this effect especially for decrease of toughness can be hidden in the formation of rod-like structures. IR spectra indicate formation of β-sheet structures starting from 3 mol%, while showing random structures for 0.5-1 mol% conjugate content (**Fig. 37 c**). These observations can be eventually correlated with the data presented in aggregate-size distribution diagrams, where aggregates above 1 µm start to appear from 3 mol%. These correlations could be an indication that aggregates large then 1 µm of these structures give rise to β-sheet like structures in IR spectra. Surprisingly, improvement in toughness was observed for composites only for 0.5 and 1 mol% and decreasing starting from 3 mol% (**Fig. 37 a**). Drawing these parallels leads one to assume that aggregation of rods prominent for certain conjugate concentration impacts negatively the toughness. Aggregation of rods large then 1 µm would represents as aggregation of particles additional weak point in the polymer matrix, leading to fact that elastic modulus and toughness decrease. This assumption could be potentially correlated to the tendency of conjugate to interact with themselfs by rising concentration. In this case conjugate would be primarily consumed for this interaction and not available for the interface interaction, although one should note that this phenomenon was not investigated in a great detail within this thesis.

Comparison with the existing literature allows us to conclude that such phenomenon of toughness improvement through particle addition and their size variation in the nanorange for ductile matrices was very rarely described. This again emphasizes the novelty of the concept and opportunities hidden in biomaterials and their structural principles. This could be explained by the fact that only in the last years the nanoeffects came into focus of researches and nanocomposites are still not well understood. However, as proven with many examples, for ductile matrices, particulate fillers increase brittleness of composites if there is no or very weak interfacial adhesion, while in brittle matrices the reverse effect is observed and the brittleness is reduced. [144] Although there are no rigorous studies

available on the size effects and toughness, there are some studies presented below available, where comparable connectives were pointed out. The modification of polypropylene with calcium carbonate particles lead to toughness improvement, but it was dependent on the particle size, where 50 nm particles were more efficient then micron ones. [173] Toughness improvement for semi-crystalline polymer blends was achieved again through calcium carbonate particles of different sizes, although the dependency the toughness from particle size was evaluated mainly for micron or submicron particles. Authors concluded that toughness has its source in the plastic extensibility of the matrix material in the interparticle ligaments. [174]

One should point out that changes of toughness are complex and several toughening mechanisms may act simultaneously. Apart from the possible impact of size effect and reinforcement of the amorphous phase, the modification of the interface may significantly contribute to the toughness increase, improving connectivity between the inorganic and organic phases. This phenomenon is well known and was discussed in the literate review, although most known compatibilizer lead to improved toughness but have either little or negative impacts on the elastic modulus.

3.2. Bioinspired interfaces in composites

All results discussed in the previous chapters prove a significant impact of the conjugate on the composite material. All the studies are based on one peptide sequence GTQYYAYSTTQKS-PEG though, which was selected out of initial experiments as the most efficiently binding sequence. The principle of the surface recognition by peptides and the proposed method of selection of those sequences- phage display- will all the time deliver a set of well binding sequences. This fact creates the necessity to find out the parameters and methods to select the most appropriate candidates among the sequences obtained in the phage display read-out. In addition to the selection of the most appropriate sequences, the obvious question arises, if will all the sequences deliver a similar performance and if not what would be the difference between them and the reasons behind it. All these aspects are covered in this chapter.

3.2.1. Variation of peptide sequences in conjugates

Table 6. Peptide sequences represented with single letter code and abbreviation of the sequence selected from phage display screening as selective binder for MgF_2 particles

Abbreviation	Sequence in single letter code
Pep-I	GTQYYAYSTTQKS
Pep-II	GMIVDHLPIQVNT
Pep-III	GEYDYACGVVGYE
Pep-IV	GTQAIRVHTISSQ
Pep-V	GSYPKASLALLAP
Pep-VI	GGLNQVLRIPSPI
Pep-VII	GSPKHNLDMVKMM

The biopanning on MgF_2 nanoparticles (NPs) delivered seven different 12mer peptides (**Table 6)**. All obtained sequences are different in their nature and contain quite a broad range of amino acids residues. This situation required to find the method to select the most appropriate candidate out of the set. The selection was based on washing-elution experiments, performed to identify the most suitable candidate, which is able to strongly adsorb to the NP surface. [24] These experiments include several steps. At first, fluorescent tag marked peptides are incubated first with particles, where peptides have time to adsorb on the surface and concentration of peptide is measured with fluorescence spectroscopy. After that several washing experiments are performed and fluorescence intensity is measured in the left solution. This allows defining the amount of peptide left in the solution and correspondingly calculating the amount of peptides adsorbed at the particles. This test

revealed the pep-I-PEG as the promising candidate.[24] However, diversity of the obtained sequences brings a rather broad range of polarity within the different sequences. This makes peptide solubility and tendency to self-aggregate to very important parameters that have to be considered as they change behavior of peptides and conjugates. They may impact the availability and efficiency of compatibilizers at the internal material interfaces.

3.2.2. Solubility and aggregation behavior of conjugates

Solubility of peptides can be estimated by employing predictive tools that rely on increment system analysis (**Fig. 38**). Hydrophilicity values according to Hopp and Woods et all offer the first indications for solubility estimation **(Fig. 38, Tab.I**).[175] According to the prediction tool, among considered peptide sequences the majority evidences poor solubility with only exception of pep-VII-PEG, being well soluble. The sequences with negative hydrophilicity values differ only slightly from each other thoug, enabling no reliable sorting of the peptides. To be able to differentiate among them, analysis of amino acid composition was included (**Fig. 38, Tab.II**).

Phage display read-out		I. Preliminary analyis		
	Sequence	Hydrophilicity value		Solubility
I	GTQYYAYSTTQKS	-0.4	-	poor
II	GMIVDHLPIQVNT	-0.6	-	poor
III	GEYDYACGVVGYE	-0.2	-	poor
IV	GTQAIRVHTISSQ	-0.2	-	poor
V	GSYPKASLALLAP	-0.4	-	poor
VI	GGLNQVLRIPSFI	-0.6	-	poor
VII	GSPKHNLDMVKMM	0.1	+	good

II. Amino acid composition analysis			Selected seq.
Hydrophobic	Charged	Forming H-bond. network	
15%	8%	**85%**	**pep-I-PEG**
54%	15%	38%	
54%	23%	38%	
38%	15%	54%	
54%	8%	31%	
62%	8%	31%	**pep-VI-PEG**
46%	**31%**	46%	**pep-VII-PEG**

Fig. 38. Representation of set of peptide sequences identified for MgF_2 NP as strong binders and selecting procedure to find sequences with a different solubility and aggregation behavior. Left tables represents amino acid sequence, corresponding solubility and hydrophilicity value calculated by Hopp and Woods, where sequences are grouped and identified as "+" with positive value and "-" for negative ones. Second table analyses percentage of hydrophobic (after Hopp and Woods), charged and residues capable to form hydrogen bonding network in comparison to total amount of residues (13). Through analysis 3 sequences were identified for further investigation: with good solubility – green, with poor solubility – yellow. The amino acids residues were considered as following: E,D,R,K,H – charged amino acids; S,T;E,D,K,R,H,N,Q,Y - amino acids capable of forming extensive intermolecular hydrogen bonding, V, I, L, F, M, C, A, G – hydrophobic amino acids. Picture was adapted from reference [176]

The prediction for solubility of peptides is based on its polarity and can be estimated based on the presence and percentage of certain amino acids group, which makes peptides more or less soluble. Higher percentage of amino acids with non—polar (hydrophobic) side chains will contribute dramatically and lowers the solubility of peptide.[177] Mostly of all considered peptides have higher abundance of hydrophobic residues, which explains low solubility of most considered sequences. Pep-VI offers with 62% the highest percentage of hydrophobic residues. In the opposite to the hydrophobic residues presence of charged residues improve solubility of the whole peptide. Most of the considered peptides show also low abundance of charged residues. A combination, where peptides contain mostly hydrophobic residues and small portion of charged residues, would explain why most of peptides have low solubility. Conclusively, the highest percentage of charged residues with 31% evidenced by pep-VII contributes significantly to its good water solubility. The amino acid analysis revealed further for pep-I, with 85% the highest amount of residues capable to establish H-bonding, this leads to the formation of hydrogels, which was experimentally observed. Taking into account bespoke aspects pep-I and pep-VI will be taken into account for further studies as representatives with low solubility and high aggregation tendency, respectively. Pep-VII differs from other sequences and shows good water solubility and will be further considered as an example of well soluble peptide. Thus the other peptide sequences show intermediate values and considering simplicity of the predictions only the candidates with extreme values have been further investigated.

3.2.2.1. Circular Dichroism (CD) spectroscopy study

Application of prediction tools allows to cluster the sequences in well and poorly soluble and to select the sequences for the further investigation out of each group. Characterization of secondary structures is needed in order to explain the aggregation issues of peptides. Only conjugates will be considered without any addition of inorganic component.

The conjugates with different peptide sequences were investigated with Circular Dichroism (CD) spectroscopy in order to check the secondary structures (**Fig. 39**). The measurements were performed for 1mg/ml concentration in water in the region from 190 to 260 nm. CD spectroscopy measurements evidenced for all three conjugates negative cotton effects at about 198-200 nm typical for a statistical chain-segment conformation (random coils) although showing some variations. They provide no evidence of β-sheet formation as a distinct motif found in self-assembling peptides. The major differences correspond to the position of the CD peak and their intensities. Conjugate pep-VII-PEG shows the most intensive CD signal, while conjugates pep-I-PEG and pep-VI-PEG show two times weaker signal. Interestingly all conjugates evidence slightly different position of the peak minimum, where pep-VI-PEG is slightly shifted to the right and pep-I-PEG to the left relatively to pep-

VII-PEG. This behavior of CD signal can be related to the aggregation issues. It is known that CD signal loses its intensity when aggregation takes place, and the position of negative maxima depend on the side chain and zwitterion-cation equilibrium and may vary slightly. [178][179] Also for peptides undergoing self-aggregation, CD signal shifts to the higher wavelength by aggregation. [180, 181] [181] To sum up all observations and reports from the literature, one can conclude that based on the position and intensity of the peak, pep-VII-PEG processes lower tendency to aggregation among studied conjugates, while other conjugates tend to self-aggregate even with very low concentration.

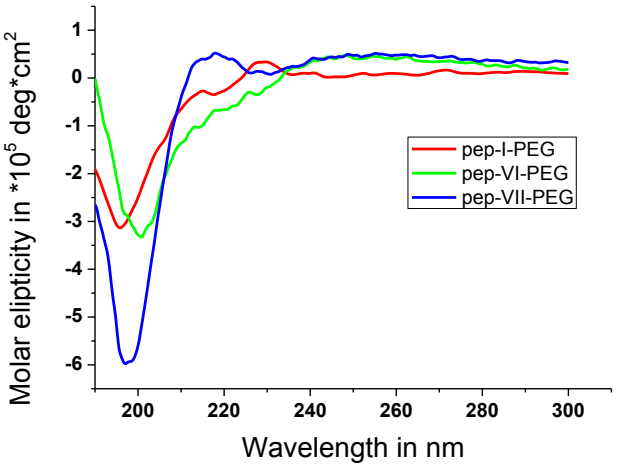

Fig. 39. CD spectra of conjugates: pep-I, VI&VII-PEG measured in water. Spectra evidence random coil structures for all considered conjugates.

3.2.2.2. Diffusion Ordered Spectroscopy (DOSY)

Diffusion Ordered Spectroscopy (DOSY) was used to characterize aggregation behavior of conjugates in the solution. This method is able to determine the diffusion coefficient D of supramolecular aggregates as described by the Stokes–Einstein equation (see experimental section). This diffusion coefficient is inversely related to the radius of the diffusing species, and one might expect that larger molecules or complexes will tend to exhibit smaller diffusion coefficients. This method was used to find out the differences between aggregation behavior of conjugates but not as a method to identify the size of aggregates. 2 mg of each conjugate were dissolved in methanol d_3 and DOSY experiments were measured The obtained diffusion coefficients for all the studied conjugates can be found in the **Table 7**. The measured values shows difference in aggregation behavior of conjugates, diffusion coefficients change from 2.91×10^{-10} to 2.2×10^{-10} and 1.72×10^{-10} m^2/s for pep-VII-, pep-VI and pep-I-PEG correspondingly. According to Stockes-Einstein equation, diffusion coefficient is inversely proportional to the radius of measured species. This would mean that pep-VII-PEG would build the smallest aggregates and pep-I-PEG the biggest ones in terms of size among considered conjugates. It goes in line with the solubility predictions,

where pep-VII-PEG shows good solubility. The measured values for diffusion coefficient would correspond to the conjugates in the range of 5-10 nm. Taking into account previous measurements and mechanical experiments, it is getting clear that with increasing conjugate concentration aggregation increases. It would mean that depending on the conjugate concentration taken for a specific measurement, aggregation will be pronounced to a different extent. Due to that, DOSY was not used for the aggregate size calculation but rather identification differences between conjugates. The calculated sizes of conjugates would be correct only for measured concentration. Also these observations and reported vales are comparable with values mentioned previously. [182]

Table 7. Diffusion coefficient for pep-I, VI&VII-PEG determined out of the DOSY spectra.

Sequence	D in $*10^{-10}$ m^2/s
Pep-I-PEG	1.72
Pep-VI-PEG	2.20
Pep-VII-PEG	2.91

3.2.3. Interaction of conjugate with nanoparticles

Previous sections focused on the solubility and aggregation aspect of peptide sequences, where only pep-PEG conjugates were considered without involvement of other components. This chapter will describe the impact of aggregation and different solubility on the interaction of conjugates with the nanoparticles in the solution. To address this topic, NMR titration experiments will be performed, which allowed following the changes occurring with conjugates upon NP addition by monitoring changes in NMR spectra.

NMR-titration experiments provide insights into effective stabilizer fraction and thus reveal indirectly availability of the stabilizer to act at the particle interface. To 1 mmol solutions of conjugates (pep-I-PEG, pep-VI-PEG & pep-VII-PEG) in CD_3OH (methanol d3) successive MgF_2 sols were titrated in 10 µL (2 µmol MgF_2) steps to monitor changes in 1H NMR spectra of the peptide segments. After each addition of conjugate, ^1H NMR spectra was recorded to be able to monitor the spectra. The amount of particles, which ca be titrated, was evaluated based on two factors: broadening of the spectra to such extend that the signals disappear and possibility to perform shimming for the measurements. Above a certain amount, the system became so inhomogeneous that shimming became impossible. It is worth to note that these experiments are not intended to evaluate the residue involved in the interaction due to the dilution effect causing shifts in NMR spectra.

Table 8. Amount of MgF_2 particles from methanolic sol in µl possible to titrate to the methanolic solution (d_3) of pep-I-PEG, pep-VI-PEG and pep-VII-PEG.

Sequence	Titrated amount of nanoparticles
Pep-I-PEG	60 µL
Pep-VI-PEG	40 µL
Pep-VII-PEG	90 µL

As a result of conjugate-particle interaction NMR signals broaden. Ultimately, the characteristic peptide resonances nearly vanish at a critical particle concentration. Interestingly, to the different conjugates different amounts of MgF_2 sols could be added, indicating different effectivity/availability of stabilizers (**Table 8**)**.** Conjugate pep-VI-PEG with low solubility accommodated 40 µL of particle sol, while conjugate pep-VII-PEG with higher solubility can stabilize with 90 µL more than double of the amount. The fact that conjugates can accommodate different amounts of MgF_2 sols appears to be straightforward correlated with the aggregation issues. Conjugates with higher tendency to form colloidal aggregates with each other are apparently less available to interact and stabilize inorganic particle surfaces. This situation leads to the situation where more and more particles with further titrations are present in the system leading to higher inhomogeneity of the whole system and experimental problems. Based on the analysis of titrated amounts, we can conclude that from studied sequences pep-VII-PEG shows higher availability for interaction with nanoparticles, which means that pep-VII-PEG is less prone to interact with each other.

Behavior of the conjugates differ not only in term of how much particles can be accommodated but also which amount of NP causes shifts in NMR resonances. For pep-I-PEG, even 5 µL of particles cause strong broadening of the spectra and vanishing of some signals, where further addition does not impact significantly the spectra (**Fig. 40**). It might be potentially explained by the aggregation of conjugate before they come to the contact with NP. Especially for the pep-I-PEG, the very broad resonances and overall quality of NMR spectra indicate that pep-I-PEG aggregates and eventually only the small amount is available for the interaction at the nanoparticle surface.

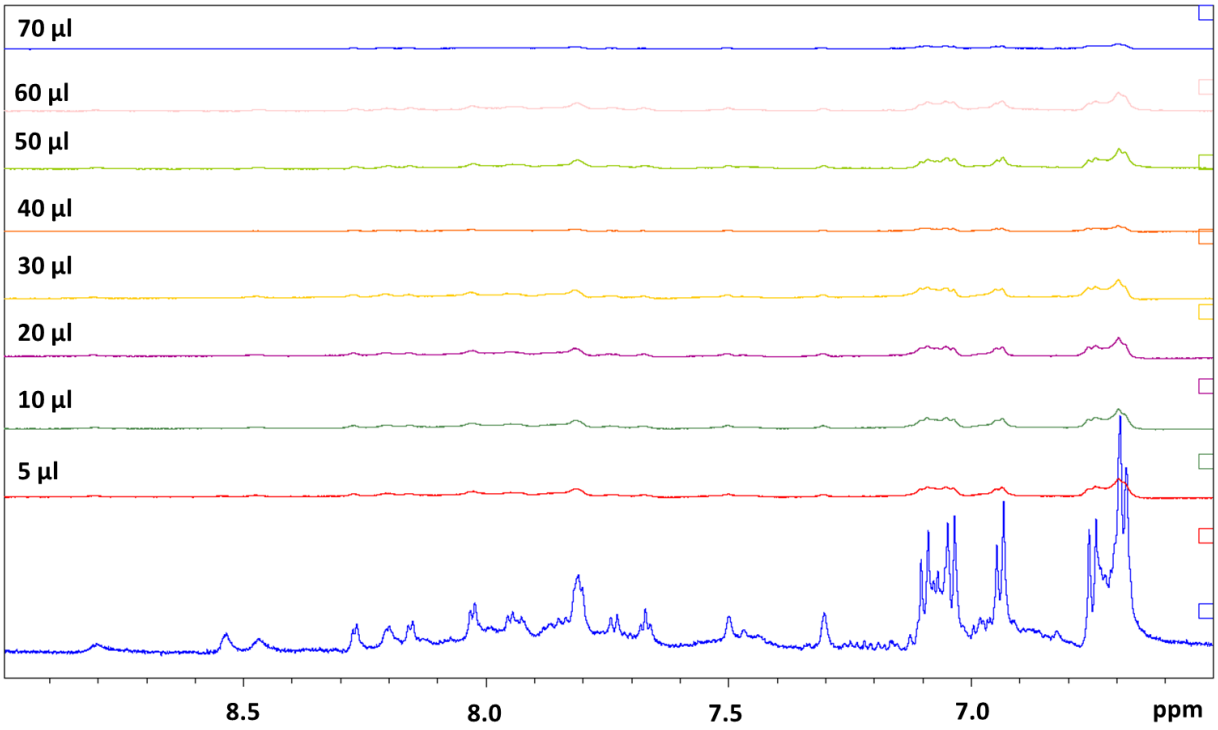

Fig. 40. ^{1}H NMR spectra (NH and aromatic region) of pep-I-PEG representing titration serie of MgF_2 NP in the sol form added to the conjugate in 10µl (2 µmol MgF_2)and corresponding changes in the spectra. NMR spectra shows broadening and vanishing of the signals in the presented region.

Quite different is the behavior of pep-VI & VII-PEG. The same 5 µl does not cause extreme broadening for conjugate pep-VI & VII-PEG (**Fig. 41**). In the case of pep-VII-PEG signals broaden and partially vanish with each titration consequently up to 20 µl. For pep-VI-PEG, 10 µL are required to cause strong line broadening. Again pep-VI-PEG show quite broad signals in NMR spectra suggesting aggregation in the solution. But potentially this aggregation is less prominent as for pep-I-PEG and this conjugate is more available for the interaction with NP. In contrast, pep-VII-PEG shows very clear NMR signals suggesting that aggregation is not that prominent for this sequence ensuring higher availability for NP. Also observed changes might be impacted by different speed of interaction with NP, although this issue was not explored in detail in this study.

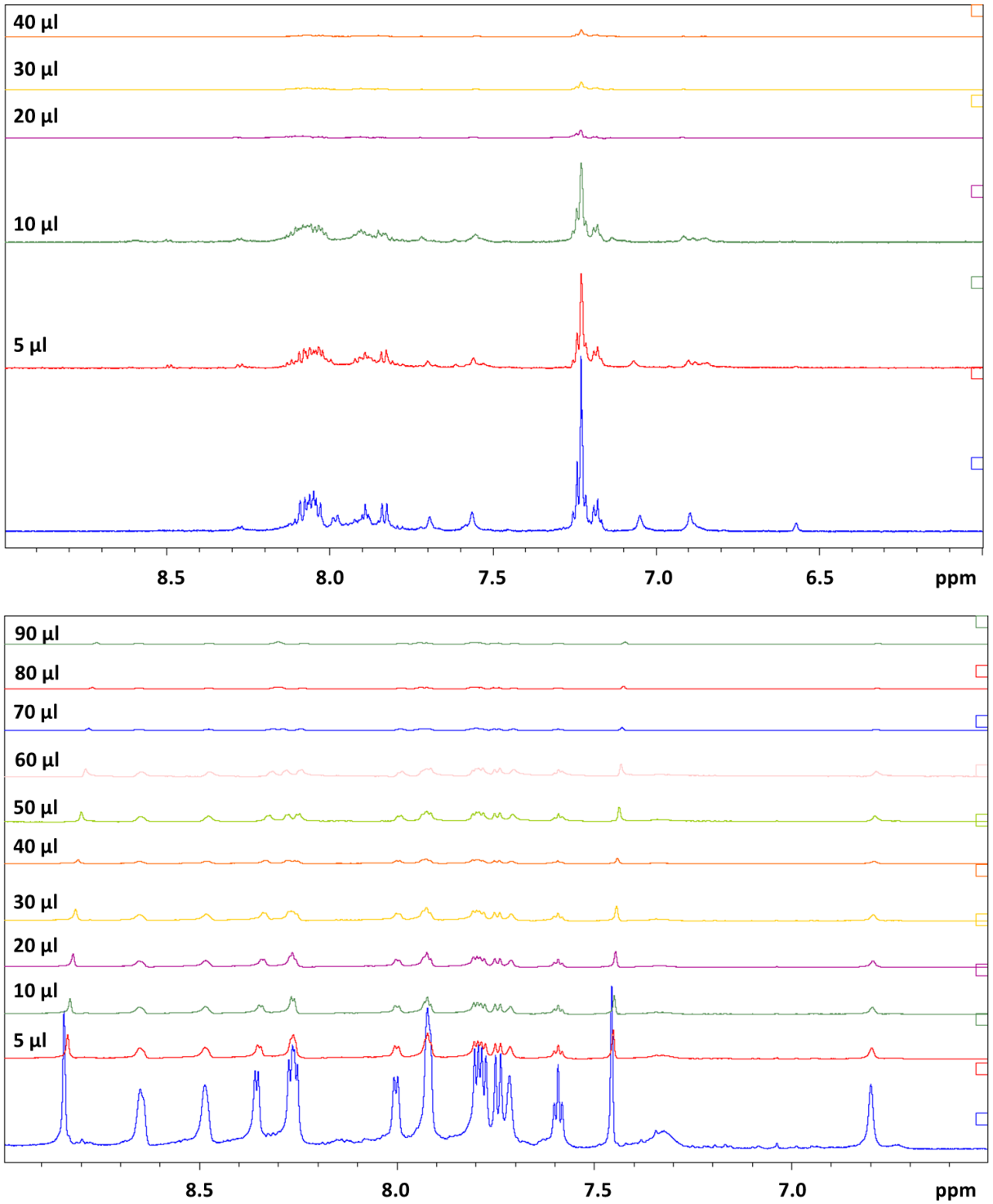

Fig. 41. ^{1}H NMR spectra (NH and aromatic region) of pep-VI-PEG (upper picture) and pep-VII-PEG representing titration serie of MgF_2 NP in the sol form added to the conjugate in 10µl (2 µmol MgF_2) and corresponding changes in the spectra.

3.2.4. Impact of peptide sequence on mechanical properties of composites

Studies based on the predictive tools and analysis of secondary structures of conjugates and interaction of conjugates with nanoparticles together suggest that considered sequences have different affinity to aggregation. Ultimately, the hypothesis should be tested if the self-aggregation tendency and effective interface stabilization would correlate with interface availability of the compatibilizers in composites, which in turn would be reflected in material properties as they are critically affected by internal interface stabilization. To assess the mechanical performance of the composites, tensile testing experiments were performed on the 15wt% MgF_2 filled composites with 0.5 mol% conjugate concentration. This concentration was found from the previous experiments sufficient to achieve an improvement in mechanical properties but small enough that aggregation issues due to high concentration would not dominate the system.

Tensile toughness of stabilized composites from PEO and MgF_2 was monitored as an integral parameter that is sensitively impacted through interface modification. [183] This property of materials is significantly impacted by the compatibilizers and modification of interfaces of materials, which was shown in various reviews. [13, 45, 144] Other properties can be also affected by the interface changes but this impact is more indirect. The changes in toughness can be achieved either through higher stretching capabilities of materials expressed in higher elongation at break values or through improved yield strength allowing the material to absorb more energy and leading consequently to larger area under the curve often accompanied with increased ultimate stress values. (**Fig. 42 b**) Certainly both properties combined together will also contribute to the increase in toughness.

Elongation at break measures how much bending and shaping a material can withstand without breaking. The measured elongations at break values are an indication of the ductility of a polymer. Yield strength of a material is the ability to withstand an applied load without failure or plastic deformation.

Tensile testing experiments performed with composites having different peptide sequences incorporated in a conjugate clearly show that mechanical properties vary and depend on the peptide sequence. Tensile toughness of the studied composites can increase with application of other sequences (**Fig. 42 a**). Intriguingly, pep-VII-PEG leads to composites that show 270 MJ/m^3, the average tensile toughness of 150-170 MJ/m^3 was found for composites with either pep-I-PEG or pep-VI-PEG respectively. The changes in the tensile toughness obviously correlate well with aggregation tendency in the pool of the different conjugates, making it likely that this reflects the fraction of available conjugates to act at the interface.

Elongations at break values are also dependent of peptide sequences and again pep-I-PEG turn out to be the candidate with smallest values among considered sequences (**Fig. 42 c**). Pep-VII-Peg with best solubility shows the highest values for elongation at break in average of 1200%, pep-VI-PEG shows the intermediate performance of 1000% followed by

pep-I-PEG with 900%. The difference in elongation at break between considered conjugates is 300%. Increase in toughness can be directly correlated with the changes in elongation at break. Higher extensibility of composites expressed in higher elongation at break values allows to adsorb more energy. This can be observed in improved toughness values, higher elongation at break values would increase area under the stress-strain curve. This phenomenon is well known in material science and also described for natural materials like silk, where elongation at break values for differently processes silk fibers significantly impact tensile toughness. [45, 184, 185]

Analysis of values for yield strength shows that variation of the sequences from the pool selected by phage display as specific binders does not influence yield strength significantly (**Fig. 42 d**). It would mean that yield strength does not contribute to toughness increase, and this is solely based on the changes of elongation at break parameters. The contribution of only elongation at break to higher toughness would also mean toughness changes are significantly impacted by the interface phenomena meaning that aggregation and corresponding efficiency of conjugate significantly impacts it.

Each of considered sequences turned out surprisingly to be better in terms of their mechanical properties (except yield strength) than an original sequences pep-I-PEG. Pep-I-PEG was selected as the most promising one among selected by phage display based on the adhesion-elution experiments. [24] The fact that pep-I-PEG appeared as the most promising one from washing-elution experiments and turned out to be the less efficient in the mechanical experiments, can be explained by the aggregation issues, which were neglected as a parameter in the washing-elution experiments. The adhesion experiments were based on the measurements of concentration before and after exposure of the conjugates to the inorganic surface and resistance of adhesion to the washing steps. But ability of conjugates and peptides to interact with each other would also lead to higher amount of adsorbed molecules and would significantly influence the adhered amounts.

Composites differ in their toughness and elongation at break depending on conjugate sequences, but yield strength remain unaffected. Interestingly, in the previous experiments performed with pep-I-PEG sequence on the example of 15wt% filled composites, yield strength increased in composites with conjugate addition, but did not change with conjugate concentration changes. The yield strength parameter is also considered in the material science studies as an indicative parameter characterizing strength of binding between the matrix and the filler modified by coupling agents, compatibilizers or grafting. [183] Based on that, one can consider yield strength as a parameter indirectly indicating the strength of peptide binding to the inorganic surface. Simultaneously it means that different peptide sequences provide comparable binding between the matrix and the filler. The assumption is that peptides bind with the same strength, but this conclusion cannot be drawn from these experiments. It is possible that the forces of interaction between the peptides and particles similar to each that the differences are not large enough to create difference on the macroscopic level in the material.

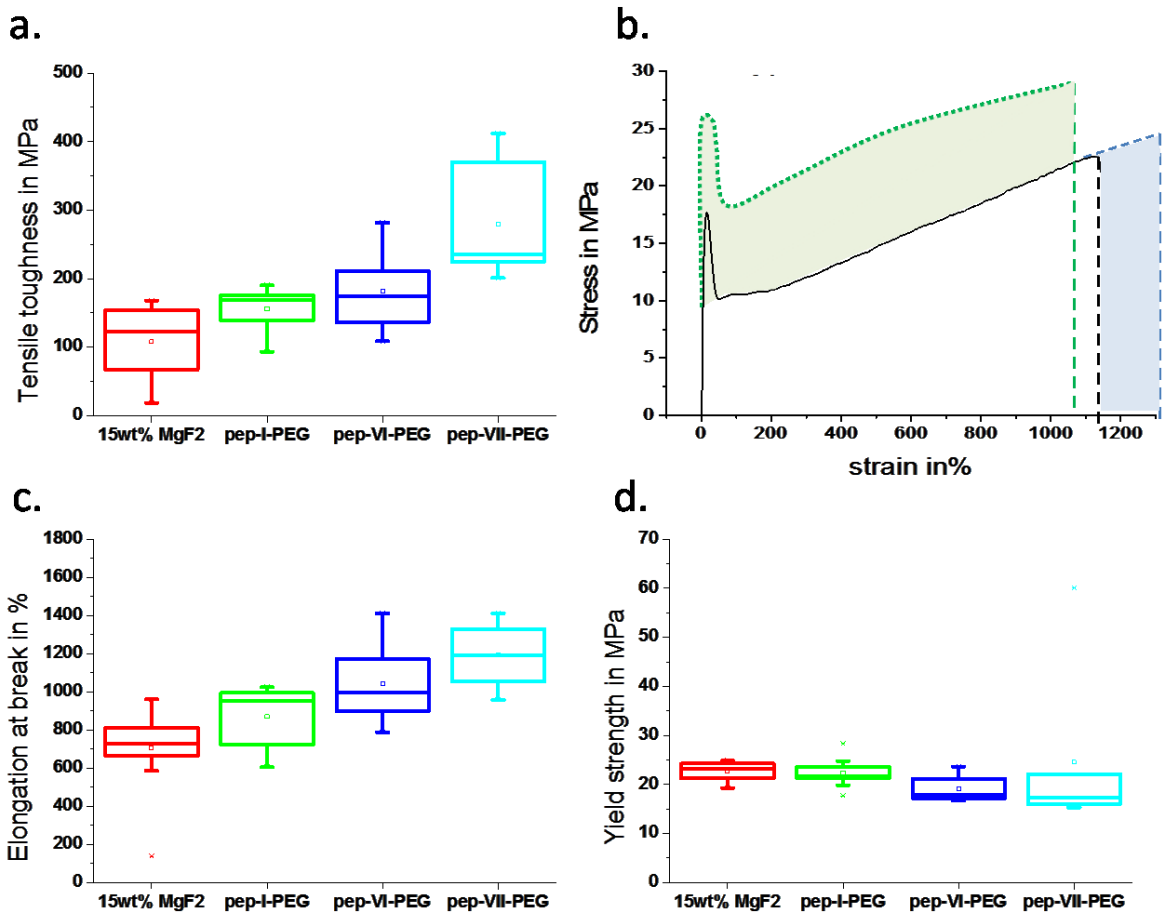

Fig. 42. Mechanical properties of composites containing 15wt% MgF_2 and 0.5 mol% of conjugates pep-I-PEG, pep-VI-PEG, pep-VII-PEG. Changes of toughness (a), elongation at break (c) and yield strength (d) are presented. Tensile toughness is calculated as area under the stress-strain curve. (b) shows typical stress-strain curve and the ways to improve toughness through elongation at break (blue) or yield strength (green).

3.2.5. Summary

This study shows that the affinity of peptides to interact with themselves significantly impacts recognition events of inorganic surfaces. Peptides can be categorized in good and poor soluble based on the results for the solubility prediction of peptides (**Fig. 43, I).** Peptides with poor solubility have much higher tendency to form aggregates (**Fig. 43, II).** The smaller the affinity for peptide-peptide interaction, the higher the availability of peptide sequences for an inorganic surface. As proven in this study, sequences with low solubility due to aggregation are less efficient in surface recognition and following material science applications (**Fig. 43, III)**. This differentiation cannot be done during the phage display screening itself and needs to be performed afterwards. Utilization of predictive tools for estimation of peptide solubility and aggregation behaviour simplifies significantly selection of most appropriate candidates from the pool of sequences identified in the screening. This finding represents a significant differentiating criterion for the sequences identified by phage display for certain surfaces.

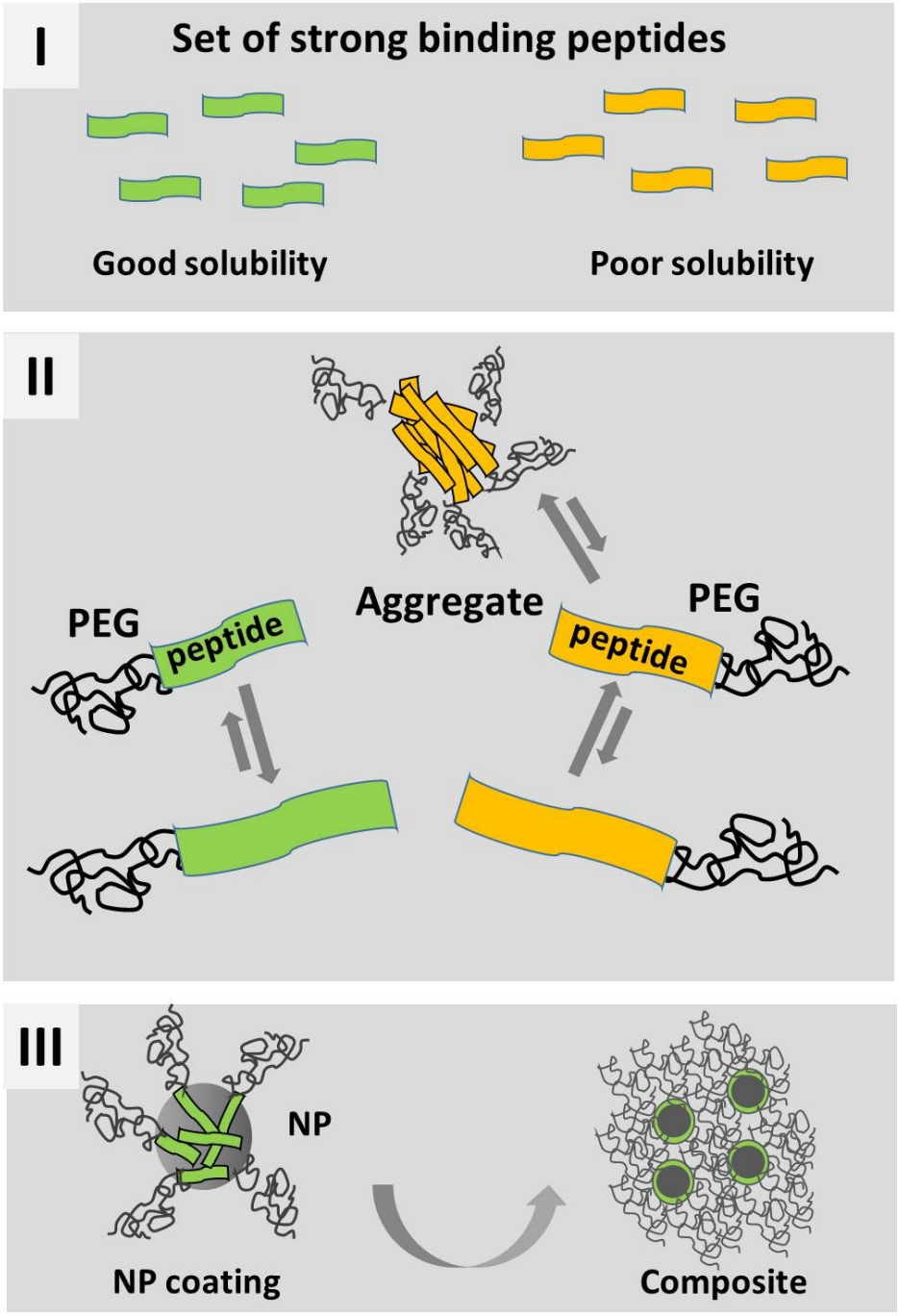

Fig. 43. Schematic representation of difference in tendency to peptide-peptide interaction and aggregation for sequences selected by phage display as binders for a given inorganic surface. Sequences can be differentiated based on their solubility in good and poorly soluble ones. (I) Peptides with good solubility interact with a target surface, while for poorly soluble peptides tend to interact with them self and build aggregates (II). Both types of sequences were used in form of peptide-PEG conjugates for NP coating and dispersion in polymer matrix leading to a hybrid material (III). Picture was adapted from reference [176]

3.3. NMR study of peptide – nanoparticle interactions

In the previous chapters, it was discussed what is the impact of peptide-polymer conjugates on the composite material, but the ways how different peptides interact with the MgF_2 particles remain unclear. This section will be dedicated to the advanced NMR analysis aiming to gain a more in depth understanding of interaction type of conjugates with the surface and to address the question of the role of particular amino acids in the interaction. For this analysis, the best performing sequence pep-VII-PEG (Gly-Ser-Pro-Lys-His-Asn-Leu-Asp-Met-Val-Lys-Met-Met-PEG_{3200}) was selected.

Dried out of the sol MgF_2 particles were added to the system and 2D NMR spectra was recorded before and after addition of particles. 5mg of the conjugate were dissolved in deuterated methanol. Selection of methanol d_3 as a solvent was predetermined by the following reasons. Original nanoparticles exist and are stable in the metabolic solution in a form of sol. This fact defined selection of the solvent media for the experiments for composites development. Having all experiments with composites performed in methanol, the same solvent was selected for NMR study. Additionally, solid particles are stable in methanolic solution and do not sediment, while it was the case in water.

Addition of particles may cause changes in pH, which can significantly impact the interaction of peptides with the nanoparticle surface. Upon addition up to 4 mg particles, pH changes in the moderate range: from 4.7 to 3.7. Taking into account pKa values for residues, only aspartic acid could be influenced in this range and shift in NH region for this residue could be additionally caused by pH changes. Maintaining of pH would be possible in a buffer solution, but absent stability of particles in water solution and sedimentation did not allow performing these experiments.

For this study to the mathanolic (d_3) solution of conjugate MgF_2 particles was added in a solid form (2 mg) and TOCSY spectra was recorded before and after addition of NP. **Fig. 44** represents superimposed TOCSY spectra of conjugate before and after NP addition. The upper picture focuses on the shifts for NH protons and lower picture specifically indicates shifts in aliphatic region with black triangles. Shifts in TOCSY spectra clearly indicates that several amino acids residues are involved in the peptide-MgF_2 interactions. The total chemical shift perturbation calculated out of spectra is presented in the **Fig. 45.**

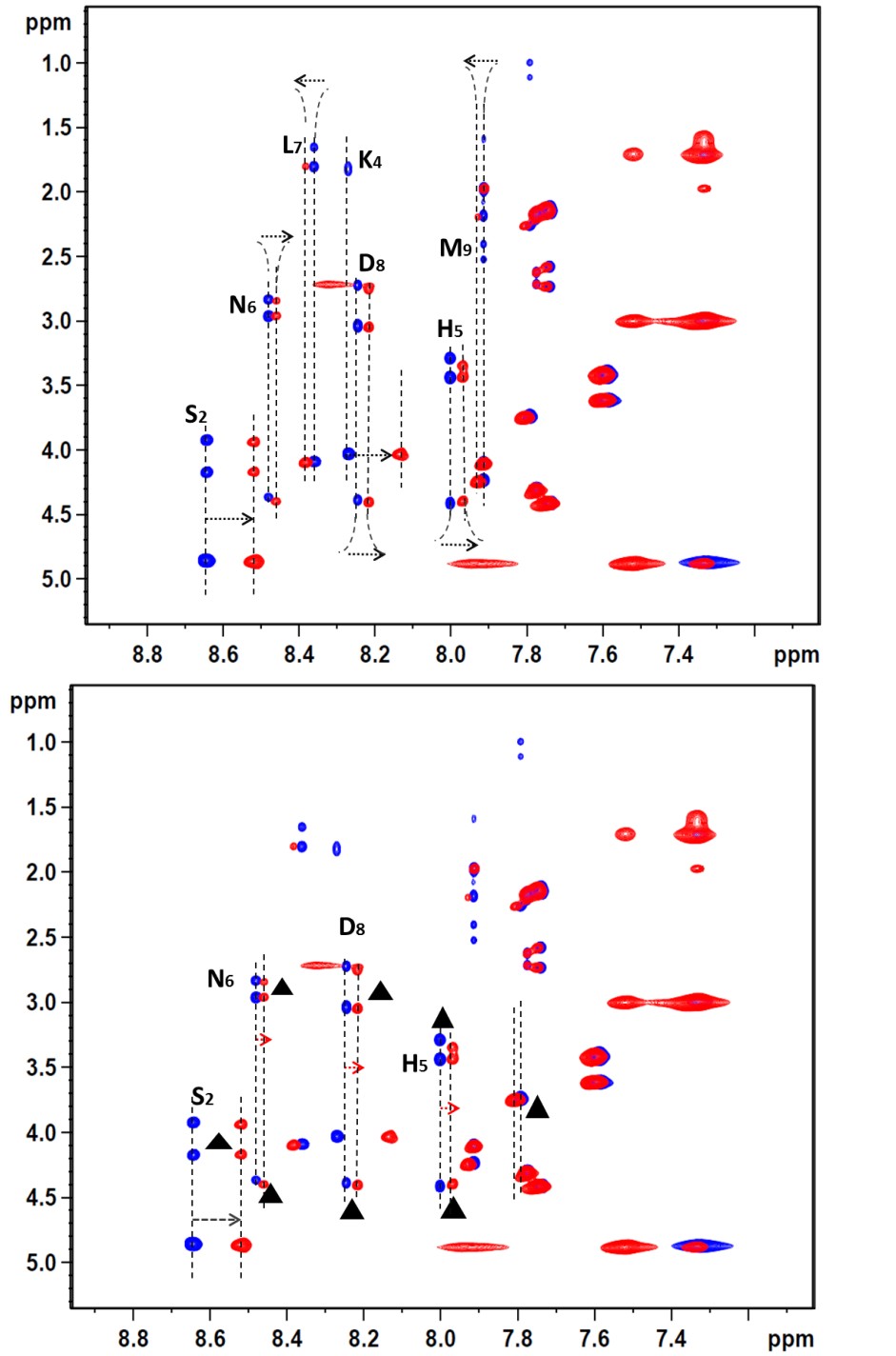

Fig. 44. Superimposed TOCSY spectra of NH and aromatic region of pure pep-VII-PEG in methanolic solution d3 before (blue signals), and after addition of 2 mg of MgF_2 NP (red signals). Dotted red lines with arrows in-between represent shift for spin system position (interaction of NH protons) of a certain amino acids marked with single letter code. Shifts of other protons after NP addition are marked with black triangles. Both spectra are identical, upper pictures represents only shift for spin system position, lower picture shows shifts of other protons of amino acids. Two separate pictures are presented for clarity purposes.

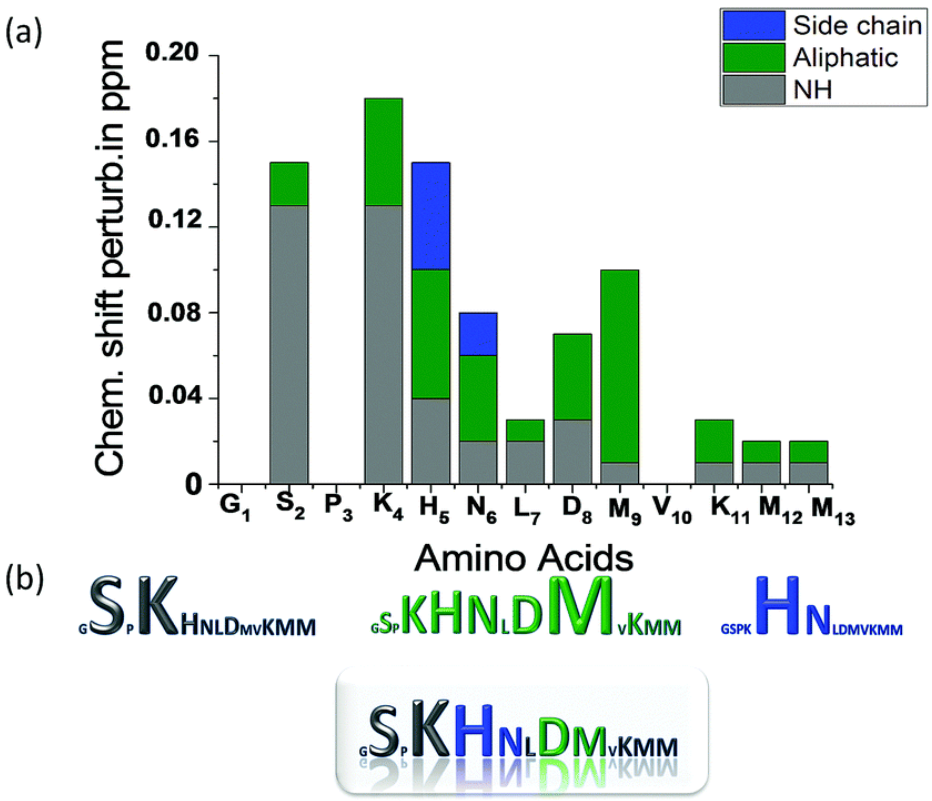

Fig. 45. Total chemical shift perturbation of conjugate signals upon addition of NP revealing interaction modes via backbone (grey), polar side chain (red) and unipolar side chain (blue) contacts to occur depending on residues (a) The perturbation represented a total value calculated from shift in NH, aliphatic and side chain protons irrespective of shift direction out of NMR spectra. Interaction mode motif analysis (b) showing schematically the importance of residue for different contact modes and the overall contact profile (b, inset bottom). Figure was adapted from the reference [27]

Particular evidence for contacts can be assigned to a double cationic segment close to the N-terminus, where Ser2, Lys4 and His5 provide most contributions. However, with less intense shifts also several other contacts are present e.g. Met9, Asp8 and Asn6. Minor contributions are found at the PEGylated C-terminus were Lys11 and Met12&13 are positioned.

Most significant shifts in the NH region experience Serine and Lysine in the 4th position, both shift to lower ppm over 0.1 ppm. As these residues should be not affected by slight pH change and therefore these changes can be considered as a sign for involvement of these residues into the binding event. All other residues except Gly, Pro and Val evidence small shifts 0.01-0.04 ppm and seem to provide small contribution from their NH protons. Nearly all residues with smaller shifts shifts also to lower ppm, only methionine at the 9th position and Leucine show very minor shift to higher ppm. NH_2 protons of Lysine (4th) are not visible in the original TOCSY spectra, but becoming visible after addition of nanoparticles. This fact would suggest that Lys is involved in the interaction and upon binding become “fixated” in its position, what makes his NH_2 side chain protons visible. The same phenomenon was not observed for Lys 11, suggesting no significant contribution to binding.

Also close proximity to PEG $_{3200}$ could also explain this fact, that PEO can hinder side chains of Lys 11th for the interaction with the surface.

All the residues apart Gly, Pro and Val show again shifts in aliphatic region upon addition of nanoparticles, which again supports the statement that many of residues in the sequences are involved in the interaction and cause the shift in TOCSY spectra. Shift cannot be caused by small changes in pH, specially taking into account the fact that aliphatic protons are much less sensitive to pH changes. In opposite to the shift in NH region, where Ser and Lys showed the most prominent shift, in aliphatic region, most of protons shift come from Methionine (9th) followed by comparably equal shifts by Lys4, His and Asp and Asn. The chemical shift perturbation in aliphatic region in overall smaller then observed for NH region and is in the range of 0.04 - 0.09 ppm. It is worth to note that the same amino acids show shift as NH as aliphatic region, suggesting that these shifts have its origin in the interaction nature with the surface and are not originating from pH sensitivity.

Only two residues contribute to the interaction with their side chain protons as Asn and His. Both experienced cumulative shifts up to 0.04 ppm. The biggest contribution for Serine and Lysine (4th position) are coming mainly from NH protons, while chemical shift perturbation for others mainly is driven by shift for aliphatic protons and side chain for Histidine and Asparagin.

Analysis of NMR spectra revealed a set of residues responsible for binding of considered sequences pep-VII-PEG to the surface of NP. Interestingly the correlation of these results with previous published studies revealed that magnesium fluoride complexes in enzymes involved in phosphoryl transfer reactions show similar set of residues as Lys, Asp, Asn and Ser involved in the interaction. [186, 187] Apart consideration of binding motifs for magnesium fluoride surface, the involvement of His in the binding was already mentioned in several publication as the residues quite often involved in binding to different inorganic surfaces. [85, 132]

NMR analysis of pep-VII-PEG conjugate interactions with the surface of MgF_2 particles shows that 10 out of 13 residues are involved into binding process, evidencing multipoint, multimode interactions, which might explain the strong and robust binding of this sequence to filler particles. Ser2, Lys4 and His5 provide the biggest contribution to the binding taking into account chemical shift perturbation measured by NMR. The type of amino acids in the sequences and their degree of involvement to establish the binding suggests that binding is dominated by the electrostatic interactions.

4. Conclusion

This work was inspired by natural hybrid materials such as bone and nacre. An intriguing concept evident in these biomaterials is the utilization of proteins that are able to specifically recognize inorganic surfaces acting as ‘‘interfacial glue’’ and allowing very efficient mediation of interface between inorganic and organic components. This thesis is dedicated to the exploration and transfer of this recently explored structural principle of biomaterials – biomolecules at interface - to synthetic hybrid composites. This study shows that the concept of interface biomolecules is applicable to synthetic composites allowing significant improvement of mechanical properties. Peptide-polymer conjugates used as a simplified version of protein-based interface molecules are able to act as a tailor-made compatibilizer in the material and act simultaneously as a stabilizer of nanoparticles in the polymer matrix. This finding represents a new application of peptide-polymer conjugates as compatibilizers for hybrid materials.

Application of peptide-polymer conjugates allowed improving mechanical properties of final composites making them stiffer and tougher simultaneously. Improved stiffness expresses in 2-3 times higher elastic modulus values achieved through compatibilizer addition. Structural studies on composites revealed that conjugates cause aggregation suppression ensuring transition from larger to smaller aggregates with rising conjugate concentration, this transition is called size effect. Correlation of composite structure with changes of mechanical properties revealed that size effect is responsible for improvement of elastic modulus, as elastic modulus is sensitive to size changes and corresponding distribution of the filler specially in the nanometer range. Together with improvement in stiffness, toughness increased, expressed in higher elongation at break values. Performed studies suggest that improvement of toughness is driven by the size effect too.

Stiffness and toughness improved with the increasing conjugate concentration up to a certain level, beyond which it leads to the deterioration of both properties. Studies on the conjugate behavior revealed that at high concentrations conjugate start to interact with each other and lead to formation of self-assembled structures. These structures increase in size with the rising conjugate concentration and act as distorting point in the polymer matrix lowering stiffness and toughness to the level of unstabilized composites.

Comparison of different peptides sequences, identified previously as specific binders to MgF_2 particles, shows that the affinity of peptides to peptide-peptide interaction impacts recognition events of inorganic surfaces. The smaller the affinity for peptide-peptide interaction and aggregation, the higher the availability of peptide sequences for an inorganic surface. Sequences with high solubility can be proved to be more effectively available for interface stabilization and ultimately leading to composites with 200% improved toughness. In opposite, sequences with low solubility due to aggregation are less efficient in surface recognition and consequently less efficient compatibilizer identified through lower tensile

toughness values in comparison to the well soluble peptide sequences at the same concentration. This correlation represents relevant differentiating factor for the sequences identified by phage display for certain surfaces. Utilization of predictive tools for estimation of peptide solubility and aggregation behavior simplifies selection of most appropriate peptide sequences out phage display screening.

The way how the conjugate interact with the surface of nanoparticles was revealed using NMR analysis. NMR study on the best performing sequences identified 10 out of 13 amino acids residues involved into the interaction, allowing the strong and robust binding of this sequence to filler particles. The type of amino acids in the sequences and the degree of involvement to establish the binding suggests that binding is dominated by electrostatic interactions.

This work shows that it is possible to transfer an architectural principles of biomaterials to the synthetic systems, opening a big space for variation of components and correspondingly of properties of final materials. Nevertheless, it is becoming clear that transfer of one principle of biomaterials to the synthetic systems does not give improvement in mechanical performance, which biomaterials evidence. The outstanding mechanical performance is achieved by a very sophisticated interplay of different architectural principles and mechanisms applied together, which can be an inspiration for next class of bioinspired materials.

5. Outlook

This work shows that the concept of interface biomolecules can be transferred to synthetic composites allowing significant improvement of mechanical properties. Peptide-polymer conjugates used as a version of protein-based interface molecules are able to act as a tailor-made compatibilizer. The core of bespoke concept is adhesion of peptides in a conjugate form to the inorganic surface. Application of NMR analysis allows getting more insight into the interaction mechanism, but still the understanding of interaction of different peptides with the inorganic surface remains limited. Some aspects of these issues such as aggregation tendency and solubility were addressed in this work, but the question of the strength of interaction and if there are any differences between selectively binding peptides in the forces of interactions remained untouched. Clear and easy applicable strategies for sequence differentiation and selection would speed up and allow better control of peptide interactions with surfaces for targeted applications. A possible solution for this challenge could be single molecule force spectroscopy, which currently allows measurements of forces between molecules located at the cantilever and the surfaces underneath.[188, 189] It could be realized in the following set-up: peptide can be attached to the cantilever of the AFM microscope and cantilever can approached to the surface, which could contain a layer of inorganic materials and then pulled away. Analysis and averaging of thousands of measured force curves allows obtaining average force of interaction. The information about the forces of interaction of different peptides with the same surface could provide a significant contribution for the understanding of nature of this interaction and biotic-abiotic interface in general.

More information about the ways of interaction and understanding the mechanisms behind it would allow to replace peptides/conjugates by polymers, which mimick peptides with their functional groups. This could allow possibly recognition of surfaces by polymers.

Some aspects of peptide interaction with inorganic surfaces can be addressed by advanced analytical techniques. One of such aspects is the analysis of core-shell structures, possibly consisting of particles covered by peptides layers. Such structures could be visualized by the TEM coupled with Electron Energy Loss Spectroscopy (EELS). This nanoanalytical method has its advantages over the Energy Dispersive X-Ray spectroscopy (EDX) technique, allowing acquiring chemical information on the nanometer level, by measuring loss in energy of electrons interacted with the matter and mapping it for different elements. These studies could potentially answer the questions about the thickness of formed shells and behavior of peptides at the interface. More understanding and insight into the mechanisms hidden behind toughness changes and interfaces in the materials can be acquired through performance of in-situ WAXS studies combined with tensile testing accompanied by Raman spectroscopy.

This thesis focused only on the application of one structural principal derived from biomaterials to the synthetic composites. The next steps for the elaboration of the studied principal would be redesigning of system considering again examples of materials from

nature. The filler of the composites can be also optimized using filler of different shapes. Again for this topic nature represents a big source of inspiration as natural materials utilize extremely successfully inorganic components of different shapes, where elongated elements such as rods seem to be more preferred.[190] One more approach would be increasing degree of filling and reducing percentage of matrix, potentially achieving composites consisting only of filler distributed in the compatibilizer. This is again inspired by biomaterials e.g nacre, where high percentage of filler can be incorporated into the system without deterioration the mechanical properties of the final composite.[4]

Apart certain form of components, 3D arrangement of components seems to be of a crucial importance.[191] Lots of information is available about architecture of natural composites, but transfer of this knowledge to the synthetic systems still remains problematic. This difficulty has its origin in the fact that this type of arrangements found in biomaterials is very difficult or nearly impossible to achieve in the synthetic systems due to lack of technologies and manufacturing methods.

Considering the state of the art knowledge about the biomaterials and the examples of composites mimicking biomaterials, the most promising way for development of future bioinspired materials would be combining different structural principles of biomaterials in one material. Nature all the time uses interplay of several mechanisms to achieve an outstanding mechanical performance.

6. Experimental part

6.1. Materials

For conjugate synthesis

Sidechain-protected L-amino acids Fmoc-Gly-OH, Fmoc-Thr(*t*Bu)-OH, Fmoc-Gln(Trt)- OH, Fmoc-Tyr(*t*Bu)-OH, Fmoc-Ala-OH, Fmoc-Ser(*t*Bu)-OH, Fmoc-Lys(Boc)-OH, Bromotrimthylsilane (TMSBr), *N*-methyl-2-pyrrolidone (NMP, 99.9+%, peptide synthesis grade), 2-(1H-benzotriazole-1-yl)-1,1,3,3- tetramethyluronium hexafluorophosphate (HBTU), 1-Hydroxybenzotriazole (HOBt), dichloromethane (DCM, peptide grade), used for peptide synthesis, were purchased by IRIS Biotech (Marktredwitz, Germany). NMP was filtrated before use, DCM was distilled, other chemicals were used as received. *N*,*N*-diisopropylethylamine (DIPEA, peptide grade), piperidine (peptide grade), Trifluoracetic acid (TFA, peptide grade), 2,5-dihydroxybenzoic acid (DHB) (MALDI MS matrix) were purchased by Acros Organics (Thermo Fisher Scientific) (Watham, MA, USA). Guanidinium chloride (99.5%) was obtained from Carl Roth (Karlsruhe, Germany). TentaGel® PAP resin (PEG attached peptide resin, loading: 0.24 mmol g-1; Mn = 3200) was obtained from Rapp Polymere (Tübingen, Germany).

DMSO d6 with 99,9% purity and methanol d_3 were obtained in ampules from Deutero GmbH (Kastellen, Germany).

For composites preparation

PEO, used as a matrix with Mn=900.000, PEG for reference experiments with Mn= 3000; methanol (≥99.6%) and magnesium turnings (99.98%) for magnesium fluoride synthesis were obtained from Sigma Aldrich (St. Luois, U.S.A). Hydrogen fluoride (>99%) was obtained from Solvay Fluor (Hannover, Germany)) and used as methanolic solution. Methanol (LC-MS grade) was bought from Acros Organics.

6.2. Methods

6.2.1. Synthetic methods

6.2.1.1. Synthesis of MgF_2 particles

The synthesis of MgF_2 was performed under inert atmosphere (Ar) using Schlenk techniques. Mg turnings (2.43 g, 100 mmol) were dissolved in 500 mL dried methanol to yield $Mg(OMe)_2$ at a concentration of 0.2 M. To initiate fluorolysis a stoichiometric amount of HF dissolved in methanol was slowly added under vigorous stirring to give the desired product. Aging for 2-3 weeks resulted in optically clear sols. The particles were obtained from a Kemnitz Group at Humboldt University Berlin, where they were synthesized according to a specific procedure, developed by the group, leading to a material with very high specific surface area.

6.2.1.2. Conjugate synthesis

Solid-phase supported peptide synthesis (SPPS): Peptide-PEO conjugates were synthesized according to standard Fmoc procedures with side-chain protected amino acids (AA). ABI-Fastmoc protocols (single coupling for 1st to 10th AA, double coupling afterwards, capping; *N*-terminal acetylation followed in NMP using TentaGel® PAP resin. AA coupling was facilitated by HBTU/DIPEA. After final deprotection the resin was washed thoroughly with NMP and DCM. The cleavage was done with TFA/TMSBr/Thioanisol = 94:1:5 (v/v/v) for 2 x 1 h. The conjugates were precipitated in cold diethyl ether and centrifuged. The dried conjugates were dissolved in water with guanidine hydrochloride (0.1% w/v). Conjugates are then dialyzed against Milli-Q® water for ca. 4 days with change of solvent at least three times per day.

6.2.2. Preparation of composites

Composites consist out of three components: inorganic component – MgF_2 nanoparticles present in a sol form, peptide-polymer conjugate and PEO with the molecular weight of 900 000 g/mol as a matrix.

The preparation procedure of the composites consisted of two steps: solution casting and hot pressing (Fehler! Verweisquelle konnte nicht gefunden werden.). An appropriate amount of the peptide-polymer conjugate was dissolved in methanol (LC-MS grade), after

which a certain amount of MgF_2 sol was added. Different amount of the nanoparticles were tested: 10, 15, 30 wt%. Also several concentrations of the conjugate were added starting from 0.5 mol% and covering the range to 8 mol%. Mol% (mole fraction for the component multiplied by 100 %) are calculated in relation to MgF_2 The mixture was stirred for a minimum of 4 hours to allow the conjugate to adhere to the inorganic surface. A 5 wt% aqueous solution of PEO (900 kg mol^{-1}) was added and all components were mixed for another 30 min. The total volume of the prepared solution was 5 ml. The solution was cast into a small bowl and the material was dried under an extraction hood for 12 hours. The material that was obtained after the solution casting step was not suitable for the mechanical testing experiments, which require even and homogeneously thick composites. A hot pressing procedure was applied to prepare composite materials in order to eliminate unevenness in thickness of composites (**Fig. 46**).

Hot pressing of the composite materials was performed on the SPECAC machines from Specac Limited (Orington, UK) at a constant temperature of 70°C. First the composites are heated without load for 3 min, then 1 ton of pressure is applied for 1 min, followed by 2 tons of pressure for 3 min. The composites are cooled down in the special cooling device with circulating water for 2 min. To prevent sticking of the composite to the pressing plates and to ensure quick release from the pressing plates, Polyethylene terephthalate (PET) foil is used. The average thickness of the composite ranges from 80-120 µm. The thickness of the composite can be varied using different rings. The duration of a the cooling step may differ depending on the composition. Composites containing higher content of inorganic filler needed longer cooling (3 min) and composites with higher conjugate content (6 mol%) needed faster cooling (1.5 min).

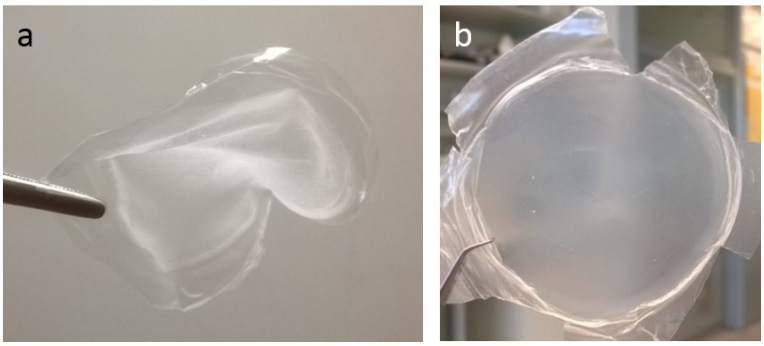

Fig. 46. Composites before (a) and after hot pressing step (b).

6.2.3. Mechanical testing of composites

To evaluate a mechanical performance, tensile testing experiments were performed for all composites described in the thesis.

Samples in a typical bone form a length of 18 mm and a width of 6 mm were punched out of pressed composites (**Fig. 47 a**). Normally 4 bone shaped samples can be made out of

one composite. The stamp was also developed and produced in the Max-Planck Institute of Colloids and interfaces (MPI) (**Fig. 47 b**) The size of the samples was constructed in such a way that it fits to small tensile testing devices used in this study. The thickness of the samples was in the range of 100-150 μm.

Experiments were performed on the two tensile testing machines: small devices for precise measurements of small forces and at standard Zwick machine.

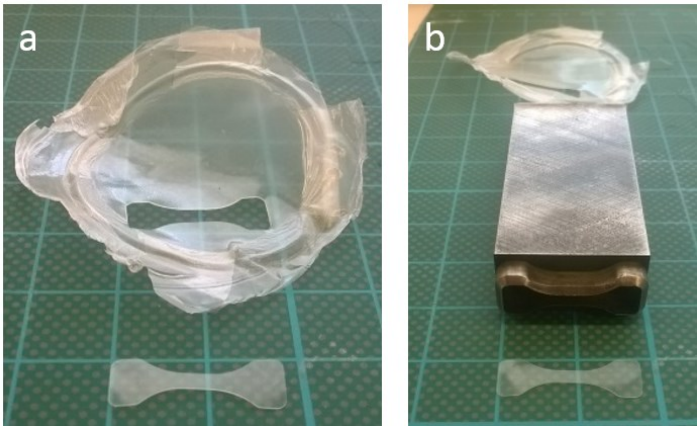

Fig. 47. Samples in a typical bone form stamped out of composite (a) and stamp used for the experiments (b).

For the tensile testing experiment, a sample is fixed in the holder of the mashine. The sample will be pulled apart with the constant speed, while the needed force and the displacement will be measured.

Stress σ is defined as the force F per unit area action on a plane in the material having a cross section area A. The normal stress is calculated by dividing the force by the area.

$$\sigma = F/A$$

Due to effect of stresses, the relative shape changes, called **strain**. In normal cases, strain ε is a function of length change *L* to the initial length (L_0).

$$\varepsilon = L\text{-}L_0/\ L_0$$

Plotting of stress against strain lead to a stress-strain curve, which describes mechanical response of material to the applied stress. Analysis of each curve allows calculating the mechanical properties of the studied material. The parameters derived from the curve correspond to the characteristic points in the diagram (**Fig. 48**).

The initial linear part of the stress-strain curve is characterized by a linear relation between stress and strain, in accordance with Hooks law and often corresponds to a reversible strain. From this linear part the **elastic modulus** (modulus of elasticity, Young's Modulus) is calculated.

$$E = \Delta\sigma/\Delta\varepsilon$$

Elastic modulus is a measure of the stiffness of a material. A solid material will deform when a load is applied to it. If it returns to its original shape after the load is removed, elastic deformation occurs. In the range where the ratio between load and deformation remains constant, the stress-strain curve is linear.

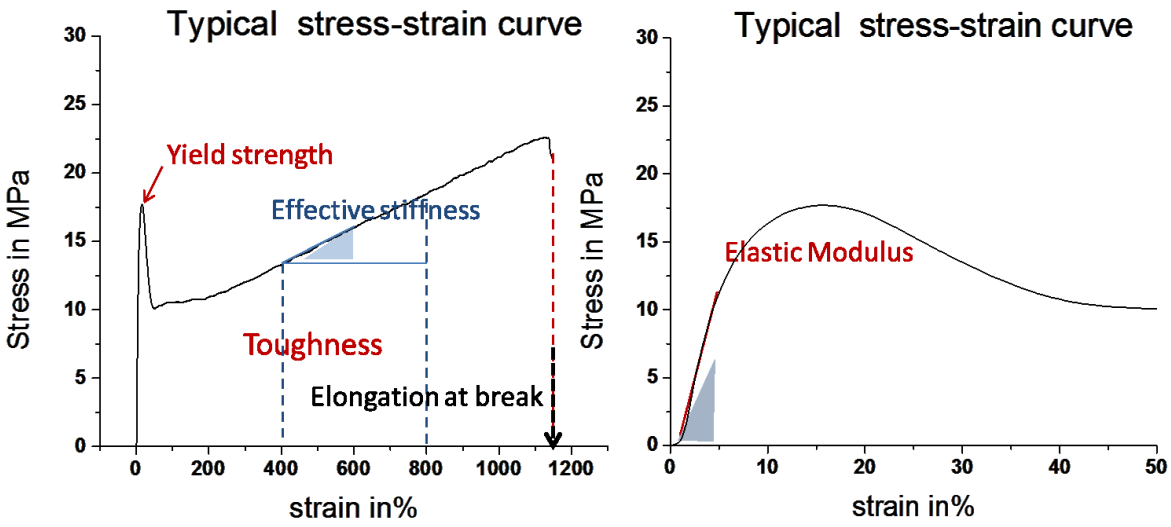

Fig. 48. Typical stress-strain curve obtained for composites with indication for yield strength, toughness, elongation at break and effective stiffness (left) and enlarged area of the curve (0-50% strain) showing elastic modulus, which is calculated as a slope of the stress-strain curve and indicated as triangle (right).

In materials science, the strength or **yield strength** of a material is the ability to withstand an applied load without failure or plastic deformation. It is the material property defined as the stress at which a material begins to deform plastically. Prior to the yield point the material will deform elastically and will return to its original shape when the applied stress is removed. Once the yield point is passed, some fraction of the deformation will be permanent and non-reversible. It represents the upper limit to forces that can be applied without permanent deformation.

Elongation at break is the ratio between increased length and initial length after breakage of the tested specimen at a controlled temperature. It is related to the ability of a plastic specimen to resist changes of shape without cracking. The elongation is calculated as the relative increase in length and expressed in %.

Toughness is the ability of a material to absorb energy and plastically deform without fracturing. One definition of material toughness is the amount of energy per unit volume that a material can absorb before rupturing. Toughness requires a balance of strength and ductility. Is is calculated as area under the stress-strain curve.

All the obtained values for mechanical properties will be resented in a form of box diagram. The purpose of this representation type is to show the range of all obtained values, which might be for some interpretation of importance e.g. how broad or how narrow the distribution of the values. 25-75% of all obtained values are located within the box. The higher and the lowest points are minimum and maximum values correspondingly. The

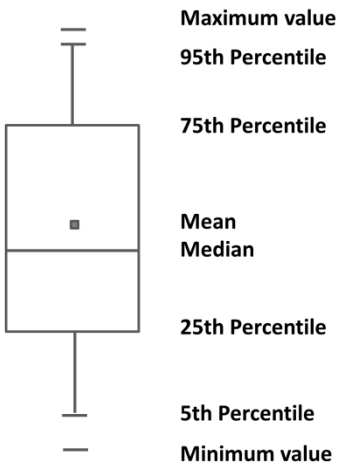

Fig. 49. Schematic representation of a box diagram, which will be used for the representation of obtained values.

Median is the value separating the higher half of a data sample, from the lower half. For a data set, it may be thought of as the "middle" value. The **mean** of a set of observations is the arithmetic average of the values.

Tensile testing

Tensile experiments were performed with two tensile testing devices: custom-made tensile testing stage developed and constructed at MPI and universal ZWICK tensile testing machine (**Fig. 50 a, c**).

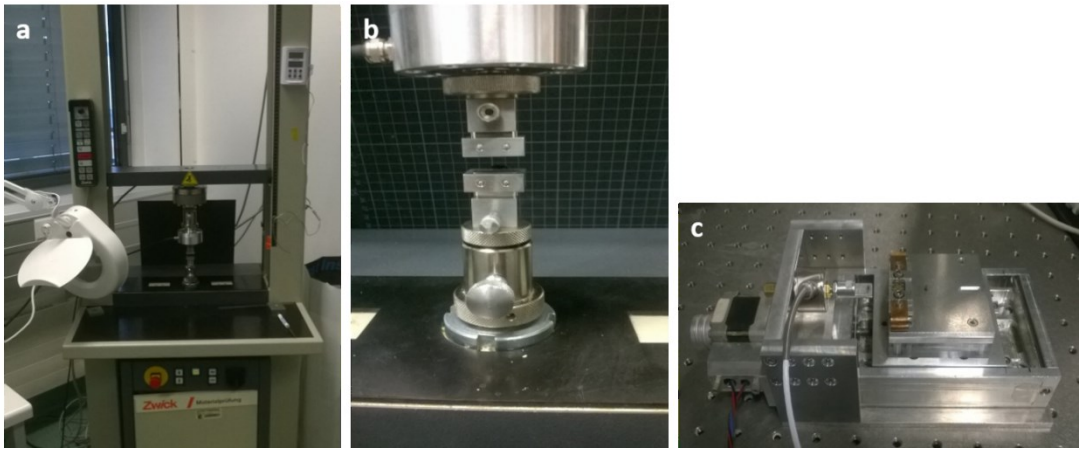

Fig. 50. Zwick tensile testing machine (a) with specially developed holder for thin and small samples (b) and small tensile testing machine developed at MPI for combined experiments in microscopes (c).

The small tensile testing machine was designed in such a way that it can fit to the E-SEM to perform combined experiments. These experiments were performed but the obtained information did not provide substantial contribution to this work. A very similar stage was also developed for in-situ X-Ray experiments with tensile testing at the synchrotron BESSYII, which was the goal of the collaborative project on the same samples. Due to these reasons, the small tensile testing stage was employed for the first experiments to allow compatibility of results and elastic modulus was calculated based on these experiments. Additionally, very slow movement was possible and the test was done with the speed of 5 µm/s. Being a small device, the custom-made tensile testing stage has a limited moving distance, which turned out to be a serious limitation for our study with ductile PEO. This fact led us to use ZWICK testing machine, where the limitation due to small moving distance is excluded. To be able to test small samples in a big ZWICK device, a new holding device was developed for small and thin samples (**Fig. 50 b**). The ZWICK testing device was mainly used to be able to test samples until they break and to calculate toughness.

The small tensile testing machine was also equipped with the videoextensiometry, a supporting tool that allows more précised measurements of displacement. It is done by the matching of two parallel lines of the tool with lines of the polymer, which are placed on the bone-like sample before the experiment (**Fig. 51**). They were placed in such a way that the borders of bone form remain parallel. The position of the lines is registered in the program, so displacement can be precisely measured. There was a video control of experiments, meaning for every fifth measurement point, a picture was taken in order to be able to control and check results after experiments. The composites were stretched until the black lines were out of the optical microscope field view.

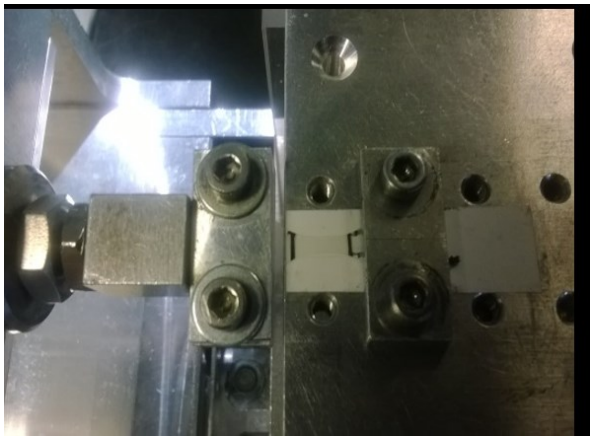

Fig. 51. Composite sample inside a small tensile testing machine.

The load cells used for measurements were max for 50N for both devices. The measurements on the ZWICK were performed with the speed of 200 mm/min.

8 samples were tested per concentration in each type of experiment. Samples showed very high sensitivity to the defects especially for energy to failure experiments. The stress is calculated as the engineering stress, or maximum force divided by initial effective cross-sectional area. The correction for the true stress was not done, due to very different

behavior of the composites depending on the concentration and not applicability of the correction to all curves. Elastic modulus was calculated based on the data obtained with videoextentiometry. The modulus is calculated as the initial slope of the stress strain curve. Linear fit to evaluate elastic modulus was performed with Origin Lab. Obtained values were involved in the calculation only if the obtained fit was better than 98%. Tensile toughness was calculated as area under the stress-strain curve. For all measurements 6 mm was the initial length, which corresponds to the parallel middle part of the bone-shaped sample, Effective stiffness was calculated as slope at the interval between 400-800% strain to catch the differences in the behavior of conjugates.

6.2.4. Analytical methods

6.2.4.1. Scanning electron microscopy (SEM)

Scanning electron microscopy pictures were done with two devices: an environmental scanning electron microscope (E-SEM) Quanta 600 FEG (FEI Europe) and a Jeol LEO 1550 (Oberkochen, Germany). E-SEM was used to screen over several samples and was particularly suitable to obtain overview pictures with low magnification. The accelerating voltage was 5-7 keV and no sputtering was needed to generate the micrograph. A JEOL high resolution scanning electron microscope (HR-SEM) was used to obtain micrographs with the high magnification. In contrast to E-SEM, sputtering was essential and the samples were sputtered with Pt/Pd before measurement. Electron microscopy pictures were done with acceleration voltage 9 keV, which was revealed as the optimal accelerating voltage for these samples. Lower voltage level did not eject enough backscattered electrons to generate sufficient contrast. As a drawback of a quite high voltage level, samples can be quickly damaged during measurement leading to cracks visible in micrographs.

Micrographs were obtained in secondary (SE) and backscattered electron (BSE) mode. Backscattered electrons were detected in order to distinguish the particles from the matrix. In comparison to the secondary electrons, backscattered electrons are sensitive to the different elemental composition and penetrate more deeply into the sample, providing information not only about the surface. MgF_2 particles will appeared as bright spots.

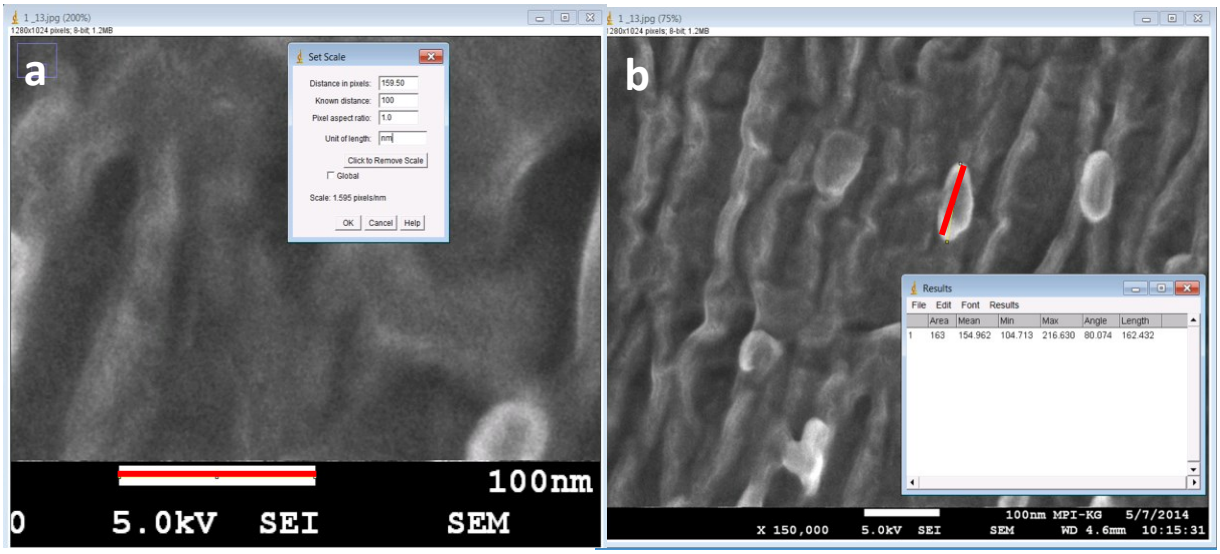

Fig. 52. Procedure of particle-size estimation performed with Image J, where first the scale bar of the picture is measured and depicted as red line to know number of corresponding pixels (a) and followed by the measuring the number of pixels for a particle (shown in red) (b) and calculating the size.

To build up the particle-size distribution diagram, 200 particles were randomly selected per sample. The size of the particles was measured with Image J. First the scale bar on the picture is measured to determine how many pixels it represents (**Fig. 52 a**). Then the objects on the micrograph are measured (**Fig. 52 b**). Knowing how many pixels objects on the micrograph and scale bar contain, solving the proportion, the size of objects can be calculated in nm. It should be noted that this procedure does not consider the particles below 10 -20 nm due to limits in resolution of the method.

6.2.4.2. Transmission electron microscopy (TEM)

Electron microscopy: Transmission electron microscopy (TEM) measurements were performed on the Philips CM200 (Eindhoven, Netherlands) operating at 200 keV accelerating voltage in bright field (BF) mode. Specimens for imaging by TEM were prepared by evaporating a droplet of composite solution onto carbon coated copper grid.

6.2.4.3. Atomic force microscopy (AFM)

AFM micrographs were obtained on the combined Raman and AFM device Alpha 300 A of WiTec (Ulm, Germany). Small pieces of composites were fixed on the glass slides and 5*5 µm squares were obtained from different spots on the sample.

6.2.4.4. Circular dichroism spectroscopy (CD)

Circular dichroism (CD) spectroscopy is a form of light absorption spectroscopy that measures the difference in absorbance of right- and left-circularly polarized light (rather than the commonly used absorbance of isotropic light) by a substance. The phenomenon of circular dichroism is very sensitive to the secondary structure of polypeptides and proteins. It has been shown that CD spectra between 260 and approximately 180 nm can be analyzed for the different secondary structural types: alpha helix, parallel and antiparallel β-sheet, turn, and other.

Circular dichroism spectra were recorded on a JASCO 700 (JASCO Germany, Gross-Umstadt, Germany) spectrometer using quartz cuvetts of 1 cm path length at 25 °C. The measurements were performed for 1mg/ml concentration in water in the region of 190 to 260 nm

6.2.4.5. IR spectroscopy

Attenuated total reflection Fourier-Transform-Infrared Spectroscopy (ATR FTIR) analysis was performed on a FT-IR spectrometer Vertex 70 from Bruker Optik GmbH (Leipzig Germany) with diamond ATR crystal with a resolution of 4 cm^{-1}. Conjugate was measured in a solid state and solid composites were investigated after hot pressing. All the samples were measured in vacuum.

6.2.4.6. NMR spectroscopy

NMR study was performed on Bruker AVANCE II 500 and AVANCE 600. ^{1}H, standard 2D experiments (ROESY; TOCSY) and DOSY measurements were performed on Bruker AVANCE II 500. Titrations experiments were realized on Bruker AVANCE 600. Various solvents were used for experiments. Conjugates with strong tendency to aggregation were dissolved in DMSO d_6 99,8%. Methanol d_3 was used for all other conjugates.

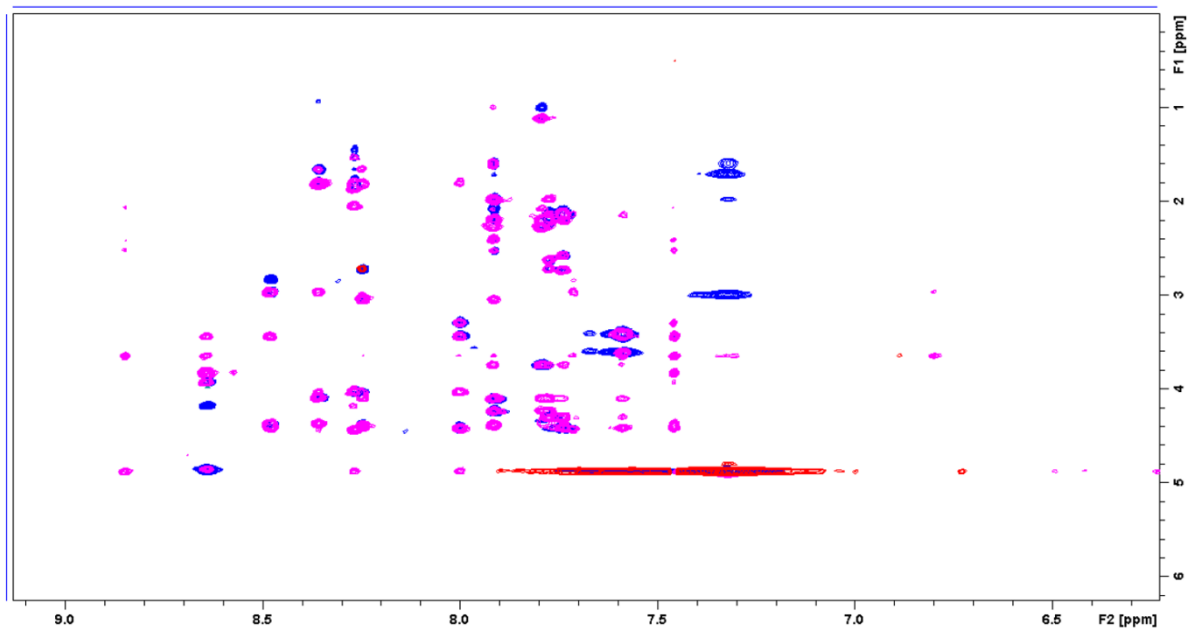

Fig. 53. Superimposed TOCSY and ROESY spectra of conjugate 6, where blue peaks represent TOCSY and pink peaks belong to ROESY measured in methanol d_3.

The assignment of protons in ^{1}H spectra of peptides is essential to be able to monitor role of amino acid residues in the interaction of peptides with the inorganic surfaces. For the assignment of the protons in 1H spectra of peptides application of 2D homonuclear NMR techniques is necessary.

TOCSY: *Total Correlation Spectroscopy*

A TOCSY experiment contains all cross peaks due to protons of the same spin system. Protons from different amino acids always belong to different spin systems, because there is no scalar coupling across the amide bond. Analysis of spin systems allows deciding to which type of amino acids the spin system belongs. Possible criteria are: Occurrence or absence of methyl groups, length of the spin system and positions of chemical shifts in the spin system. On the horizontal axis there is the chemical shift of H(N), on the vertical axis there are chemical shifts of α, β, γ protons. By knowing the chemical shift of α, β protons we can find amino acids. The chemical shift of amide proton cannot be considered as very reliable information, because it varies depending on the conditions of the experiment.

NOESY and ROESY

Cross peaks in the **NOESY** (Nuclear Overhauser Effect Spectroscopy) are due to dipolar couplings resulting from interactions of spins *via space* and hence only depend on the distance but not on the number of intervening bonds. Dipolar couplings are averaged to zero in solution but give rise to the very important relaxation phenomena, one of which is

the NOE (nuclear Overhauser effect, NOE) - The strong dependence of the cross peak intensity on the distance separation explains why this parameter is the most useful for structure determination. The NOESY not only contains peaks from which distances are derived for the structure calculation but is also heavily used during the sequential resonance assignment process. Considering that scalar couplings are restricted to protons within a single amino acids, sequential correlations (correlations between protons of neighboring amino acids) need to be taken from the NOESY. The greatest problem associated with NOE is the existence of “zero-crossing region”, where NOE becomes increasingly small. It typically occurs for mid-size molecules of around 1000-2000 Da depending on solution conditions. To solve the problem **ROESY** (Rotating Overhausser Effect spectroscopy). ROESY is similar to NOESY, except that the initial state is different. Instead of observing cross relaxation from an initial state of *z*-magnetization, the equilibrium magnetization is rotated onto *x* axis and then spin-locked by an external magnetic field so that it cannot evolve. ROESY has a different dependence between the correlation time and the cross-relaxation rate constant. In NOESY the cross-relaxation rate constant goes from positive to negative as the correlation time increases, giving a range where it is near zero, whereas in ROESY the cross-relaxation rate constant is always positive

For assignment two spectra (TOCSY and ROESY) will be acquired and superimposed (**Fig. 54**). Due to the reason stated above, for all conjugates ROESY spectra were acquired, as all conjugates with 13 amino acids residues fall in the range of 1000-2000 Da. The information from both spectra will be used to find positions of certain amino acids and connect with another one. TOCSY peaks will give information about which amino acid it is, while sequential correlations (correlations between protons of neighboring amino acids) need to be taken from the NOESY.

It is very important for interpretation to find the starting point, which often is not the last and not the first amino acid in the sequence. It should be amino acid, which has a very specific chemical shift for some H and should be only one in the given sequence in the best case. As far as one amino acid abbreviated as A is defined by finding the spin system in TOCSY spectra, ROESY peak can be found on the same horizontal line as TOCSY peak. Following A+1 amino acid can be found. Looking for the ROESY peak on the vertical line of TOCSY peak previous A-1 amino acid can be identified. (**Fig. 54**).

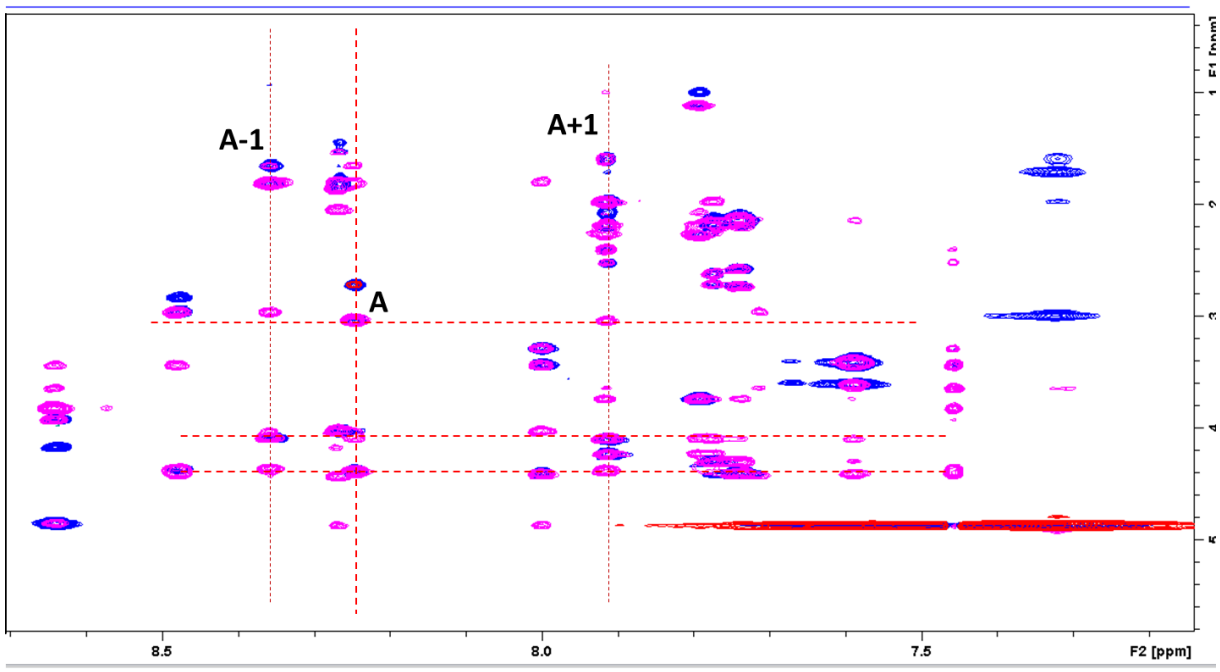

Fig. 54. Example of assignment of the protons in peptide based on TOCSY and NOESY spectra.

Titration experiments

Titrations experiments were realized on Bruker AVANCE 600 in methanol d_3 used in ampules of 0.75 ml in volume. At first, 5 mg of each of the studied conjugate were mixed with the methanol d_3. Some of the conjugates were soluble and they were used for further analysis excluding the insoluble samples. From the obtained samples 2D spectra (TOSCY and ROESY) were measured to be able to assign protons. The same amount of sol particle was stepwise titrated to each conjugate sample. These experiments were performed to analyze the amount of particles, which can be accommodated by the system indicating the availability of particular conjugate for an interaction. At the same time these experiments are not correctly designed to evaluate the residue involved in the interaction. The reason for it is presence of not deuterated methanol in the particles sol, whose amount increases with the rising amount of titrated sol particles. This leads to dilution effect causing shifts in NMR spectra. Due to this the titration experiments were performed with the best soluble conjugate and particles were added in methanolic conjugate solution in a solid form. After each addition of conjugate ^{1}H NMR spectra was recorded to be able to monitor shifts in the spectra caused by the interaction of conjugate with the inorganic particles.

Diffusion Ordered Spectroscopy (DOSY)

The Diffusion Ordered Spectroscopy technique (DOSY) is applied to monitor molecular interactions. DOSY is a NMR technique that provides a semiquantitative estimation of the translational diffusion coefficient (D) of a given molecule or mixture of molecules. Self-diffusion arises from the random Brownian motion of molecules driven by thermal energy of the system. In an isotropic system the average displacement of a molecule over time in three dimensions is zero, the mean square displacement is non-zero such that the distance travelled by a molecule in a single direction during a period t is

$$Z= (2Dt)^{1/2}$$

Here z represents the root mean square distance travelled as a time average for many molecules. The diffusion coefficient is therefore a measure of the rate of mean square displacement of a molecule and consequently has units of m^2s^{-1}.

This diffusion coefficient is directly related to the hydrodynamic radius of the molecular entity and therefore, to the molecular weight (MW) of the species in solution. Characterization rate of diffusion of molecules or their complexes may be related to their size and shape, providing insight into molecular structures and their solution behavior. This behavior is regulated through the Stokes–Einstein equation, which is for sphere

$$D= k_bT/6\pi\eta r_s$$

where k_b – Boltzmann constant, T-absolute temperature, η – solution viscosity, r_s- stokes Radius of the sphere.

This equation demonstrates that the diffusion coefficient is inversely related to the size(radius) of the diffusing species, as one might expect that larger molecules or complexes will tend to exhibit smaller diffusion coefficients. Diffusion coefficients may be extracted directly from regression fits of the peak intensity versus gradient strength.

In fact, the typical representation of DOSY corresponds to a simple 2D spectrum in which one dimension corresponds to chemical shifts and the second to log D. Moreover, if a complex is formed, the extracted diffusion coefficient for the supramolecular complex will be different to that of the individual interacting entities, since the MW of the complex will be larger, as well as the corresponding hydrodynamic radius. However, the proper interpretation of DOSY data requires the establishment of a proper experimental protocol. In fact, different factors and parameters need to be considered, from the chemical nature of the entity to be studied to the acquisition and processing parameters.

6.2.4.7. Mass spectrometry

Matrix-assisted laser desorption/ionization (MALDI) is a soft ionization technique used in mass spectrometry, mostly used for analysis of large organic molecules or biomolecules. After mixing of the sample with the suitable matrix, pulsed laser irradiates the sample triggering ablation and desorption of the sample and matrix material. Ionized molecules protonated or deprotonated can be accelerated and guided to the mass spectrometer for analysis. Mostly single charged ions are produced.

Mass spectrometry was done by Bruker autoflex III smartbeam with matrix assisted laser desorption/ionization (MALDI) and time of flight detector (MALDI-ToF-MS) (Rheinstetten, Germany). For MALDI-MS the samples were dissolved in water, while the matrix was dissolved in water/acetonitrile/TFA (1:1:0.1%, v/v/v). As was 2,5-dihydroxybenzoic acid (DHB) used. Matrix and sample solutions were mixed directly on the plate in a ratio of 2:1. It was measured in linear positive mode.

6.2.4.8. X-Ray diffraction (XRD)

Diffraction patterns were obtained with a Bruker D8 from Bruker AXS (Karlsruhe, Germany) device with Cu Kα (λ=1.5418 Å) radiation equipped with a scintillator detector. To determine the degree of crystallinity, data evaluation was performed by using the software program EVA. The degree of crystallinity of a polymer can be investigated by comparing the area under the crystalline peaks to the total scattered intensity.

6.3. Conjugate characterization

Ac-GTQYYAYSTTQKS-PEG (pep-I-PEG)

Mass spectrometry

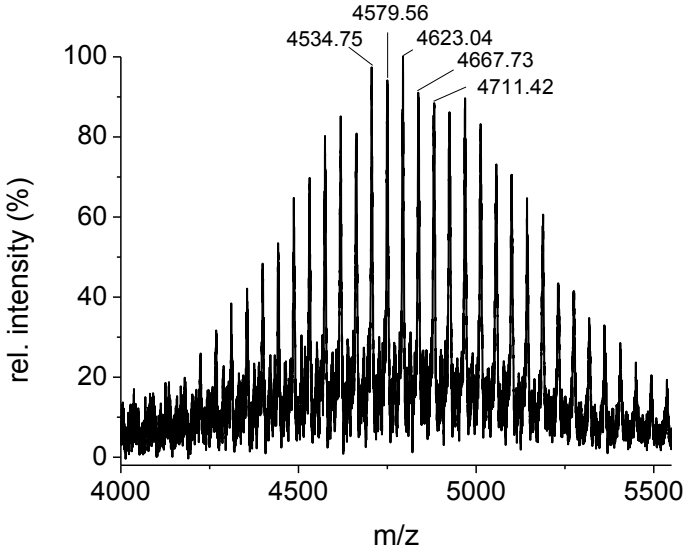

Figure S1. MALDI-ToF-MS of conjugate.

MS (MALDI-ToF) *m*/*z*: $[M + H]^+$ calc, 4579.06 g/mol; found, 4579.56 g/mol; calculated with 69 EO units.

$[M + Na]^+$ calc, 4601.06 g/mol; found, 4601.35 g/mol; (the underlying peak)

Δm = 44.05 g/mol, characteristic for repeating ethylene oxide (EO) units;

The mass can be assigned within ± 0.5 g/mol accuracy.

NMR

$G_1T_2Q_3Y_4Y_5A_6Y_7S_8T_9T_{10}Q_{11}K_{12}S_{13}$ -PEG

^{1}H NMR (500 MHz, DMSO-d_6, δ): 0.97 (3H, CH_3γ T_2), 1.02-1.10 (6H, γ CH_3 $T_{9,}$ T_{10}), 1.17 (2H, γ, δ K12), 1.28-1.37 (3H, γ, δ K12), 1.72-1.65 (2H, Hß A6, δ K12), 1.94-1.72 (4H, Hß Q_3, G_{11}), 1.98-2.18 (4 Hγ Q_3, G_{11}), 2.56-2.98 (8H, Hß + CH S_8, Y_4; Y_5, Y_7), 3.21 (2H, Hß S_{13}), 3.51 (326H, CH_2 PEO), 3.59 (1H, Hß S_8), 3.63-3.67 (3H, CH Y_4; Y_5, Y_7), 3.78 (1H, Hα G_1), 3.97 (1H, Hß T_2), 4.01-

4.12 (2H, Hß $T_{9,}$ T_{10}), 4.37-4.15 (9H, Hα T_2 Q_3 Q_{11} A_6 T_{10} K_{12} S_{13} Y_4 T_9), 4.39-4.46 (2H, Hα Y_5 S_8), 4.50 (1H, Hα Y_7), 5.03- 5.14 (2H, OH S_8 S_{13}) 6.58-6.66 (6H, Hε Y_4 Y_5 Y_7), 6.76-6.83 (2H, NH_2δ Q_3 Q_{11}), 6.92-6.98 (2H, CHδ Y_4), 6.99-7.05 (4H, CHδ Y_5 Y_7), 7.22-7.29 (2H, NH_2δ Q_3 Q_{11}), 8.21—8.13 (2H. NH G_1 S_8), 8.07-7.94 (5H, NH $K_{12,}$ A_6 Q_3 Q_{11} Y_5), 7.79-7.71 (3H, NH Y_7 T_{10} T_2), 7.94-7.81 (6H, NH S_{13} T_9 $Y_{4;}$ 1H ε NH^{3+} $K_{12,}$ 2 H δ NH2 Q_3 Q_{11})

IR spectroscopy

FT-ATR-IR: *v* = 3283 (*m*; Amid A); 2890 (*w*, C-H); 1624; 1665; 1697 (*s*, Amid I); 1518 (*m*, Amid II); 1467 (m), 1343 (m), 1280 (m). 1241 (m), 1203 (w, Amide III); 1145 (w); 1104 (s); 1062 (w); 962 (m); 842 (m); 722 (vw, Amide IV).

Ac- GAKTSYTYQSTYQ – PEG (pep-I-PEG*)

Mass spectrometry

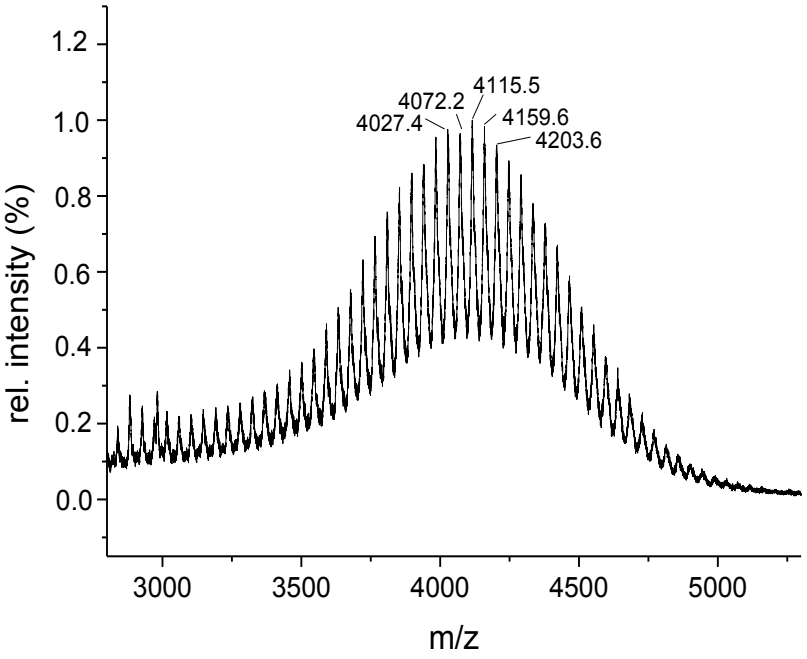

Figure S2. MALDI-ToF-MS of scrambled conjugate.

MS (MALDI-ToF) *m*/*z*: $[M + Na]^+$ calc, 4115.6 g/mol; found, 4115.5 g/mol; calculated with 59 EO units.

Δm = 44 g/mol, characteristic for repeating ethylene oxide (EO) units;

The mass can be assigned within ± 0.1 g/mol accuracy.

NMR

$G_1A_2K_3T_4S_5Y_6T_7Y_8Q_9S_{10}T_{11}Y_{12}Q_{13}$-PEG

^{1}H NMR (500 MHz, DMSO) δ 8.55 (s, 1H) NH S_5 , 8.18 (s, 1H) NH Y_6, 8.11 – 7.90 (m, 8H) NH $A_2K_3T_4$ T_7Q_9 Q_{13}, 7.83 (d, *J* = 8.0 Hz, 2H) NH Y_8 T_{11}, 7.74 (s, 1H) NH S_{10}, 7.24 (s, 1H) δNH_2 Q_9 , 7.03 (dd, *J* = 26.7, 8.4 Hz, 6H) δCH Y_6 Y_8 Y_{12}, 6.78 (s, 1H) δNH_2 Q_9, 6.62 (dd, *J* = 8.5, 2.8 Hz, 2H) δNH_2 Q_{13}, 5.11– 4.91 (m, 5H) OH S_5 S_{10} T_7 T_{11} T_4, 4.39 - 4.17 (m, 11H) αH $A_2K_3T_4S_5$

$T_7Y_8Q_9S_{10}T_{11}Y_{12}Q_{13}$, 3.99 (s, 2H) ßH T_7 T_{11}, 3.60 - 3.43 (m, 328 H) CH_2 PEG, ßH S_5 A_2 S_{10} K_3T_4 αH G_1 3.26 – 3.08 (m, 2H) ßH $S_{10}S_5$, 2.91 (m, 3H) ßH Y_6 Y_8 Y_{12}, 2.78 – 2.60 (m, 3H) ßH Y_6 Y_8 Y_{12}, 2.15 – 2.01 (m, 3H) ßH Q_9 Q_{13}, 1.88 - 1.72 (s, 4H) ßH Q_9 Q_{13} γH Q_9, 1.38 – 1.19 (m, 4H) γ, δ H K_3, 1.17 – 0.94 (dd, 3H) γH T_7 T_{11} T_4

IR – spectroscopy

ATR-IR: *v* = 3273(*m*; Amid A); 2880 (*m*, C-H); 1625; 1661; (*s*, Amid I); 1535 (*m*, Amid II); 1463 (m), 1356 (m), 1343 (m), 1280 (m). 1243 (m), 1200 (vw, Amide III); 1092 (m); 960 (m); 861(m)

Ac- GGLNQVLRIPSFI – PEG (Pep-VI-PEG)

Mass spectrometry

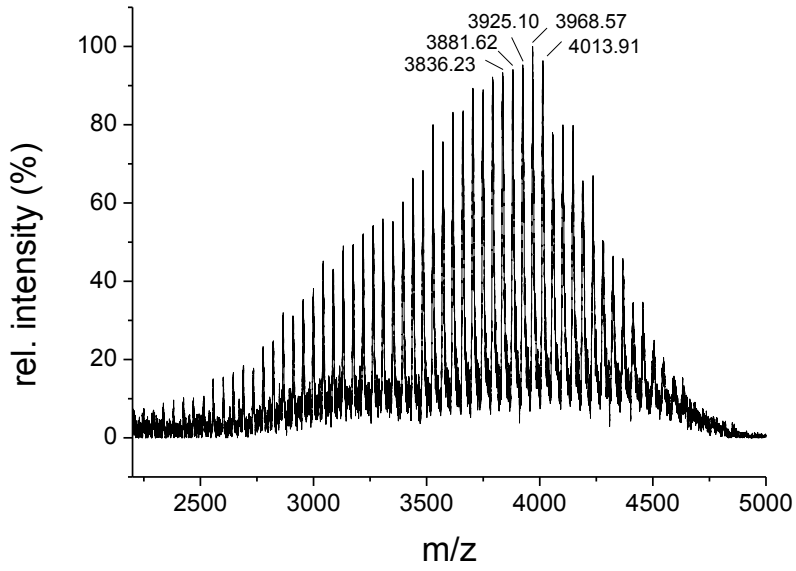

Figure S3. MALDI-ToF-MS of Pep-VI-PEG.

MS (MALDI-ToF) *m/z*: $[M + H]^+$ calc, 3968.57 g/mol; found, 3968.57 g/mol; calculated with 58 EO (m=44.05 g/mol) units.

The mass can be assigned within ± 0.0 g/mol accuracy.

NMR

$G_1G_2L_3N_4Q_5V_6L_7R_8I_9P_{10}S_{11}F_{12}I_{13}$ -PEG

^{1}H NMR (600 MHz, MeOD) δ 8.29 – 8.26 (m, 1H) NH L_3 , 8.15 – 7.96 (m, 9H) NH S_{11} NH R_8 I_{13} F_{12} N_4 I_9 Q_5 V_6 L_7, 7.89 (tt, *J* = 62.1, 18.5 Hz, 2H) NH G_1G_2, 7.69 (s, 1H) γNH_2 N_4 , 7.56 (s, 1H) δ NH_2 Q_5, 7.27 – 7.16 (m, 7H) 5H Ar F_{12},) δNH_2 Q_5 γNH_2 N_4 7.05 (s, 1H) γNH_2 N_4, 6.89 (m, 1H) δNH_2 Q_5, 5.41 – 5.15 (m, 1H) OH S_{11} 4.62 (s, 1H) Hα I_9, 4.46 – 4.29 (m, 6H) Hα S_{11} R_8 F_{12} L_3 Q_5 P_{10}, 4.17 (t, *J* = 8.4 Hz, 2H) Hα I_{13} N_4, 4.11 – 4.06 (m, 1H) Hα L_7, 3.88 – 3.75 (m, 3H) Hß S_{11} Hß N_4 Hδ P_{10},3.75 – 3.69 (m, 4H) Hß S_{11} Hß N_4 , 3.62 (s, *J* = 4.5 Hz, 470H), CH_2 PEO , 3.56 – 3.47

(m, 4H) Hα G_1 G_2 Hδ R_8 , 3.17 (dd, *J* = 14.6, 4.9 Hz, 1H) Hß F_{12}, 2.97 (m, *J* = 14.3, 8.7 Hz, 1H) Hß F_{12}, 2.84 – 2.66 (m, 2H) Hß P_{10} 2.59 (s, 1H), 2.50 – 2.41 (m, 2H) Hγ Q_5 2.37 – 2.25 (m, 1H) Hß L_3 , 2.17 – 1.75 (m, 10H) Hß I_{13} I_9 Q_5 V_6 L_7 Hγ L_3 $L_{7\,(2)}$ P_{10} Hγ P_{10}, 1.67 – 1.41 (m, 8H) Hß R_8 Q_5, Hδ L_3 Hγ I_{13} I_9 , 1.27 (s, 2H), Hγ R_8 , 1.20 – 1.07 (m, 2H) Hγ I_{13}, I_9 , 0.99 – 0.80 (m, 6H) Hδ I_{13} I_9 (2)L_7 (2)Hγ V_6.

IR spectroscopy

ATR-IR: *v* = 3275(*m*; Amid A); 2884 (*m*, C-H); 1627; 1663; (*s*, Amid I); 1537 (*m*, Amid II); 1464 (m), 1358 (m), 1344 (m), 1281 (m). 1241 (m), 1202 (vw, Amide III); 1095 (m); 962 (m); 863 (m)

Ac- GSPKHNLDMVKMM-PEG (Pep-VII-PEG)

Mass spectrometry

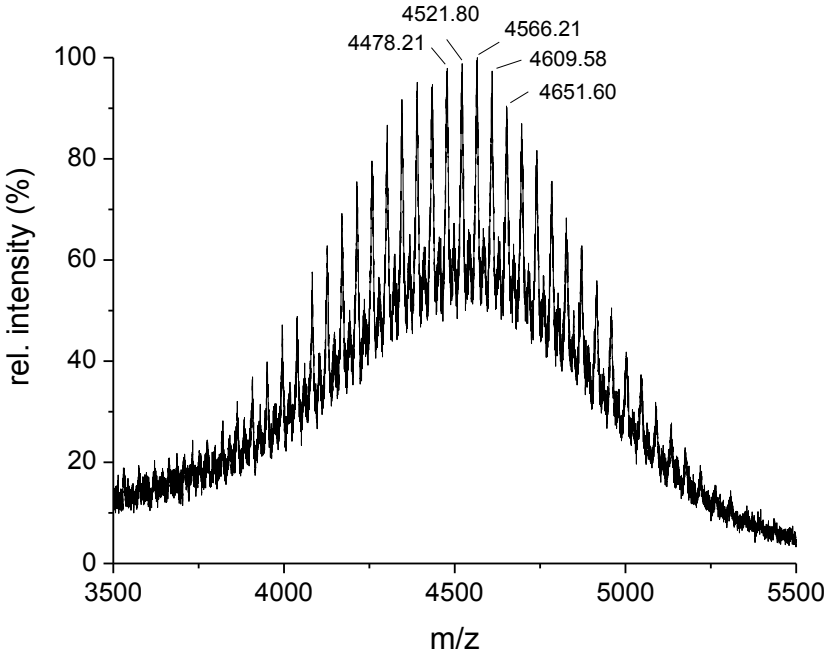

Figure S4. MALDI-ToF-MS of Pep-VII-PEG.

MS (MALDI-ToF) *m/z*: $[M + K]^+$ calc, 4565.27 g/mol; found, 4566.21 g/mol; calculated with 69 EO (m=44.05 g/mol) units.

The mass can be assigned within ± 0.94 g/mol accuracy.

NMR

$G_1S_2P_3K_4H_5N_6L_7D_8M_9K_{11}M_{12}M_{13}$ - PEG

^{1}H NMR (600 MHz, MeOD) δ 8.85 (s, 1H) H_5, 8.65 (s, 1H) NH S_2, 8.48 (s, 1H) NH N_6, 8.36 (d, *J* = 5.0 Hz, 1H) NH L_7, 8.26 (dd, *J* = 14.0, 4.9 Hz, 2H) NH K_4 D_8, 8.00 (d, *J* = 5.6 Hz, 1H) NH H_5, 7.92 (d, *J* = 5.0 Hz, 2H) NH M_9 K_{11}, 7.79 (dd, *J* = 11.2, 6.0 Hz, 1H) V_{10}, 7.76 – 7.70 (m, 2H) $M_{12}M_{13}$, 7.59 (t, *J* = 5.9 Hz, 1H) G_1 , 7.46 (s, 1H) H_5, 7.36 – 7.28 (m, *J* = 11.3 Hz, 1H) Hγ N_6, 6.80 (s, 1H) γNH_2 N_6 , 4.48 – 4.34 (m, 4H) Hα H_5 M_{13} N_6 D_8, 4.33 – 4.28 (m, 1H) Hα M_{12}, 4.26 – 4.21 (m, 1H) Hα M_9, 4.20 – 4.15 (m, 1H) Hα S_2 , 4.14 – 4.06 (m, 2H) Hα K_{11} L_7 , 4.06 – 3.95 (m, 2H)

Hα K_4 P_3 , 3.95 – 3.89 (m, 1H) H_δ P_3 3.80 – 3.72 (m, 2H) Hα V_{10} $H_ß$ S_2,, 3.71 – 3.59 (m, *J* = 8.5 Hz, 301H) CH_2 PEO , 3.48 – 3.38 (m, 3H) Hß H_5 Hα G_1 Hδ P_3 , 3.29 (s, 1H) Hß H_5 , 3.05 – 2.94 (m, 5H) Hß N_6 D_8, Hε K_4 K_{11}, 2.85 (d, *J* = 4.2 Hz, 1H) Hß N_6 , 2.77 – 2.69 (m, *J* = 13.7, 11.8, 4.8 Hz, 3H) Hß D_8 Hγ $M_{12}M_{13}$, 2.66 – 2.61 (m, 1H) Hγ M_{12} , 2.61 – 2.57 (m, *J* = 8.7, 4.9 Hz, 1H) Hγ M_{13} , 2.52 (dd, *J* = 13.3, 6.2 Hz, 1H) Hγ M_9, 2.46 – 2.35 (m, 1H) Hß M_9, 2.30 – 2.25 (m, 1H) $H_ß$ V_{10}, 2.22 – 2.13 (m, 5H) Hß P_3, Hε $M_9M_{12}M_{13}$, 2.11 – 2.03 (m, 5H) Hε M_9M_{12} M_{13}, 1.98 (dd, *J* = 15.5, 7.6 Hz, 2H) Hδ K_4 Hε M_9, 1.89 – 1.42 (m, 9H) Hß K_4 $K_{11}L_7$ Hγ K_4 K_{11} L_7 Hδ K_4, 1.36 – 1.27 (m, 2H) Hγ L_7 K_{11}, 1.12 (d, *J* = 6.9 Hz, 2H) Hγ V_{10}, Hδ L_7 1.02 – 0.89 (m, 4H) Hγ V_{10} Hδ L_7 Hγ K_4 K_{11}

IR spectroscopy

ATR-IR: *v* = 3273(*m*; Amid A); 2884 (*m*, C-H); 1627; 1665; (*s*, Amid I); 1539 (*m*, Amid II); 1468 (m), 1415 (m),1344 (m), 1279 (m). 1243 (m), 1202 (vw, Amide III); 1097 (m); 962 (m); 841 (m).

7. References

[1] Studart AR. Towards High-Performance Bioinspired Composites. Adv Mater. 2012;24:5024-44.
[2] Wegst UGK, Bai H, Saiz E, Tomsia AP, Ritchie RO. Bioinspired structural materials. Nat Mater. 2015;14:23-36.
[3] Munch E, Launey ME, Alsem DH, Saiz E, Tomsia AP, Ritchie RO. Tough, Bio-Inspired Hybrid Materials. Science. 2008;322:1516.
[4] Fratzl P, Weinkamer R. Nature's hierarchical materials. Progr Mat Sci. 2007;52:1263-334.
[5] Peter Fratzl JD, Richard Weinkamer. Materials Design Inspired by Nature: Function Through Inner Architecture. Cambridge, UK: RSC Publishing; 2013.
[6] Studart AR. Turning brittleness into toughness. Nat Mater. 2014;13:433.
[7] Erb RM, Libanori R, Rothfuchs N, Studart AR. Composites Reinforced in Three Dimensions by Using Low Magnetic Fields. Science. 2012;335:199-204.
[8] Munch E, Launey ME, Alsem DH, Saiz E, Tomsia AP, Ritchie RO. Tough, Bio-Inspired Hybrid Materials. Science. 2008;322:1516-20.
[9] Aizenberg J, Fratzl P. Biological and Biomimetic Materials. Adv Mater. 2009;21:387-8.
[10] Fratzl P, Burgert I, Gupta HS. On the role of interface polymers for the mechanics of natural polymeric composites. Phys Chem Chem Phys 2004;6:5575-9.
[11] Smith BL, Schaffer TE, Viani M, Thompson JB, Frederick NA, Kindt J, et al. Molecular mechanistic origin of the toughness of natural adhesives, fibres and composites. Nature. 1999;399:761-3.
[12] Suzuki M, Saruwatari K, Kogure T, Yamamoto Y, Nishimura T, Kato T, et al. An Acidic Matrix Protein, Pif, is a Key Macromolecule for Nacre Formation. Science. 2009.
[13] Ritchie RO. The conflicts between strength and toughness. Nat Mater. 2011;10:817.
[14] Börner HG. Strategies exploiting functions and self-assembly properties of bioconjugates for polymer and materials sciences. Progr Polym Sci. 2009;34:811-51.
[15] Schnitzler T, Herrmann A. DNA Block Copolymers: Functional Materials for Nanoscience and Biomedicine. Acc Chem Res 2012;45:1419-30.
[16] Broecker F, Hanske J, Martin CE, Baek JY, Wahlbrink A, Wojcik F, et al. Multivalent display of minimal Clostridium difficile glycan epitopes mimics antigenic properties of larger glycans. Nat Commun. 2016;7:11224.
[17] Börner HG. Precision Polymers—Modern Tools to Understand and Program Macromolecular Interactions. Macromol Rapid Commun. 2011;32:115-26.
[18] Hartmann L, Börner HG. Precision Polymers: Monodisperse, Monomer-Sequence-Defined Segments to Target Future Demands of Polymers in Medicine. Adv Mater. 2009;21:3425-31.
[19] Günay KA, Klok H-A. Identification of Soft Matter Binding Peptide Ligands Using Phage Display. Bioconjug Chem 2015;26:2002-15.
[20] Klem MT, Willits D, Solis DJ, Belcher AM, Young M, Douglas T. Bio-inspired Synthesis of Protein-Encapsulated CoPt Nanoparticles. Adv Func Mater 2005;15:1489-94.
[21] Li Y, Whyburn GP, Huang Y. Specific Peptide Regulated Synthesis of Ultrasmall Platinum Nanocrystals. J Am Chem Soc. 2009;131:15998-9.
[22] Mandal D, Tiwari RK, Nasrolahi Shirazi A, Oh D, Ye G, Banerjee A, et al. Self-assembled surfactant cyclic peptide nanostructures as stabilizing agents. Soft Matter. 2013;9:9465-75.
[23] Pérez Y, Mann E, Herradón B. Preparation and characterization of gold nanoparticles capped by peptide–biphenyl hybrids. J Colloid Interface Sci. 2011;359:443-53.
[24] Hanßke F, Kemnitz E, Börner HG. Generic Biocombinatorial Strategy to Select Tailor-Made Stabilizers for Sol–Gel Nanoparticle Synthesis. Small. 2015;11:4303-8.
[25] Noack J, Emmerling F, Kirmse H, Kemnitz E. Sols of nanosized magnesium fluoride: formation and stabilisation of nanoparticles. J Mater Chem. 2011;21:15015-21.
[26] Lellouche J, Kahana E, Elias S, Gedanken A, Banin E. Antibiofilm activity of nanosized magnesium fluoride. Biomaterials. 2009;30:5969-78.

[27] Samsoninkova V, Seidt B, Hanßke F, Wagermaier W, Börner HG. Peptide–Polymer Conjugates for Bioinspired Compatibilization of Internal Composite Interfaces: via Specific Interactions toward Stiffer and Tougher Materials. Advanced Materials Interfaces. 2016:n/a-n/a.
[28] Meyers MA, McKittrick J, Chen P-Y. Structural Biological Materials: Critical Mechanics-Materials Connections. Science. 2013;339:773.
[29] Currey JD, Taylor JD. The mechanical behaviour of some molluscan hard tissues. J Zool 1974;173:395-406.
[30] Currey JD. Mechanical Properties of Mother of Pearl in Tension. Proc R Soc Lond B Biol Sci. 1977;196:443.
[31] Jackson AP, Vincent JFV, Turner RM. The Mechanical Design of Nacre. Philos Trans R Soc Lond B Biol Sci. 1988;234:415.
[32] Dunlop JWC, Weinkamer R, Fratzl P. Artful interfaces within biological materials. Mater Today. 2011;14:70-8.
[33] Barthelat F, Yin Z, Buehler MJ. Structure and mechanics of interfaces in biological materials. Nat Rev Mater. 2016;1:16007.
[34] Aizenberg J, Weaver JC, Thanawala MS, Sundar VC, Morse DE, Fratzl P. Skeleton of Euplectella sp.: Structural Hierarchy from the Nanoscale to the Macroscale. Science. 2005;309:275.
[35] Keckes J, Burgert I, Fruhmann K, Muller M, Kolln K, Hamilton M, et al. Cell-wall recovery after irreversible deformation of wood. Nat Mater. 2003;2:810-3.
[36] Puxkandl R, Zizak I, Paris O, Keckes J, Tesch W, Bernstorff S, et al. Viscoelastic properties of collagen: synchrotron radiation investigations and structural model. Philos Trans R Soc Lond B Biol Sci. 2002;357:191-7.
[37] Gupta HS, Seto J, Wagermaier W, Zaslansky P, Boesecke P, Fratzl P. Cooperative deformation of mineral and collagen in bone at the nanoscale. Proc Natl Acad Sci. 2006;103:17741-6.
[38] Barthelat F, Tang H, Zavattieri PD, Li CM, Espinosa HD. On the mechanics of mother-of-pearl: A key feature in the material hierarchical structure. J Mech Phys Solids. 2007;55:306-37.
[39] Levi-Kalisman Y, Falini G, Addadi L, Weiner S. Structure of the Nacreous Organic Matrix of a Bivalve Mollusk Shell Examined in the Hydrated State Using Cryo-TEM. J Struct Biol 2001;135:8-17.
[40] Rousseau M, Lopez E, Stempflé P, Brendlé M, Franke L, Guette A, et al. Multiscale structure of sheet nacre. Biomaterials. 2005;26:6254-62.
[41] Marin F, Luquet G, Marie B, Medakovic D. Molluscan Shell Proteins: Primary Structure, Origin, and Evolution. Cur Top Dev Biol Academic Press; 2007. p. 209-76.
[42] Shen X, Belcher AM, Hansma PK, Stucky GD, Morse DE. Molecular Cloning and Characterization of Lustrin A, a Matrix Protein from Shell and Pearl Nacre of Haliotis rufescens. J Biol Chem. 1997;272:32472-81.
[43] Wustman BA, Weaver JC, Morse DE, Evans JS. Characterization of a Ca(II)-, Mineral-Interactive Polyelectrolyte Sequence from the Adhesive Elastomeric Biomineralization Protein Lustrin A. Langmuir. 2003;19:9373-81.
[44] Rothon RN. Particulate-Filled Polymer Composites: Raupe Technology Limited; 2003.
[45] Goerg H. Michler FJB-C. Nano- and Micromechanics of Polymers Hanser Verlag; 2012.
[46] J.Pritchard. Plastics Additives. Shropshire: Rapra Technology Limited; 2005.
[47] Pukánszky B, Fekete E, Tüdós F. Surface tension and mechanical properties in polyolefin composites. Makromol Chem Macromol Symp 1989;28:165-86.
[48] Fekete E, Pukánszky B, Tóth A, Bertóti I. Surface modification and characterization of particulate mineral fillers. J Colloid Interface Sci. 1990;135:200-8.
[49] Papirer E, Schultz J, Turchi C. Surface properties of a calcium carbonate filler treated with stearic acid. Eur Polym J. 1984;20:1155-8.
[50] Jančář J, Kučera J. Yield behavior of polypropylene filled with CaC03 and Mg(OH)2. I: “Zero” interfacial adhesion. Polym Eng Sci. 1990;30:707-13.
[51] Pukánszky B, Maurer FHJ. Composition dependence of the fracture toughness of heterogeneous polymer systems. Polymer. 1995;36:1617-25.
[52] Particulate-filled polymer composites. Shawhury: Rapra Technology Limited; 2003.

[53] Ishida H, Miller JD. Substrate effects on the chemisorbed and physisorbed layers of methacryl silane-modified particulate minerals. Macromolecules. 1984;17:1659-66.
[54] Plueddemann EP. Adhesion Through Silane Coupling Agents. J Adhesion. 1970;2:184-201.
[55] Zolotnitsky M, Steinmetz JR. Comparative study of organofunctional water-borne silanes as couplants in nylon-66 composites. J Vinyl Add Techn. 1995;1:109-13.
[56] Sharma YN, Patel RD, Dhimmar IH, Bhardwaj IS. Studies of the effect of titanate coupling agent on the performance of polypropylene–calcium carbonate composite. J Appl Polym Sci. 1982;27:97-104.
[57] Landry CJT, Coltrain BK, Teegarden DM, Long TE, Long VK. Use of Organic Copolymers as Compatibilizers for Organic−Inorganic Composites. Macromolecules. 1996;29:4712-21.
[58] Zhou X, Xiong R, Lin Q. Effect of block copolymer coupling agents on properties of mica reinforced polymeric composites. J Mat Sci 2006;41:7879-85.
[59] Kim J-Y, Peck JH, Hwang S-H, Hong J, Hong SC, Huh W, et al. Preparation and mechanical properties of poly(vinyl chloride)/bamboo flour composites with a novel block copolymer as a coupling agent. J Appl Polym Sci. 2008;108:2654-9.
[60] Li Y, Chen L, Zhou X. Interfacial crystalline behavior in glass-fiber/polypropylene composites modified by block copolymer coupling agents. J Mat Sci 2008;43:5083-91.
[61] Kumar SK, Jouault N, Benicewicz B, Neely T. Nanocomposites with Polymer Grafted Nanoparticles. Macromolecules. 2013;46:3199-214.
[62] Asai M, Zhao D, Kumar SK. Role of Grafting Mechanism on the Polymer Coverage and Self-Assembly of Hairy Nanoparticles. ACS Nano. 2017;11:7028-35.
[63] Gao J, Li J, Benicewicz BC, Zhao S, Hillborg H, Schadler LS. The Mechanical Properties of Epoxy Composites Filled with Rubbery Copolymer Grafted SiO2. Polymers. 2012;4:187.
[64] B.Pulkanszky EF. Advances in Polymer Science. Springer-Verlag Berlin Heidelberg1999.
[65] Johns A, Morris S, Edwards K, Quirino RL. Asolectin from soybeans as a natural compatibilizer for cellulose-reinforced biocomposites from tung oil. J Appl Polym Sci. 2015;132:n/a-n/a.
[66] Luyt AS, Geethamma VG. Effect of oxidized paraffin wax on the thermal and mechanical properties of linear low-density polyethylene–layered silicate nanocomposites. Polym Test 2007;26:461-70.
[67] Rozman HD, Tan KW, Kumar RN, Abubakar A, Mohd. Ishak ZA, Ismail H. The effect of lignin as a compatibilizer on the physical properties of coconut fiber–polypropylene composites. Eur Polym J. 2000;36:1483-94.
[68] Lee S-H, Wang S. Biodegradable polymers/bamboo fiber biocomposite with bio-based coupling agent. Compos A: Appl Sci Manuf 2006;37:80-91.
[69] Bourmaud A, Riviere J, Le Duigou A, Raj G, Baley C. Investigations of the use of a mussel-inspired compatibilizer to improve the matrix-fiber adhesion of a biocomposite. Polym Test 2009;28:668-72.
[70] Phua SL, Yang L, Toh CL, Guoqiang D, Lau SK, Dasari A, et al. Simultaneous Enhancements of UV Resistance and Mechanical Properties of Polypropylene by Incorporation of Dopamine-Modified Clay. ACS Appl Mater Interfaces. 2013;5:1302-9.
[71] Ferrer A, Hoeger IC, Lu X, Rojas OJ. Reinforcement of polypropylene with lignocellulose nanofibrils and compatibilization with biobased polymers. J Appl Polym Sci 2016;133:n/a-n/a.
[72] Launey ME, Ritchie RO. On the Fracture Toughness of Advanced Materials. Adv Mater. 2009;21:2103-10.
[73] Song F, Soh AK, Bai YL. Structural and mechanical properties of the organic matrix layers of nacre. Biomaterials. 2003;24:3623-31.
[74] Wang RZ, Suo Z, Evans AG, Yao N, Aksay IA. Deformation mechanisms in nacre. J Mat Res 2011;16:2485-93.
[75] Crookes-Goodson WJ, Slocik JM, Naik RR. Bio-directed synthesis and assembly of nanomaterials. Chem Soc Rev 2008;37:2403-12.
[76] Dickerson MB, Sandhage KH, Naik RR. Protein- and Peptide-Directed Syntheses of Inorganic Materials. Chem Rev 2008;108:4935-78.

[77] Arakaki A, Masuda F, Amemiya Y, Tanaka T, Matsunaga T. Control of the morphology and size of magnetite particles with peptides mimicking the Mms6 protein from magnetotactic bacteria. J Colloid Interface Sci. 2010;343:65-70.
[78] Hoess RH. Protein Design and Phage Display. Chem Rev. 2001;101:3205-18.
[79] Sarikaya M, Tamerler C, Jen AKY, Schulten K, Baneyx F. Molecular biomimetics: nanotechnology through biology. Nat Mater. 2003;2:577-85.
[80] Johnny X. Huanga, and SLB-H, Coopera MA, . Development of Anti-Infectives Using Phage Display: Biological Agents against Bacteria, Viruses, and Parasites. Antimicrob Agen Chemother 2012;56:4569–82.
[81] Brown S. Metal-recognition by repeating polypeptides. Nat Biotechnol. 1997;15:269-72.
[82] Sano K-I, Shiba K. A Hexapeptide Motif that Electrostatically Binds to the Surface of Titanium. J Am Chem Soc. 2003;125:14234-5.
[83] Carter CJ, Ackerson CJ, Feldheim DL. Unusual Reactivity of a Silver Mineralizing Peptide. ACS Nano. 2010;4:3883-8.
[84] Puddu V, Perry CC. Peptide Adsorption on Silica Nanoparticles: Evidence of Hydrophobic Interactions. ACS Nano. 2012;6:6356-63.
[85] Rothenstein D, Claasen B, Omiecienski B, Lammel P, Bill J. Isolation of ZnO-Binding 12-mer Peptides and Determination of Their Binding Epitopes by NMR Spectroscopy. J Am Chem Soc. 2012;134:12547-56.
[86] Thai CK, Dai H, Sastry MSR, Sarikaya M, Schwartz DT, Baneyx F. Identification and characterization of Cu2O- and ZnO-binding polypeptides by Escherichia coli cell surface display: toward an understanding of metal oxide binding. Biotechnol Bioeng. 2004;87:129-37.
[87] Nygaard S, Wendelbo R, Brown S. Surface-Specific Zeolite-Binding Proteins. Adv Mater. 2002;14:1853-6.
[88] Estephan E, Saab M-B, Martin M, Larroque C, Cuisinier FJG, Briot O, et al. Phages recognizing the Indium Nitride semiconductor surface via their peptides. J Pep Sci 2011;17:143-7.
[89] Serizawa T, Techawanitchai P, Matsuno H. Isolation of Peptides that Can Recognize Syndiotactic Polystyrene. ChemBioChem. 2007;8:989-93.
[90] Wang S, Humphreys ES, Chung S-Y, Delduco DF, Lustig SR, Wang H, et al. Peptides with selective affinity for carbon nanotubes. Nat Mater. 2003;2:196-200.
[91] Cui Y, Kim SN, Jones SE, Wissler LL, Naik RR, McAlpine MC. Chemical Functionalization of Graphene Enabled by Phage Displayed Peptides. Nano Lett. 2010;10:4559-65.
[92] Guo J, Catchmark JM, Mohamed MNA, Benesi AJ, Tien M, Kao T-h, et al. Identification and Characterization of a Cellulose Binding Heptapeptide Revealed by Phage Display. Biomacromolecules. 2013;14:1795-805.
[93] Sethi M, Pacardo DB, Knecht MR. Biological Surface Effects of Metallic Nanomaterials for Applications in Assembly and Catalysis. Langmuir. 2010;26:15121-34.
[94] Sethi M, Knecht MR. Experimental Studies on the Interactions between Au Nanoparticles and Amino Acids: Bio-Based Formation of Branched Linear Chains. ACS Appl Mater Interfaces. 2009;1:1270-8.
[95] Sethi M, Joung G, Knecht MR. Linear Assembly of Au Nanorods Using Biomimetic Ligands. Langmuir. 2009;25:1572-81.
[96] Majzik A, Fülöp L, Csapó E, Bogár F, Martinek T, Penke B, et al. Functionalization of gold nanoparticles with amino acid, β-amyloid peptides and fragment. Colloids Surf B Biointerfaces. 2010;81:235-41.
[97] Krpetić Ž, Nativo P, Porta F, Brust M. A Multidentate Peptide for Stabilization and Facile Bioconjugation of Gold Nanoparticles. Bioconjug Chem 2009;20:619-24.
[98] Fabris L, Antonello S, Armelao L, Donkers RL, Polo F, Toniolo C, et al. Gold Nanoclusters Protected by Conformationally Constrained Peptides. J Am Chem Soc. 2006;128:326-36.
[99] Barlow SM, Haq S, Raval R. Bonding, Organization, and Dynamical Growth Behavior of Tripeptides on a Defined Metal Surface: Tri-l-alanine and Tri-l-leucine on Cu{110}. Langmuir. 2001;17:3292-300.

[100] Aili D, Enander K, Rydberg J, Nesterenko I, Björefors F, Baltzer L, et al. Folding Induced Assembly of Polypeptide Decorated Gold Nanoparticles. J Am Chem Soc. 2008;130:5780-8.
[101] Graf P, Mantion A, Foelske A, Shkilnyy A, Mašić A, Thünemann AF, et al. Peptide-Coated Silver Nanoparticles: Synthesis, Surface Chemistry, and pH-Triggered, Reversible Assembly into Particle Assemblies. Chem Eur J. 2009;15:5831-44.
[102] Higuchi M, Nagata K, Abiko S, Tanaka M, Kinoshita T. Stimuli Induced Structural Changes of Gold Nanoparticle Assemblies Having Sequential Alternating Amphiphilic Peptides at the Surface. Langmuir. 2008;24:13359-63.
[103] Merg AD, Slocik J, Blaber MG, Schatz GC, Naik R, Rosi NL. Adjusting the Metrics of 1-D Helical Gold Nanoparticle Superstructures Using Multivalent Peptide Conjugates. Langmuir. 2015;31:9492-501.
[104] Aryal S, Bahadur K. C R, Bhattarai SR, Prabu P, Kim HY. Immobilization of collagen on gold nanoparticles: preparation, characterization, and hydroxyapatite growth. J Mater Chem. 2006;16:4642-8.
[105] Jakhmola A, Bhandari R, Pacardo DB, Knecht MR. Peptide template effects for the synthesis and catalytic application of Pd nanoparticle networks. J Mater Chem. 2010;20:1522-31.
[106] Song C, Blaber MG, Zhao G, Zhang P, Fry HC, Schatz GC, et al. Tailorable Plasmonic Circular Dichroism Properties of Helical Nanoparticle Superstructures. Nano Lett. 2013;13:3256-61.
[107] Merg AD, Boatz JC, Mandal A, Zhao G, Mokashi-Punekar S, Liu C, et al. Peptide-Directed Assembly of Single-Helical Gold Nanoparticle Superstructures Exhibiting Intense Chiroptical Activity. J Am Chem Soc. 2016;138:13655-63.
[108] Sharma N, Top A, Kiick KL, Pochan DJ. One-Dimensional Gold Nanoparticle Arrays by Electrostatically Directed Organization Using Polypeptide Self-Assembly. Angew Chem Int Ed. 2009;48:7078-82.
[109] Schwemmer T, Baumgartner J, Faivre D, Börner HG. Peptide-Mediated Nanoengineering of Inorganic Particle Surfaces: A General Route toward Surface Functionalization via Peptide Adhesion Domains. J Am Chem Soc. 2012;134:2385-91.
[110] Wang T, Mitchell J, Borner H, Colfen H, Antonietti M. BaCO3 mesocrystals: new morphologies using peptide-polymer conjugates as crystallization modifiers. Phys Chem Chem Phys. 2010;12:11984-92.
[111] Kim J, Rheem Y, Yoo B, Chong Y, Bozhilov KN, Kim D, et al. Peptide-mediated shape- and size-tunable synthesis of gold nanostructures. Acta Biomater. 2010;6:2681-9.
[112] Kim J, Rheem Y, Yoo B, Chong Y, Bozhilov KN, Kim D, et al. Peptide-mediated shape- and size-tunable synthesis of gold nanostructures. Acta Biomaterialia. 2010;6:2681-9.
[113] Li Y, Tang Z, Prasad PN, Knecht MR, Swihart MT. Peptide-mediated synthesis of gold nanoparticles: effects of peptide sequence and nature of binding on physicochemical properties. Nanoscale. 2014;6:3165-72.
[114] Belser K, Vig Slenters T, Pfumbidzai C, Upert G, Mirolo L, Fromm KM, et al. Silver Nanoparticle Formation in Different Sizes Induced by Peptides Identified within Split-and-Mix Libraries. Angew Chem Int Ed 2009;48:3661-4.
[115] Naik RR, Stringer SJ, Agarwal G, Jones SE, Stone MO. Biomimetic synthesis and patterning of silver nanoparticles. Nat Mater. 2002;1:169-72.
[116] Chiu C-Y, Li Y, Huang Y. Size-controlled synthesis of Pd nanocrystals using a specific multifunctional peptide. Nanoscale. 2010;2:927-30.
[117] Tao K, Wang J, Li Y, Xia D, Shan H, Xu H, et al. Short peptide-directed synthesis of one-dimensional platinum nanostructures with controllable morphologies. Sci Rep 2013;3:2565.
[118] Forbes LM, Goodwin AP, Cha JN. Tunable Size and Shape Control of Platinum Nanocrystals from a Single Peptide Sequence. Chem Mater. 2010;22:6524-8.
[119] Whaley SR, English DS, Hu EL, Barbara PF, Belcher AM. Selection of peptides with semiconductor binding specificity for directed nanocrystal assembly. Nature. 2000;405:665-8.

[120] Dickerson MB, Jones SE, Cai Y, Ahmad G, Naik RR, Kröger N, et al. Identification and Design of Peptides for the Rapid, High-Yield Formation of Nanoparticulate TiO2 from Aqueous Solutions at Room Temperature. Chem Mater. 2008;20:1578-84.
[121] Ruan L, Ramezani-Dakhel H, Chiu C-Y, Zhu E, Li Y, Heinz H, et al. Tailoring Molecular Specificity Toward a Crystal Facet: a Lesson From Biorecognition Toward Pt{111}. Nano Lett. 2013;13:840-6.
[122] Coppage R, Slocik JM, Sethi M, Pacardo DB, Naik RR, Knecht MR. Elucidation of Peptide Effects that Control the Activity of Nanoparticles. Angew Chem Int Ed. 2010;49:3767-70.
[123] Patwardhan SV, Patwardhan G, Perry CC. Interactions of biomolecules with inorganic materials: principles, applications and future prospects. J Mater Chem. 2007;17:2875-84.
[124] Fears KP, Clark TD, Petrovykh DY. Residue-Dependent Adsorption of Model Oligopeptides on Gold. J Am Chem Soc. 2013;135:15040-52.
[125] Nel AE, Madler L, Velegol D, Xia T, Hoek EMV, Somasundaran P, et al. Understanding biophysicochemical interactions at the nano-bio interface. Nat Mater. 2009;8:543-57.
[126] Briggs BD, Knecht MR. Nanotechnology Meets Biology: Peptide-based Methods for the Fabrication of Functional Materials. J Phys Chem Let. 2012;3:405-18.
[127] Yu J, Becker ML, Carri GA. The Influence of Amino Acid Sequence and Functionality on the Binding Process of Peptides onto Gold Surfaces. Langmuir. 2012;28:1408-17.
[128] Tang Z, Palafox-Hernandez JP, Law W-C, E. Hughes Z, Swihart MT, Prasad PN, et al. Biomolecular Recognition Principles for Bionanocombinatorics: An Integrated Approach To Elucidate Enthalpic and Entropic Factors. ACS Nano. 2013;7:9632-46.
[129] Skelton AA, Liang T, Walsh TR. Interplay of Sequence, Conformation, and Binding at the Peptide−Titania Interface as Mediated by Water. ACS Appl Mater Interfaces. 2009;1:1482-91.
[130] Horinek D, Serr A, Geisler M, Pirzer T, Slotta U, Lud SQ, et al. Peptide adsorption on a hydrophobic surface results from an interplay of solvation, surface, and intrapeptide forces. Proc Natl Acad Sci. 2008;105:2842-7.
[131] Patwardhan SV, Emami FS, Berry RJ, Jones SE, Naik RR, Deschaume O, et al. Chemistry of Aqueous Silica Nanoparticle Surfaces and the Mechanism of Selective Peptide Adsorption. J Am Chem Soc. 2012;134:6244-56.
[132] Mirau PA, Naik RR, Gehring P. Structure of Peptides on Metal Oxide Surfaces Probed by NMR. J Am Chem Soc. 2011;133:18243-8.
[133] Mandal HS, Kraatz H-B. Effect of the Surface Curvature on the Secondary Structure of Peptides Adsorbed on Nanoparticles. J Am Chem Soc. 2007;129:6356-7.
[134] Shaw CP, Middleton DA, Volk M, Lévy R. Amyloid-Derived Peptide Forms Self-Assembled Monolayers on Gold Nanoparticle with a Curvature-Dependent β-Sheet Structure. ACS Nano. 2012;6:1416-26.
[135] Katoch J, Kim SN, Kuang Z, Farmer BL, Naik RR, Tatulian SA, et al. Structure of a Peptide Adsorbed on Graphene and Graphite. Nano Lett. 2012;12:2342-6.
[136] Hnilova M, Oren EE, Seker UOS, Wilson BR, Collino S, Evans JS, et al. Effect of Molecular Conformations on the Adsorption Behavior of Gold-Binding Peptides. Langmuir. 2008;24:12440-5.
[137] Coppage R, Slocik JM, Briggs BD, Frenkel AI, Naik RR, Knecht MR. Determining Peptide Sequence Effects That Control the Size, Structure, and Function of Nanoparticles. ACS Nano. 2012;6:1625-36.
[138] Slocik JM, Govorov AO, Naik RR. Plasmonic Circular Dichroism of Peptide-Functionalized Gold Nanoparticles. Nano Lett. 2011;11:701-5.
[139] Zoroddu MA, Medici S, Peana M, Anedda R. NMR studies of zinc binding in a multi-histidinic peptide fragment. Dalton Trans. 2010;39:1282-94.
[140] Gammon E. General Chemistry, Enhanced Edition. 9th edition ed: Brooks/Cole; ; 2011.
[141] Lellouche J, Friedman A, Lellouche J-P, Gedanken A, Banin E. Improved antibacterial and antibiofilm activity of magnesium fluoride nanoparticles obtained by water-based ultrasound chemistry. Nanomedicine 2012;8:702-11.

[142] Gentleman E, Stevens MM, Hill RG, Brauer DS. Surface properties and ion release from fluoride-containing bioactive glasses promote osteoblast differentiation and mineralization in vitro. Acta Biomater 2013;9:5771-9.
[143] Xu X, Liu F, Jiang L, Zhu JY, Haagenson D, Wiesenborn DP. Cellulose Nanocrystals vs. Cellulose Nanofibrils: A Comparative Study on Their Microstructures and Effects as Polymer Reinforcing Agents. ACS Appl Mater Interfaces. 2013;5:2999-3009.
[144] Fu S-Y, Feng X-Q, Lauke B, Mai Y-W. Effects of particle size, particle/matrix interface adhesion and particle loading on mechanical properties of particulate–polymer composites. Compos B: Eng. 2008;39:933-61.
[145] B.Seidt. Characterization of bioinspired hybridmaterials by multi-scale analysis [Doctoral Thesis]: Technical University Berlin; 2016.
[146] Pati D, Kalva N, Das S, Kumaraswamy G, Sen Gupta S, Ambade AV. Multiple Topologies from Glycopolypeptide–Dendron Conjugate Self-Assembly: Nanorods, Micelles, and Organogels. J Am Chem Soc. 2012;134:7796-802.
[147] Stuart BH. Infrared Spectroscopy: Fundamentals and Applications Infrared Spectroscopy: Fundamentals and Applications: John Wiley & Sons, Ltd; 2005. p. 137-65.
[148] Wang H, Keum JK, Hiltner A, Baer E. Impact of Nanoscale Confinement on Crystal Orientation of Poly(ethylene oxide). Macromol Rapid Commun. 2010;31:356-61.
[149] Burba CM, Frech R, Grady B. Stretched PEO–LiCF3SO3 films: Polarized IR spectroscopy and X-ray diffraction. Electrochim Acta. 2007;53:1548-55.
[150] Su Z, Li J, Li Q, Ni T, Wei G. Chain conformation, crystallization behavior, electrical and mechanical properties of electrospun polymer-carbon nanotube hybrid nanofibers with different orientations. Carbon. 2012;50:5605-17.
[151] Lee JH, Shofner ML. Dispersion of polymer-decorated hydroxyapatite nanoparticles in poly(ethylene oxide) at low grafting densities. Polymer. 2012;53:5146-54.
[152] Waddon AJ, Petrovic ZS. Spherulite Crystallization in Poly(ethylene oxide)-Silica Nanocomposites. Retardation of Growth Rates through Reduced Molecular Mobility. Polym J. 2002;34:876-81.
[153] Vaisman L, Marom G, Wagner HD. Dispersions of Surface-Modified Carbon Nanotubes in Water-Soluble and Water-Insoluble Polymers. Adv Funct Mater. 2006;16:357-63.
[154] Osman MA, Atallah A. High-Density Polyethylene Micro- and Nanocomposites: Effect of Particle Shape, Size and Surface Treatment on Polymer Crystallinity and Gas Permeability. Macromol Rapid Com 2004;25:1540-4.
3ketone)/ZnO bionanocomposites. J Mater Chem B. 2014;2:3065-78.
[156] K.Friedrich. Crazing in polymers. Berlin Heidelberg: Springer verlag; 1986.
[157] Strawhecker KE, Manias E. Crystallization Behavior of Poly(ethylene oxide) in the Presence of Na+ Montmorillonite Fillers. Chem Mater. 2003;15:844-9.
[158] Bing-Xing Y, Jia-Hua S, Pramoda KP, Suat Hong G. Enhancement of stiffness, strength, ductility and toughness of poly(ethylene oxide) using phenoxy-grafted multiwalled carbon nanotubes. Nanotechnology. 2007;18:125606.
[159] Xi J, Qiu X, Zheng S, Tang X. Nanocomposite polymer electrolyte comprising PEO/LiClO4 and solid super acid: effect of sulphated-zirconia on the crystallization kinetics of PEO. Polymer. 2005;46:5702-6.
[160] Burgaz E. Poly(ethylene-oxide)/clay/silica nanocomposites: Morphology and thermomechanical properties. Polymer. 2011;52:5118-26.
[161] Jurkin T, Pucić I. Poly(ethylene oxide) irradiated in the solid state, melt and aqueous solution—a DSC and WAXD study. Radiat Phys Chem 2012;81:1303-8.
[162] Adams WW, Yang D, Thomas EL. Direct visualization of microstructural deformation processes in polyethylene. J Mat Sci. 1986;21:2239-53.
[163] Martin J, Ponçot M, Bourson P, Dahoun A, Hiver J-M. Study of the crystalline phase orientation in uniaxially stretched polypropylene by Raman spectroscopy: Validation and use of a time-resolved measurement method. Polym Eng Sci. 2011;51:1607-16.

[164] Lazzeri A, Thio YS, Cohen RE. Volume strain measurements on CACO3/polypropylene particulate composites: The effect of particle size. J Appl Polym Sci 2004;91:925-35.
[165] Suprapakorn N, Dhamrongvaraporn S, Ishida H. Effect of CaCO3 on the mechanical and rheological properties of a ring-opening phenolic resin: Polybenzoxazine. Polymer Composite 1998;19:126-32.
[166] Douce J, Boilot J-P, Biteau J, Scodellaro L, Jimenez A. Effect of filler size and surface condition of nano-sized silica particles in polysiloxane coatings. Thin Solid Films. 2004;466:114-22.
[167] Mishra S, Sonawane SH, Singh RP. Studies on characterization of nano CaCO3 prepared by the in situ deposition technique and its application in PP-nano CaCO3 composites. J Polym Sci B: Polym Phys 2005;43:107-13.
[168] Dekkers MEJ, Heikens D. The effect of interfacial adhesion on the tensile behavior of polystyrene–glass-bead composites. J Appl Polym Sci. 1983;28:3809-15.
[169] Sevostianov I, Kachanov M. Effect of interphase layers on the overall elastic and conductive properties of matrix composites. Applications to nanosize inclusion. Int J Solid Struct 2007;44:1304-15.
[170] Kontou E. Micromechanics model for particulate composites. Mech Mat 2007;39:702-9.
[171] Ji XL, Jing JK, Jiang W, Jiang BZ. Tensile modulus of polymer nanocomposites. Polym Eng Sci 2002;42:983-93.
[172] Rong MZ, Zhang MQ, Pan SL, Lehmann B, Friedrich K. Analysis of the interfacial interactions in polypropylene/silica nanocomposites. Polym Int 2004;53:176-83.
[173] Zhang L, Li C, Huang R. Toughness mechanism in polypropylene composites: Polypropylene toughened with elastomer and calcium carbonate. J Polym Sci B: Polym Phys. 2004;42:1656-62.
[174] Bartczak Z, Argon AS, Cohen RE, Weinberg M. Toughness mechanism in semi-crystalline polymer blends: II. High-density polyethylene toughened with calcium carbonate filler particles. Polymer. 1999;40:2347-65.
[175] Hopp TP, Woods KR. Prediction of protein antigenic determinants from amino acid sequences. Proc Natl Acad Sci. 1981;78:3824-8.
[176] Samsoninkova V, Venkatareddy NL, Wagermaier W, Dallmann A, Börner HG. Precision compatibilizers for composites: in-between self-aggregation, surfaces recognition and interface stabilization. Soft Matter. 2018;14:1992-5.
[177] Characterization of Protein Therapeutics using Mass Spectrometry: Springer New York Heidelberg Doredrecht London; 2013.
[178] Rocha S, Thünemann AF, Pereira MdC, Coelho M, Möhwald H, Brezesinski G. Influence of fluorinated and hydrogenated nanoparticles on the structure and fibrillogenesis of amyloid beta-peptide. Biophys Chem 2008;137:35-42.
[179] Gokce I, Woody RW, Anderluh G, Lakey JH. Single Peptide Bonds Exhibit Poly(Pro)II ("Random Coil") Circular Dichroism Spectra. J Am Chem Soc. 2005;127:9700-1.
[180] Tooke L, Duitch L, Measey TJ, Schweitzer-Stenner R. Kinetics of the self-aggregation and film formation of poly-L-proline at high temperatures explored by circular dichroism spectroscopy. Biopolymers. 2010;93:451-7.
[181] Chiti F, Webster P, Taddei N, Clark A, Stefani M, Ramponi G, et al. Designing conditions for in vitro formation of amyloid protofilaments and fibrils. Proc Natl Acad Sci. 1999;96:3590-4.
[182] FrederixPim WJM, Scott GG, Abul-Haija YM, Kalafatovic D, Pappas CG, Javid N, et al. Exploring the sequence space for (tri-)peptide self-assembly to design and discover new hydrogels. Nat Chem. 2015;7:30-7.
[183] Pukánszky B, Fekete E, Tüdós F. Surface tension and mechanical properties in polyolefin composites. Macromol Symp. 1989;28:165-86.
[184] Shao Z, Vollrath F. Surprising strength of silkworm silk. Nature. 2002;418:741.
[185] Yang Y, Chen X, Shao Z, Zhou P, Porter D, Knight DP, et al. Toughness of Spider Silk at High and Low Temperatures. Adv Mater. 2005;17:84-8.

[186] Baxter NJ, Blackburn GM, Marston JP, Hounslow AM, Cliff MJ, Bermel W, et al. Anionic Charge Is Prioritized over Geometry in Aluminum and Magnesium Fluoride Transition State Analogs of Phosphoryl Transfer Enzymes. J Am Chem Soc 2008;130:3952-8.
[187] Baxter NJ, Bowler MW, Alizadeh T, Cliff MJ, Hounslow AM, Wu B, et al. Atomic details of near-transition state conformers for enzyme phosphoryl transfer revealed by rather than by phosphoranes. Proc Nat Acad Sci. 2010;107:4555-60.
[188] Rief M, Oesterhelt F, Heymann B, Gaub HE. Single Molecule Force Spectroscopy on Polysaccharides by Atomic Force Microscopy. Science. 1997;275:1295-7.
[189] Janshoff A, Neitzert M, Oberdörfer Y, Fuchs H. Force Spectroscopy of Molecular Systems—Single Molecule Spectroscopy of Polymers and Biomolecules. Angew Chem Int Ed 2000;39:3212-37.
[190] Fratzl P, Gupta HS, Paschalis EP, Roschger P. Structure and mechanical quality of the collagen-mineral nano-composite in bone. J Mater Chem. 2004;14:2115-23.
[191] Eder M, Amini S, Fratzl P. Biological composites—complex structures for functional diversity. Science. 2018;362:543-7.

Acknowledgments

PhD represents not only a scientific work but mostly a personal transformation. This transformation and personal changes take place to some extend due to scientific knowledge, which one acquires on a way, but I believe that it is only a part. The changes mainly come from positive and as well negative experiences which one makes and people which surround. The impact of the people, who supervises you and who works with you makes the biggest difference. And I would like to express my gratitude to all people who I was working with me over the years of PhD. Special thanks goes of course to my supervisors Prof. Hans Börner and Dr. Wolfgang Wagermaier, who were guiding me over the period of the project proving scientific and personal guidance.

I would like to thank specially Prof. Fratzl from MPI of Colloids and Interfaces for very helpful scientific discussions and ideas, which were extremely valuable. I am very happy that I had a chance to work under his guidance. I am also very grateful for very valuable and helpful discussion about NMR experiments with Dr. Andre Dallmann.

A special thanks goes to my colleague in the group of Prof. Börner - Felix Hanßke. We were working together on the same cluster of topics. I am very grateful that I had colleagues to discuss the data, for his extreme dedication and readiness to help. I appreciate very much also help of Narrendra Reddy in all NMR related topic and questions and also other discussions.

Apart scientific guidance and inspiration, scientific work requires lots of experiments and measurements. I appreciate a lot the support, which I got to be able to realize number of experiments: help and supervision of Dr. Michaela Eder and Petra Leibner (MPI) in the mechanical experiments, Susann Reinhold and Heike Runge (MPI) for help in SEM measurements; Dr. Clavel (Humboldt University) in the help and supervision in TEM measurements and last but not least help of Anne Heilig in AFM measurements. Special thanks go also to former member of Prof. Börner group Katharina Linkert for the support in peptide synthesis and Dario Remmler for MALDI measurements.

I am extremely grateful for the personal help of friends, who supported me through the phase of PhD. Their help was for me extremely valuable. I appreciated a lot help and advices of Eva Maron. The support of my friend Bita Rezania is difficult to overestimate; her contribution to the PhD in terms of mental support was huge. I am also extremely thankful to Olga Ganevich and Christian Lorenz for mental support and that these very close to me people “caught” me in the “minimum of the curve”. I appreciate also professional help of Irina Theisen in a finding myself and finding a balance in all occurring situations. Special thanks goes of course to my teacher in all senses of this word Galina Berkova, who was my teacher in chemistry, analytical methods specially in NMR and later become a good friend and life coach.

Of course I am deeply grateful to my mother and my relatives for overall support and understanding and possibilities given to me.

Selbstständigkeitserklärung

Hiermit versichere ich, dass ich die vorliegende Dissertation selbstständig verfasst und keine anderen als die angegebenen Quellen und Hilfsmittel verwendet habe.

Ferner erkläre ich, dass ich nicht anderweitig mit oder ohne Erfolg versucht habe, eine Dissertation einzureichen oder mich einer Doktorprüfung zu unterziehen.

Valeria Samsoninkova